

BUCKLING LOAD PREDICTIONS IN PRESSURE VESSELS UTILIZING
MONTE CARLO METHOD

by

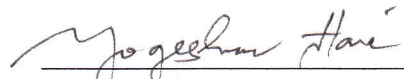
Gurinder Singh Brar

A dissertation submitted to the faculty of
The University of North Carolina at Charlotte
in partial fulfillment of the requirements
for the degree of Doctor of Philosophy in
Mechanical Engineering

Charlotte

2009

Approved by:



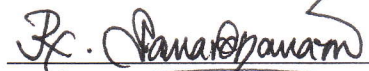
Dr. Yogeshwar Hari



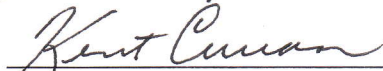
Dr. Dennis K. Williams



Dr. Russell Keanini



Dr. Rajaram Janardhanam



Dr. Kent Curran

©2009
Gurinder Singh Brar
ALL RIGHTS RESERVED

ABSTRACT

GURINDER SINGH BRAR. Buckling load predictions in pressure vessels utilizing Monte Carlo method (Under direction of DR. YOGESHWAR HARI)

In practice, large diameter, thin wall shells of revolution are never fabricated with constant diameters and thicknesses over the entire length of the assembly. These initial geometric imperfections have significant effect on the load carrying capacity of cylindrical shells. The cylindrical shell in the study is flue gas desulphurization (FGD) “vessel” which is a large hybrid tank-vessel-stack assembly in a major Canadian refinery. The function of the FGD vessel is to contain and support a proprietary process that utilizes an ammonium sulphate scrubbing system to produce environmentally friendly air emissions. FGD vessel stack has internal diameter of 6.1m, height of 45.34m and wall thickness of 9.525mm. Initial imperfections in FGD vessel is in the form of wall thickness variations. FGD wall thickness at 144 points along the circumference and elevation are measured. Monte Carlo method is employed to generate the measured data again. Test of significance is carried out to see the accuracy of the data generated. This Monte Carlo algorithm can be used to create data for any type of shell without spending time in actual measurements. Next, load carrying capacity of shell is determined considering imperfections to be axisymmetric and then asymmetric. Fourier decomposition is used to interpret imperfections as structural features can be easily related to the different components of imperfections. Further, double Fourier series is used to represent asymmetric initial geometric imperfections. The ultimate objective of these representations is to achieve a quantitative assessment of the critical buckling load considering the small axisymmetric and asymmetric deviations from the nominal

cylindrical shell wall thickness. Analysis of cylindrical shells when used as pressure vessels and are under external pressure is also carried out. Comparison of reliability techniques that employ Fourier series representations of random axisymmetric and asymmetric imperfections in axially compressed cylindrical shells and shells under external pressure with evaluations prescribed by ASME Boiler and Pressure Vessel Code, Section VIII, Division 1 and 2 is also carried out.

ACKNOWLEDGEMENTS

I would like to express my gratitude to all those who helped and inspired me during my doctoral study.

I would like to express my deep and sincere gratitude to my advisor, Dr. Yogeshwar Hari. His wide knowledge, positive suggestions, support and personal guidance provided a good basis for the present work. Throughout the thesis-writing period, he provided encouragement, sound advice, good company, and lots of good ideas.

I wish to express my warm and sincere thanks to Dr. Dennis K. Williams, who introduced me to this field, kept an eye on the progress of my work and always was available when I needed advice. I am grateful to Dr. Hari and Dr. Williams for attracting me to USA to accomplish my PhD. Without their support, my ambition to study abroad can hardly be realized.

I would also like to thank the other members of my PhD committee, Dr. Russell Keanini, Dr. Rajaram Janardhanam and Dr. Kent Curran for their detailed review, constructive criticism and excellent advice during the preparation of this thesis. Their kind support and guidance have been of great value in this study.

I am also grateful to the department of mechanical engineering, University of North Carolina at Charlotte for providing me an excellent work environment during the past years. I would like to express my sincere gratitude to Dr. Jayaraman Raja, Department Chair and Dr. Harish Cherukuri, Graduate Coordinator for their continual administrative support. The financial support from The University of North Carolina at Charlotte is gratefully acknowledged.

My deepest gratitude goes to my family for their love and support, this dissertation is simply impossible without them. I wish to thank my father, Dr. Joginder Singh Brar and mother, Mrs. Gurpreet Kaur Brar. Especially, I would like to give my special thanks to my wife, Prabhjot and my daughter, Sachleen. They have lost a lot due to my research work.

Above all, I would thank God for his blessings.

TABLE OF CONTENTS

LIST OF FIGURES	x
LIST OF TABLES	xii
LIST OF SYMBOLS	xiii
CHAPTER 1: INTRODUCTION	1
1.1 Buckling in Thin Wall Cylindrical Shells	1
1.2 Effect of Imperfections on Buckling Load	2
1.3 Background and Literature Review	4
1.4 Scope and Objectives	11
1.5 Outline of Analytical Research	11
CHAPTER 2: MONTE CARLO SIMULATION OF CYLINDRICAL SHELLS	13
2.1 Introduction	13
2.2 Monte Carlo Method	13
2.3 FGD Vessel	15
2.4 Simulation of Cylinders	18
2.5 Test of Significance	19
2.6 Summary	21
CHAPTER 3: AXISYMMETRIC ANALYSIS OF AXIAL END LOAD ON CYLINDRICAL SHELL	23
3.1 Introduction	23
3.2 Theory	23
3.3 Test of Simulated Cylindrical Shells	27
3.4 Calculation of Predicted Minimum Buckling Loads	28

3.5 Predicted Buckling Loads by Koiter's Theory	30
3.6 Summary	31
CHAPTER 4: ASYMMETRIC ANALYSIS OF AXIAL END LOAD ON CYLINDRICAL SHELL	32
4.1 Introduction	32
4.2 Theory	32
4.3 Simulated Cylindrical Shells	36
4.4 Calculation of Predicted Minimum Buckling Loads	38
4.5 Predicted Buckling Loads by Koiter's Theory	41
4.6 Summary	43
CHAPTER 5: ANALYSIS OF EXTERNAL PRESSURE ON CYLINDRICAL SHELL	44
5.1 Introduction	44
5.2 Simulated Shells	45
5.3 Calculation of Predicted Minimum Buckling Loads	46
5.4 Summary	49
CHAPTER 6: RESULTS AND COMPARISON WITH ASME B&PV CODE	50
6.1 Introduction	50
6.2 Results	50
6.3 Comparison of Results with ASME B&PV Code Sec. VIII Div. 2 Rules	52
CHAPTER 7: CONCLUSIONS	57
7.1 Recommendations	57
7.2 Future Work	59
REFERENCES	61

APPENDIX A: SIMULATED GB SHELLS	64
APPENDIX B: FOURIER COEFFICIENTS FOR GB SHELLS	89
APPENDIX C: VARIANCE COVARIANCE MATRIX FOR GB SHELLS	90
APPENDIX D: BUCKLING LOADS FOR GB SHELLS (KOITER AXISYMMETRIC THEORY)	91
APPENDIX E: ASYMMETRIC FOURIER COEFFICIENTS FOR GB SHELLS	92
APPENDIX F: BUCKLING LOAD MAP FOR GB SHELLS (AXIAL LOADING)	95
APPENDIX G: 8-MODE TREE FOR GB SHELLS (AXIAL LOADING)	96
APPENDIX H: BUCKLING LOADS FOR GB SHELLS (KOITER ASYMMETRIC THEORY)	97
APPENDIX I: BUCKLING LOAD MAP FOR GB SHELLS (EXTERNAL PRESSURE)	98
APPENDIX J: 8-MODE TREE FOR GB SHELLS (EXTERNAL PRESSURE)	99

LIST OF FIGURES

FIGURE 1.1: Load V/s Deflection Plot for Axially Loaded Cylindrical Shell	3
FIGURE 1.2: Sensitivity of the Bifurcation Load to the Amplitude of Axisymmetric Geometric Imperfections	6
FIGURE 2.1: FGD Vessel/Stack	16
FIGURE 2.2: Asymmetric Variation of Shell Wall Thickness for GB8 Shell	19
FIGURE 2.3: Axisymmetric Variation of Shell Wall Thickness for GB8 Shell	19
FIGURE 2.4: Chi-square (X^2) Values for 50 Simulated GB Shells	21
FIGURE 3.1: Auto-covariance Function for GB Shells	28
FIGURE 3.2: Non-dimensional Buckling Loads for 50 GB Shells (Axisymmetric Fourier Analysis)	29
FIGURE 3.3: Calculated Reliability Function V/S Non-dimensional Buckling Load (Axisymmetric Fourier Analysis)	29
FIGURE 3.4: Non-dimensional Buckling Loads for 50 GB Shells (Koiter Axisymmetric Theory)	30
FIGURE 3.5: Calculated Reliability Function V/S Non-dimensional Buckling Load (Koiter Axisymmetric Theory)	31
FIGURE 4.1: Koiter Circle for FGD vessel ($L/R=2.6$, $R/t=320$)	37
FIGURE 4.2: Circumferential Variation of the Half-wave Sine Fourier Representation	38
FIGURE 4.3: Axial Variation of the Half-wave Sine Fourier Representation	38
FIGURE 4.4: Non-dimensional Buckling Loads for 50 GB Shells (Multimode)	40
FIGURE 4.5: Calculated Reliability Function V/S Non-dimensional Buckling Load (Multimode)	40
FIGURE 4.6: Non-dimensional Buckling Loads for 50 GB Shells (Koiter Asymmetric Theory)	42

FIGURE 4.7: Calculated Reliability Function V/S Non-dimensional Buckling Load (Koiter Asymmetric Theory)	42
FIGURE 5.1: Non-dimensional Buckling Loads for 50 GB Shells (Shells Subjected to External Pressure)	48
FIGURE 5.2: Calculated Reliability Function V/S Non-dimensional Buckling Load (Shells Subjected to External Pressure)	48
FIGURE 6.1: Reliability Curves for Shells Subjected to Axial Compressive Load by Monte Carlo Technique	53
FIGURE 6.2: Reliability Curves for Shells Subjected to Axial Compressive Load by Koiter's Special Theory	54
FIGURE 6.3: Reliability Curves for Shells Subjected to Axial Compressive Load	55
FIGURE 6.4: Reliability Curves for Shells Under External Pressure	56
FIGURE 7.1: Reliability Curves of Simulated Shells Subjected to Axial Compressive Load by Different Methods	58
FIGURE 7.2: Reliability Curves of FGD Vessel Subjected to External Pressure by Different Methods	58
FIGURE G.1: 8-Mode Tree for GB Shells (Axial Loading)	96
FIGURE J.1: 8-Mode Tree for GB Shells (External Pressure)	99

LIST OF TABLES

TABLE 2.1:	Technical Specifications of FGD Stack Shell	17
TABLE 2.2:	Shell Wall Thickness (in.) of FGD Stack Shell	17
TABLE 2.3:	Chi-square Values of 50 Simulated GB Shells	20
TABLE 6.1:	Buckling Loads for FGD Vessel Subjected to Axial Compressive Load	51
TABLE 6.2:	Buckling Loads for FGD Vessel Subjected to External Pressure	52
TABLE A.1 – TABLE A.50:	Simulated Shell Wall Thicknesses of FGD Vessel	64-88
TABLE B.1:	Fourier Coefficients (a_i) for GB Shells	89
TABLE C.1:	Variance-covariance Matrix (σ_{ij}) for 25 GB Shells	90
TABLE D.1:	Non-Dimensional Buckling Load of GB Shells (Koiter Axisymmetric Method)	91
TABLE E.1:	Double Fourier Series Coefficient (C_{kl}) for GB Shells	92
TABLE E.2:	Double Fourier Series Coefficient (D_{kl}) for GB1 Shells	93
TABLE E.3:	Imperfection Amplitude (ξ) for GB1 Shells	94
TABLE F.1:	Buckling Load Map for GB Shells (Axial Loading)	95
TABLE H.1:	Non-Dimensional Buckling Load of GB Shells (Koiter Asymmetric Method)	97
TABLE I.1:	Buckling Load Map for GB Shells (External Pressure)	98

LIST OF SYMBOLS

λ - Non-dimensional buckling load

μ - Poisson's ratio

θ - Non-dimensional number associated with the circumferential coordinate

ξ - Non-dimensional number associated with the axial coordinate

ξ_i - Magnitude of imperfection as a fractional value of shell thickness

$\sigma_A(\xi)$ - Elements of variance-covariance matrix

$C_{w0}(\xi_1, \theta_1, \xi_2, \theta_2)$ - Auto-covariance function

$W_n(\xi, \theta)$ - Initial imperfection function

W_{cr} - Euler's crippling or buckling load

N_{xx} - Axial distributed in-plane force

N_{yy} - Circumferential in-plane force

L_{eff} - Effective length of Euler column

P_{cl} - Classical buckling load of a perfect shell

P_{cr} - Critical buckling load of a shell with imperfections

R - Radius of the shell

E - Young's modulus

L - Length of the shell

t - Wall thickness of the shell

k - Number of half waves in axial direction

l - Number of full waves in circumferential direction

D_0 - Outside diameter of the shell

I - Moment of inertia

D - Bending stiffness of cylindrical wall

w - Outward deflection in cylindrical shell wall

CHAPTER 1: INTRODUCTION

1.1 Buckling in Thin Wall Cylindrical Shells

Buckling is failure mechanism when a structural member fails under compressive load. Buckling is characterized by the appearance and growth of bulges, ripples or waves. Buckling is usually encountered in thin structural members when members show visibly large transverse displacement to the applied load. A structure is said to be in buckle when under a compressive load, structure undergoes transition in deformation, from deformation in direction of compressive load to a perpendicular direction. The load at which deformation transition takes place is called critical buckling load. Buckling failure is also described as failure due to elastic instability (sudden collapse).

Buckling is important as a structure can become unstable at load values significantly less than the ultimate compressive strength. It has been shown that for a thin cylindrical shell, compressive critical buckling load value governs the design of shell. Buckling of cylindrical shells can occur when a structural member is subjected to separate or combined action of axial compression, transverse pressure, torsion, etc.

Two approaches can be used for determining the buckling load of cylindrical shell, deterministic approach and stochastic approach. While the deterministic approach carries out analysis on the basis of some physical laws, stochastic (or probabilistic) approach takes into account several unknown factors that can affect the buckling loads. Deterministic approach does not include perturbations in the shell wall thicknesses.

Stochastic approach is used in this analytical study in order to predict the probability of buckling load in a particular confidence interval.

Buckling behavior cannot be predicted by linear theory. Classical buckling theories using non-linear equations are required to predict buckling behavior. However, classical theories include the effect of pre-buckling deformations and post-buckling investigations. Donnell's [1] linearized buckling as given by eq. (1.1) for thin cylindrical shell without the effect of pre-buckling and post-buckling effect is used in this study to predict the buckling load.

$$D\nabla^4(\nabla^4 w) - \nabla^4(N_{xx}w_{,xx} + 2N_{xy}w_{,xy} + N_{yy}w_{,yy}) + \frac{Et}{R^2}w_{,xxxx} = 0 \quad (1.1)$$

1.2 Effect of Imperfections on Buckling Load

Buckling strength of thin cylindrical shells is influenced by initial imperfections in the geometry of the cylindrical shell. Imperfections in shell wall can be in form of variations in loading, eccentricity in perfect shape, variations in material properties, variations in shell wall thicknesses etc. Pressure vessels are manufactured by welding rolled sheets. Due to manufacturing variations, fabricated shells differ from perfect shape and there can also be variations in shell wall thicknesses and material properties. When imperfections in shell come into picture load carrying capacity of shells is largely reduced. Koiter [2] was first to report that under compression test shells fail much before the classical buckling load was reached. Galambos (1988) and Chen and Lui (1987) also observed that load carrying capacity of shell is drastically reduced and the reason was the presence of imperfections in shells.[3]

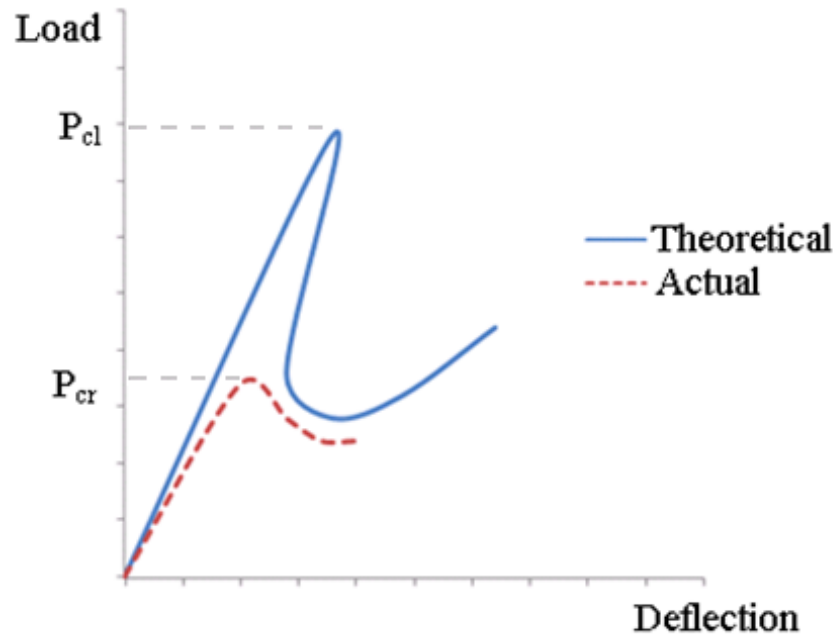


Figure 1.1: Load V/s Deflection Plot for Axially Loaded Cylindrical Shell

The effect of imperfections on load carrying capacity of cylindrical shells is shown in Fig. 1.1. Classical or theoretical buckling load (P_{cl}) as calculated from the classical theories is largely reduced due to presence of imperfections giving way to critical buckling load (P_{cr}). Non-dimensional buckling load (λ) defined in eq. (1.2) is a factor that takes into accounts the effect of imperfections and determines the critical buckling load.

$$\lambda = \frac{P_{cr}}{P_{cl}} \quad (1.2)$$

The linearized Donnell's equation as given in eq. (1.1) can also include the effect of initial imperfection (wrinkles, variations in shell wall thickness, material property etc.) for buckling load calculations.

In practice, buckling load is calculated by classical buckling theories and ASME knockdown factor as given in ASME Boiler and Pressure Vessel Code Section VIII Division 2 Rules is multiplied to classical buckling load value for including imperfection

effects. Knockdown factor is based on the experimentally determined critical buckling load values.

For calculation of buckling loads the imperfections can be treated as Axisymmetric or Asymmetric. Axisymmetric means that imperfection (or any entity) has symmetry around an axis. Symmetry can be in form of material property, loading, geometry, boundary conditions. Asymmetry refers to non symmetric behavior of an entity.

1.3 Background and Literature Review

The theory of static stability began with a paper published by Euler in 1744. Euler [4] was the first researcher to study stability of columns based on bending stress approach. Euler derived the equation for buckling of long columns by neglecting the direct stress. Considering only bending stress to calculate buckling load is one reason that Euler equation cannot be used for short columns where direct stress is considerable. Euler also included the end conditions of columns for calculating the buckling loads. Various end conditions that can be possible are one or both ends fixed or hinged, or one end free.

Some of the assumptions made in Euler's column theory are that initially the column with uniform cross-section is perfectly straight and the load applied is truly axial. Euler also assumed column material to be perfectly elastic, homogenous and isotropic, and thus obeys Hooke's law. Euler's column theory also assumed failure of column occurs due to buckling alone and the weight of the column itself is neglected.

According to Euler's theory, the crippling or buckling load, W_{cr} under various end conditions is represented by a general equation as shown in eq. (1.3):

$$W_{cr} = \frac{\pi^2 EI}{L_{eff}^2} \quad (1.3)$$

Instability of columns involves global buckling (i.e. buckling as one unit), local buckling (i.e. localized failure of compression regions) and torsional or twisting instability related to shear flow in thin walled members. Euler's column theory considers only the global buckling. Also Euler's column buckling relation shown in eq. (1.3) holds good only for long columns.

Bryan [5] developed general theory of stability based on energy criterion, which states that if potential energy in an equilibrium state is minimum than that state is said to be stable. The equations governing equilibrium state were derived by Southwell [6]. Trefftz [7] used the energy criterion and formed the stability theory from an elasticity theory for finite deformations. Kappus [8] and Biot [9] further developed the theory of elasticity for finite deformations and derived the equations for neutral equilibrium.

All the above developed theories of elasticity's involve determination of stability limit. These theories are insufficient as behavior of structure when load reaches or exceeds the stability limit (buckling or crippling load) was not considered. As load reaches crippling load there exist not only stable state but also a neighboring infinitesimally deviating equilibrium state.

Koiter [2] described that elastic behavior of structures at theoretical buckling load is characterized by neighboring equilibrium states corresponding to these loads. The discrepancy between classical buckling stress predictions and experimental buckling strengths was first shown to be predominantly caused by geometric imperfections in the shell surface by Koiter. Koiter identified that imperfections in the form of the perfect

shell buckling eigenmode would be very deleterious, and this concept was later widely adopted.

The sensitivity of the bifurcation load to geometric imperfections is, however, very dependent on the form of the imperfection, as well as the length of the shell. The peak loads are usually summarized in the form of the strength-imperfection relationship as shown in Fig. 1.2, which identifies the peak load achieved, whether this peak occurs by bifurcation into a different mode or by reaching a limit load in a mode that is already present in the geometric imperfection.[10]

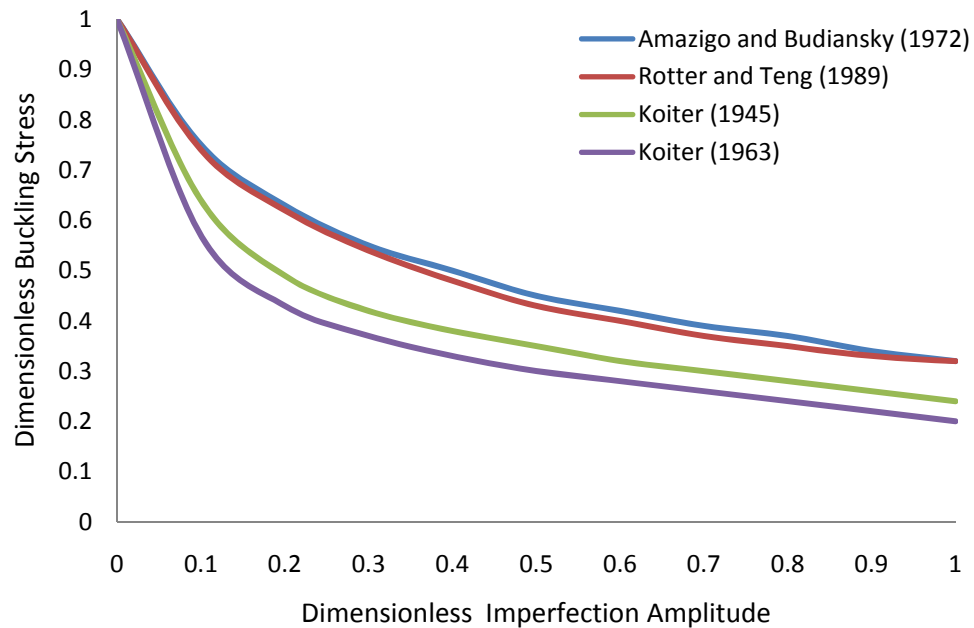


FIGURE 1.2: Sensitivity of the Bifurcation Load to the Amplitude of Axisymmetric Geometric Imperfections

Donnell and Wan [11] studied the problem of buckling in thin-walled circular cylinders under simple axial compression. The cylinders studied were long enough (more than $3/4^{\text{th}}$ of diameter) so that end conditions become unimportant and short enough (less than 10-20 times diameter) so that there is no danger of buckling of the cylinder as a tubular column. The result shows that buckling is very sensitive to imperfections or

disturbances of shape. The conclusion was that only a portion of cylindrical wall usually buckles, for which the unevenness factor may be much larger than the average for the entire wall. The effects of certain imperfections of shape were studied by large-deflection shell theory approach.

Koiter [12] discusses buckling of the symmetric configuration into a nonsymmetric form. The analysis is based on the nonlinear equations of shallow shell theory, which may be linearised for the investigation of neutral equilibrium in the symmetric configuration. Only those buckling modes are considered which are periodic in the axial direction as well as in the circumferential direction. The analysis fully confirms the predictions of the general nonlinear theory of elastic stability developed by Koiter [2].

Tennyson et. al. [13] studied the effect of axisymmetric imperfection in terms of uniformly distributed sine waves, groups of constant amplitude sine waves of varying wavelength and random distributions on the buckling behavior of circular cylindrical shells were considered. For the uniform and mixed mode distributions, it was observed that a critical axisymmetric wavelength existed that yielded a minimum buckling load for a given value of imperfection amplitude, consistent with the predictions of Koiter's extended theory.

The imperfection-sensitivity of axially compressed, long cylindrical shells with axisymmetric imperfections were analysed from statistical point of view by Roorda and Hansen [14]. Koiter's deterministic results, relating to buckling load to imperfection amplitude, are used as a nonlinear transfer function between the imperfection distribution and the critical load distribution. The failure probability of a loaded shell is investigated for various imperfection statistics.

The effects of random axisymmetric imperfections on the buckling of circular cylindrical shells under axial compression were studied by Elishakoff and Arbocz [15]. Monte Carlo technique was utilized and large numbers of shells thus created were evaluated by a deterministic analysis of buckling stress. The reliability function permits to evaluate the design stress for the whole ensemble of shells produced by a given manufacturing process, defined as the stress level for which the desired reliability is achieved.

Imbert [16] carried out a theoretical investigation of the effect of general imperfections on the buckling of a cylindrical shell under axial compression. A limit point analysis was performed to determine the buckling loads using a simplified imperfection and displacement model consisting of one axisymmetric and two asymmetric components with the same circumferential wave number. For the experimental data available the three-mode solution was found to have only a small additional effect with respect to the two-mode solution. In addition, by extrapolating imperfection coefficients for high wave numbers by means of the imperfection model, it was found that a strong interaction effect would exist between a low wave number axisymmetric mode and two classical asymmetric modes.

A correlation study between experimental buckling loads and analytical predictions based on experimentally measured initial imperfections were carried out for axially compressed isotropic and stiffened cylindrical shells by Arbocz and Babcock [17]. The amplitudes of the initial imperfections used in the analysis were calculated from the corresponding Imbert-Donnell imperfection models. The free parameters in this imperfection model were obtained by least square fitting the harmonics of the

experimentally measured initial imperfections. It was possible in all cases to achieve satisfactory correlation using only a few suitably chosen deflection and imperfection modes.

For analyzing the buckling of an axially loaded cylindrical shell, Hansen [18] considered the imperfection components corresponding to all of the classical buckling modes. The analysis represents an extension of Koiter's axisymmetric solution and in the asymptotic sense. The results obtained reveal many interesting aspects of shell buckling which arise from various imperfection forms. The buckling behavior which results is associated with both bifurcation and limit point critical stress.

Arbocz and Williams [19] presented the results of an extensive imperfection survey on a 10ft diameter integrally stiffened cylindrical shell, where modal components of the measured imperfection surface as a function of circumferential and axial wave numbers are calculated. Using fourier coefficients of the measured initial imperfections, buckling loads are calculated by solving the nonlinear Donnell type imperfect shell equations iteratively. The calculated lowest buckling load compares favorably with the values usually recommended for similar shell structures.

The effects of general nonsymmetric random imperfections on the reliability of axially compressed cylindrical shells were studied by Elishakoff and Arbocz [20]. The initial imperfection functions were simulated via a numerical procedure, and the buckling load of each realization of the simulated initial imperfections was found by the Multimode Analysis. It was shown that the results of existing Initial Imperfection data banks can be directly incorporated in the reliability analysis. Reliability based design curves for shell structures were constructed from experimental information.

The classical buckling load of a perfect shell under axial load can be calculated by eq. (1.4) as given by Fung and Sechler [21] and Amazigo and Budiansky [22]. The assumption for eq. (1.4) to hold true is that cylindrical shell; with perfect elasticity, perfect initial shape and uniform wall thickness, is under compressive load fixed in axial direction and load is uniformly distributed along the circumference.

$$P_{cl} = \frac{E}{\sqrt{3(1-\mu^2)}} \frac{t^2}{R} \quad (1.4)$$

According to Roark's formulae [23] classical buckling load for a cylindrical shell subjected to external pressure can be calculated as shown in eq. (1.5).

$$P_{cl} = 0.8 \frac{Et^2}{LR} \sqrt[4]{\left(\frac{1}{1-\mu^2}\right)^3 \frac{t^2}{R^2}} \quad (1.5)$$

Although research has been carried out on effect of imperfections on the buckling load from as early as last century, but ASME knockdown factor is still used for calculating the buckling loads. ASME knockdown empirical relations have been developed from the experimental testing of shells. Also there is a need to develop a method for calculating buckling loads when shells are used as pressure vessels and are subjected to external pressure or vacuum.

Two broad variations on how this analytical work is different from the previous work are: firstly the buckling load calculations of shell subjected to axial compressive load is carried out on the random shell wall thickness values generated, and secondly the analysis has been extended to shell under vacuum. While the analysis of axial loading of shells is important from the structural point of view, shells in vacuum have always been a consideration when shells are used in pressure vessels.

1.4 Scope and Objectives

The study aims to evaluate and verify the non-dimensional buckling load values provided by ASME Boiler and Pressure Vessels Code Section VIII Division 2 for designing the cylindrical pressure vessels subjected to axial loading and also when it is subjected to external pressure. Generally, ASME Code is used to determine the load carrying capacity of cylindrical vessel. This study also evaluates that if these pressure vessels are manufactured as per the ASME defined manufacturing tolerances, the empirical relations for calculating the Non-dimensional buckling load holds or not.

The objective of this dissertation is to verify the empirical formulae laid out in ASME code and to see the validity of the ASME Code if the shells are manufactured according to the ASME defined manufacturing tolerances. Through this study an attempt has been made to unwind the theory behind calculation of non-dimensional buckling loads. Most of the work done in this field so far has been based on one measured data of imperfections in the shell and when it is subjected to compressive loading. An attempt has been made in this study to generate a random data of imperfections within the tolerance limits and then use a stochastic technique to calculate the buckling loads.

1.5 Outline of Analytical Research

This dissertation has been divided into seven chapters. Chapter II starts with the description of Flue Gas Desulphurization (FGD) vessel which is used as example for carrying out this Dissertation. Monte Carlo method is laid out and the first step of simulating the thicknesses of the cylindrical shells is carried out in Chapter II. Chapter III presents the analysis of the simulated shells under axial load assuming thickness variations to be axisymmetric. Imperfections that are in the form of thickness variations

in simulated shells are represented in form of Fourier series. Buckling loads are then calculated by using Koiter theory. Asymmetric analysis of simulated shells is carried out in Chapter IV. Thickness imperfections in the shells are represented by Double Fourier series. Multimode analysis is used for calculating the buckling load for the shell. Results are also compared with Koiter's special theory.

Further, buckling strength of the cylindrical shell is also studied when it is subjected to external pressure. Effect of imperfections on the buckling load when cylinder is subjected to external pressure is carried out in Chapter V. Again, Multimode analysis is used for calculating the buckling loads. Chapter VI covers the discussion part. Buckling load values and probability curves from different methods are discussed in this chapter. Finally, conclusions and recommendations for future research are presented in Chapter VII.

CHAPTER 2: MONTE CARLO SIMULATION OF CYLINDRICAL SHELLS

2.1 Introduction

For determining critical buckling loads in pressure vessels, under different loading conditions, numbers of cylindrical shells having variations in shell wall thickness are required. This chapter lays out the methodology for simulation of cylindrical shells similar to the known problem example (i.e. FGD Vessel). Monte Carlo simulation technique is used as it provides flexibility and can include number of sources of uncertainty. Next the dimensions and details of FGD vessel are laid out. Shell wall thickness values of fifty cylinders are generated by Monte Carlo simulation technique that requires the use of random number generator. Random number generator used for simulating thicknesses of shells generates the numbers that follow uniform distribution. Generated shells are then compared with the actual thicknesses of FGD vessel to check the significance of simulated shell wall thicknesses. Cylindrical shells thus generated by using MathCAD code will be used in next chapters for calculation of buckling loads when shells are subjected to axial and lateral loads.

2.2 Monte Carlo Method

Monte Carlo method was invented by Stanislaw Ulam, a Polish born mathematician, in 1946 while he was determining the probabilities of winning in a card game of solitaire. The Monte Carlo method provides approximate solutions for many mathematical problems by generating random numbers and calculating what fraction of the numbers

obey some property or properties. Monte Carlo method is useful for examining numerical solutions to problems which are too complex to solve.

Nicholas Metropolis and Stanislaw Ulam [24] presented motivation and a general description of Monte Carlo method dealing with a class of problems in mathematical physics. Monte Carlo method is, essentially, a statistical approach to the study of differential equations, or more generally, of integro-differential equations that occur in various branches of the natural sciences.

In general Monte Carlo method can be performed by carrying out the following steps:-

- Define a domain of possible inputs.
- Generate inputs randomly from the domain and perform deterministic computation on them.
- Aggregate the results.

For analyzing the cylindrical shells the general Monte Carlo steps are modified as given below:-

- Domain of possible inputs – Varies from minimum to maximum allowable shell wall thickness of FGD vessel as per the manufacturing tolerance laid out in ASME B&PV Code Section VIII Division 1 (i.e. $3/8^{\text{th}}$ of an Inch. - $1/32$ of an Inch. (Manufacturing Tolerance)).
- Random Number Generator – MathCAD Code using runif command was used to generate random numbers within the domain and Multimode Analysis is used to analyze these generated random numbers.

- Reliability Function – To aggregate the results reliability function is plotted in order to calculate the buckling load.

2.3 FGD Vessel

The flue gas desulphurization (FGD) “vessel” is a large hybrid tank-vessel-stack assembly in a major Canadian refinery. The function of the FGD vessel is to contain and support a proprietary process that utilizes an ammonium sulphate scrubbing system to produce environmentally friendly air emissions. Waste ammonia is employed to scrub the air emissions, which eventually are discharged through a 6.1 m. diameter stack that extends approximately 94.2 m. above ground level. Within the hybrid FGD vessel and its associated components, slurry is processed from the scrubber whereby the final by-product of the process is a granular ammonium sulphate [25].

The overall absorber/stack assembly is shown in Fig. 2.1. Due to the vessel height of approximately 94.2 m., it is readily apparent that column-type instability must be considered in the design of the vessel. The FGD absorber/stack assembly is utilized in a petroleum refinery installation and is comprised of three major structural and geometric sections. The bottom section resembles (in many respects) an API Standard 650 storage tank [26] with its 21.3 m. diameter thin wall cylindrical construction as discussed by Williams [27]. The maximum internal design pressure of approximately 255 kPa in the storage tank portion is primarily attributed to the linearly varying hydrostatic load within the tank. The middle section of the FGD absorber/stack is comprised of both cylindrical and conical pressure vessels that are subjected to pressures ranging from -1.86 to 3.72 kPa. These intermediate sections are designed in accordance with the ASME Boiler and Pressure Vessel Code, Section VIII, Division 2 [28]. The third and upper most section is

comprised of multiple ring-stiffened sections of decreasing wall thicknesses as a function of elevation and resembles an ASME STS-1 stack [29]. Because the height of the FGD absorber/stack exceeds 91.4 m. in combination with tank diameters of approximately 21.3 m., wind loads, self-weight, and platform loads become a significant consideration in the design of the entire assembly. The aforementioned dead and live loads create both tensile and compressive stresses that must be combined with the stresses associated with both positive and negative internal pressures along the length of the hybrid FGD absorber/stack [30]. The compressive stresses in the tall, slender portion of the FGD (i.e., the stack) are the most obvious motivating forces for considering a buckling type failure.

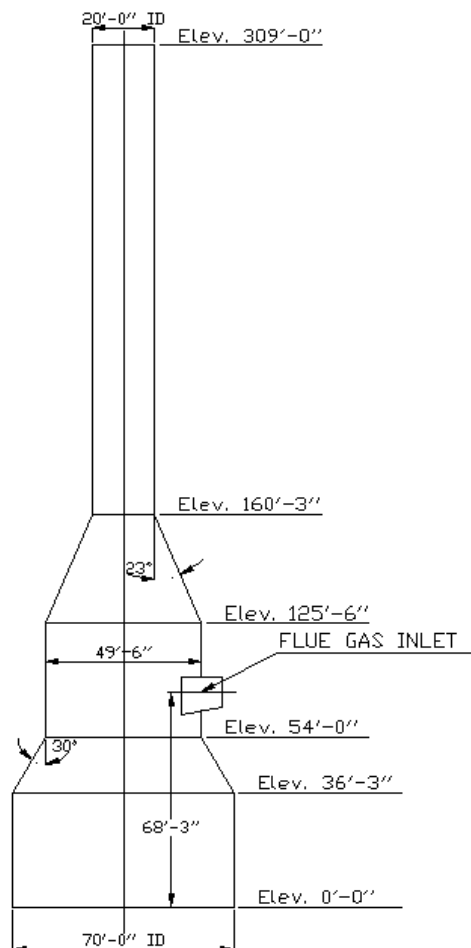


FIGURE 2.1: FGD Vessel/Stack

The cylindrical shell under study is the lower portion of stack of FGD vessel. FGD vessel stack has internal diameter of 6.1m, height of 45.339m and wall thickness of 9.525mm (0.375in.). The various dimensions and properties of FGD stack are shown in Table 2.1.

TABLE 2.1: Technical Specifications of FGD Stack Shell

Property	Value
Shell Wall Thickness, t	3/8 in.
Length of Stack, L	312 in.
Internal Radius of Shell, R	120 in.
Young's Modulus, E	3×10^7 psi
Poisson's Ratio, μ	0.31

Initial imperfections in FGD stack is in the form of wall thickness variations. Table 2.2 below shows the shell wall thickness values of the FGD stack.

TABLE 2.2: Shell Wall Thickness (in.) of FGD Stack Shell

$\theta \backslash L(\text{in.})$	13	39	65	91	117	143	169	195	221	247	273	299
0	0.360	0.358	0.363	0.382	0.357	0.366	0.355	0.375	0.379	0.371	0.365	0.376
30	0.381	0.374	0.370	0.373	0.386	0.368	0.362	0.374	0.371	0.378	0.374	0.359
60	0.373	0.371	0.387	0.357	0.366	0.376	0.357	0.369	0.376	0.381	0.366	0.376
90	0.363	0.371	0.373	0.371	0.363	0.368	0.374	0.346	0.349	0.371	0.363	0.360
120	0.375	0.359	0.377	0.359	0.367	0.353	0.375	0.373	0.382	0.355	0.365	0.358
150	0.373	0.373	0.374	0.367	0.368	0.367	0.381	0.361	0.360	0.381	0.365	0.351
180	0.352	0.362	0.362	0.376	0.362	0.379	0.377	0.361	0.377	0.365	0.374	0.367
210	0.364	0.371	0.385	0.373	0.376	0.372	0.369	0.378	0.378	0.376	0.370	0.351
240	0.372	0.375	0.377	0.365	0.354	0.379	0.376	0.362	0.366	0.359	0.373	0.366
270	0.376	0.369	0.372	0.364	0.365	0.376	0.361	0.376	0.345	0.372	0.380	0.360
300	0.373	0.368	0.380	0.361	0.364	0.368	0.361	0.372	0.369	0.358	0.367	0.364
330	0.365	0.368	0.361	0.355	0.375	0.366	0.370	0.373	0.363	0.374	0.357	0.360

Flue Gas Desulphurization (FGD) Vessel has been taken as an example in this study as vessel is subjected to elastic instability due to wind loads and self weight creating both

tensile and compressive stresses. Lower part of the FGD vessel has been taken for analysis as this part has maximum loading from the above structure, so making it critical. Also the shell wall thickness values of lower part of FGD stack were available, which gave us opportunity to check the simulated wall thickness values.

2.4 Simulation of Cylinders

An initial imperfection in FGD vessel is in the form of shell wall thickness variations. For calculation of buckling loads, 50 cylindrical shells (GB1-GB50) were simulated using MathCAD code. The code uses linear congruence method for generation of random numbers. As per the ASME Boiler and Pressure Vessel Code Section VIII Division 1 Rules [28], “The reduction in thickness shall not exceed $1/32$ in. (1mm) or 10% of the nominal thickness of the adjoining surface, whichever is less”. Therefore, shell wall thickness can vary from 0.344 in. to 0.375 in. Total 144 readings were generated for each shell, 12 readings axially and 12 circumferentially at each elevation. Table A.1 to Table A.50 in APPENDIX A gives generated shell wall thickness values for 50 GB shells.

Shell wall thickness values thus generated represent asymmetric imperfection and can be converted into axisymmetric imperfections by taking arithmetic mean of all values at a particular elevation. Fourier cosine series will be used to represent the shell wall thickness variation in GB shells for axisymmetric analysis. Double Fourier series will be used to represent the asymmetric part of the wall variations.

Fig. 2.2 shows the asymmetric variations in shell wall thickness for GB8 shell. Asymmetric data can be transformed into axisymmetric form and is shown in Fig. 2.3.

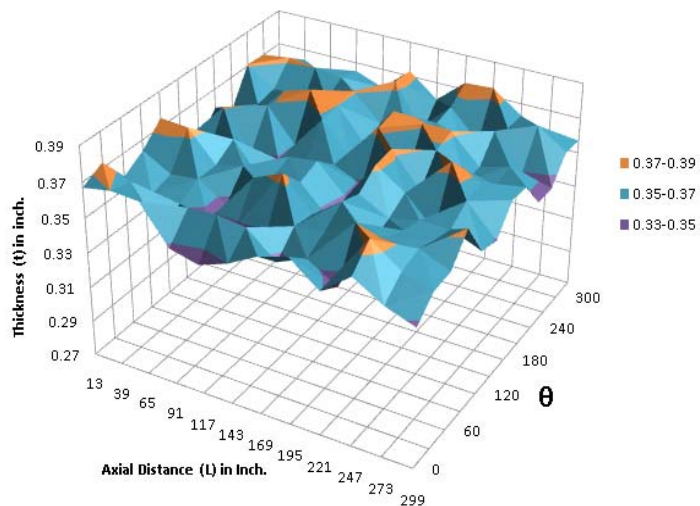


FIGURE 2.2: Asymmetric Variation of Shell Wall Thickness for GB8 Shell

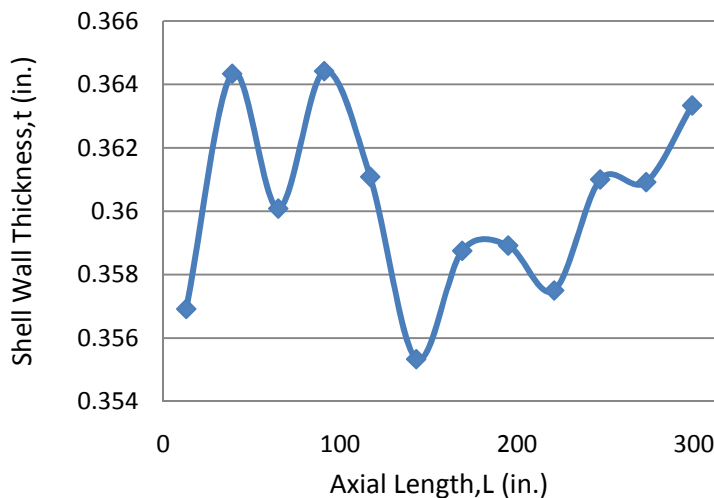


FIGURE 2.3: Axisymmetric Variation of Shell Wall Thickness for GB8 Shell

2.5 Test of Significance

In order to confirm that simulated shells agree to the actual thickness values of FGD vessel, a test of significance is required. Chi-square (X^2) test was performed on 50 simulated GB shells. Chi-square is a statistical test in which data from two sources can be confirmed for dependence. The primary purpose of Chi-square test is to compare some

observed values to the expected values. The hypothesis is that whether the two values, simulated values and actual values of the shell wall thickness, are independent or not. Eq. (2.1) gives the formulae for calculating chi-square values.

$$X^2 = \frac{(Observed-Expected)^2}{Expected} \quad (2.1)$$

Table 2.3 below shows the calculated values of Chi-square for 50 GB shells. The observed values are the simulated shell wall thickness values and expected values are actual shell wall thickness values of FGD vessel.

TABLE 2.3: Chi-square Values of 50 Simulated GB Shells

GB Shell	X ²	GB Shell	X ²
1	0.086047	26	0.080492
2	0.103374	27	0.100526
3	0.077122	28	0.092959
4	0.084597	29	0.085310
5	0.087396	30	0.078433
6	0.100768	31	0.099195
7	0.074817	32	0.093571
8	0.090447	33	0.087313
9	0.097611	34	0.085892
10	0.094665	35	0.087560
11	0.094213	36	0.095190
12	0.089677	37	0.085603
13	0.085851	38	0.090093
14	0.086000	39	0.080526
15	0.058150	40	0.082524
16	0.093256	41	0.073814
17	0.087609	42	0.100694
18	0.081147	43	0.081849
19	0.076015	44	0.080976
20	0.084279	45	0.089812
21	0.086502	46	0.090257
22	0.077483	47	0.088338
23	0.100936	48	0.095117
24	0.078848	49	0.088555
25	0.088142	50	0.078080

To summarize, a plot between Chi-square value and GB shell is shown in Fig. 2.4.

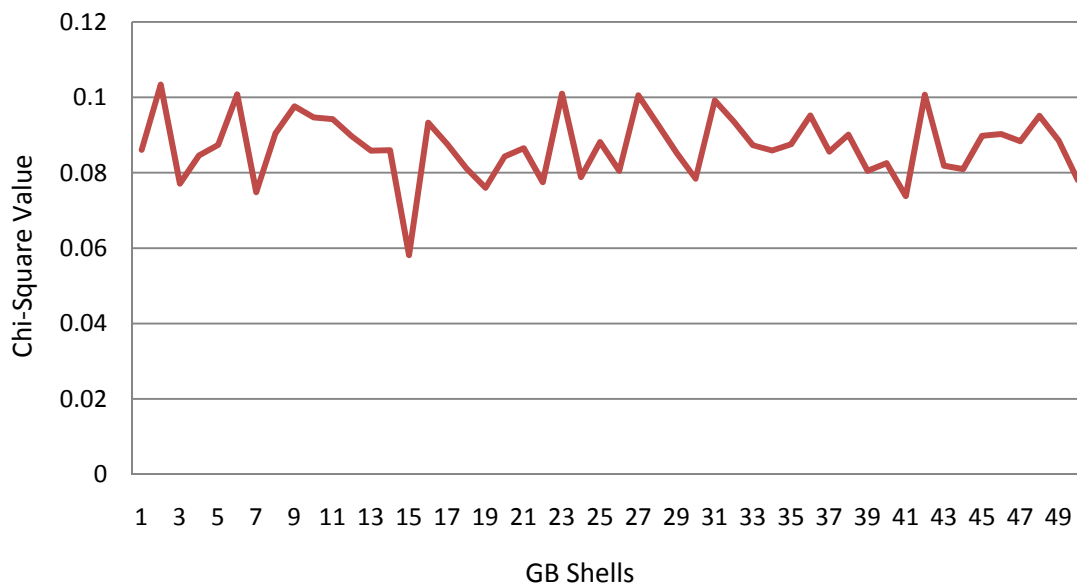


FIGURE 2.4: Chi-square (X^2) Values for 50 Simulated GB Shells

The maximum value of Chi-square comes out to be that of GB2 Shell i.e. 0.103374. The value of probability, taking level of significance of 1% and degree of freedom to be 143, comes out to be 0.9999. This means that there is 99.99% chance that actual data of FGD shell wall thickness can be simulated.

2.6 Summary

In this chapter, shell wall thicknesses for 50 shells named as GB1 to GB50 were simulated using random number generator (runif command) in MathCAD code. The runif command takes total number of random numbers to be generated, maximum and minimum values and generates random numbers that follow normal distribution. The shell wall thicknesses generated were checked against the actual wall thicknesses of FGD

vessel by Chi-square test. Chi-square test shows that there is 99.9% probability of generating the actual FGD shell wall thickness values.

GB shells generated with shell wall thickness variations in this Chapter will be analyzed to calculate the non-dimensional buckling load values in proceeding Chapters. In Chapter III, axisymmetric analysis of GB shells subjected to axial load is carried out by representing shell wall thickness variations as cosine Fourier series. Chapter IV gives asymmetric analysis for calculation of buckling loads due to axial loading of GB shells, when thickness variations are represented as a double Fourier series. Simulated GB shells are analyzed under vacuum in Chapter V.

CHAPTER 3: AXISYMMETRIC ANALYSIS OF AXIAL END LOAD ON CYLINDRICAL SHELL

3.1 Introduction

It is known that presence of geometric imperfections reduces the load carrying capacity of cylindrical shells when subjected to axial end load. In this Chapter, non-dimensional buckling load is calculated for GB shells simulated by Monte Carlo technique in the last chapter. The simulated GB shells contain imperfections in the form of variations in shell wall thickness. Shell wall thickness varies in simulated GB shells in axial direction as well as in circumferential direction. Imperfections in this Chapter are treated to be axisymmetric i.e. varying in only axial direction. Cosine Fourier series is used to represent this axisymmetric imperfection. Non-linear transfer function as proposed by Koiter is used for calculating the buckling loads. Results obtained will then be compared to non-dimensional buckling load values obtained by Koiter's special theory.

3.2 Theory

Solution of thin cylindrical shell containing axisymmetric thickness variations while subjected to an axial end load, the reliability approach employs the simulation of number of shells using Monte Carlo technique, calculation of buckling loads using Koiter's special theory [12], and calculation of non-dimensional buckling load (λ) based on reliability function. Similar to the method described by Elishakoff et al. [31], any initial

imperfection can be represented by series of cosines and sines. A review of the previously defined work [31] indicated numerous errors in the formulations and figures as published in the open literature, thereby creating the necessity to revisit the bases for the results as described by the authors. With this in mind, as given by Elishakoff and Arbocz [20] and Arbocz and Williams [19], the initial imperfection function $W_n(\xi, \theta)$ can be represented as shown in eq. (3.1):

$$W_n(\xi, \theta) = \sum_{i=0}^{N_1} a_i \cos(i\pi\xi) + \sum_{k=1}^{N_2} \sum_{l=1}^{N_3} \left[b_{kl} \sin(k\pi\xi) \cos(l\theta) + c_{kl} \sin(k\pi\xi) \sin(l\theta) \right] \quad (3.1)$$

The chosen coordinate system for the cylindrical shell utilizes axial (x) and circumferential (y) coordinates. In addition, a_i , b_{kl} and c_{kl} are Fourier coefficients of the respective terms. Eq. (3.2) gives the relation of non-dimensional numbers ξ and θ with the axial and circumferential coordinates.

$$\begin{aligned} \xi &= \frac{x}{L}, 0 \leq x \leq L \\ \theta &= \frac{y}{R}, 0 \leq \theta \leq 2\pi \end{aligned} \quad (3.2)$$

The length and radius of the cylindrical shell are represented by L and R . The first half range cosine series summation term in eq. (3.1) denotes the axisymmetric part of imperfection and second half range sine series summation term denotes the non-symmetric part. As in this chapter only axisymmetric imperfections are to be dealt with eq. (3.1) reduces to eq. (3.3):

$$W_n(x) = \sum_{i=0}^L a_i \cos\left(\frac{i\pi x}{L}\right) \quad (3.3)$$

The mean of the Fourier coefficients of N simulated shells is determined by eq. (3.4):

$$A_i^{(e)} = \frac{1}{N} \sum_{m=1}^N a_i^{(m)} \quad (3.4)$$

The elements of variance-covariance matrix are calculated by eq. (3.5):

$$\sigma_{ij} = \frac{1}{N-1} \sum_{m=1}^N (a_i^{(m)} - A_i^{(e)}) (a_j^{(m)} - A_j^{(e)}) \quad (3.5)$$

The simulation process should be checked by the auto-covariance function of the simulated N shells. The auto-covariance function $R_{w_0}(x_1, x_2)$ is then given by eq. (3.6) and has to be compared to the auto-covariance function of the initial sample. The auto-covariance function gives a measure of linear association between two variables of the same process. The prefix ‘auto’ means a reflexive act on oneself, and thus auto-covariance is the covariance that the process has with itself.

$$R_{w_0}(x_1, x_2) = \sum_i \sum_j \sigma_{ij} \cos\left(\frac{i\pi x_1}{L}\right) \cos\left(\frac{j\pi x_2}{L}\right) \quad (3.6)$$

Once the auto-covariance function of the simulated shells agrees with the actual shell and variance-covariance matrix has been investigated to be dominated by lower order buckling modes, the next step is to calculate buckling load for each simulated shell. Consider the initial imperfection in shell wall thickness of the form shown in eq. (3.7):

$$w_0(x) = t \xi_i \cos\left(\frac{i\pi x}{L}\right) \quad (3.7)$$

In eq. (3.7), ξ_i is the magnitude of the imperfection as a fractional value of the shell wall thickness. Ingeter, i represent the number of half waves in axial direction. For calculating the buckling load, assume buckling mode as shown in eq. (3.8), where k

represent number of half waves in axial direction and l represents number of full waves in circumferential direction.

$$w(x, y) = tb_{kl} \sin\left(\frac{k\pi x}{L}\right) \cos\left(\frac{ly}{R}\right) \quad (3.8)$$

The non-linear transfer function as shown in eq. (3.9) is then solved for various values of i and l to reach the buckling load value. The trick for solving eq. (3.9) is that l should be an integer, i should be an even integer and ξ_i must be negative. Eq. (3.9) is then solved for non-dimensional buckling load (λ) for each value of i and l . The minimum value of non-dimensional buckling load is the critical buckling load for that shell.

The terms in eq. (3.9) are defined in eq. (3.10). The critical buckling loads for N simulated shells can be represented in a reliability v/s non-dimensional buckling load plot and critical non-dimensional buckling load at desired reliability can be calculated as given in Elishakoff [32]. Also, absolute difference between calculated value and theoretical value can be calculated according to Kolmogorov-Smirnov test of goodness of fit as given by Massey [33].

$$\begin{aligned} & (\lambda_{ci} - \lambda)^2 (\lambda_{cki} - \lambda) + \\ & (\lambda_{ci} + \lambda) \left(\frac{c\beta_l^2}{2\alpha_k^2} \right) \left[\lambda + \frac{8\lambda_{ci}\alpha_k^4}{(\alpha_k^2 + \beta_l^2)^2} \right] \xi_i \delta_{ij} + \\ & 8c^2 \alpha_k^2 \beta_l^4 \left[\frac{1}{(9\alpha_k^2 + \beta_l^2)^2} + \frac{1}{(\alpha_k^2 + \beta_l^2)^2} \right] \lambda_{ci}^2 \xi_i^2 = 0 \end{aligned} \quad (3.9)$$

where,

$$\begin{aligned}
 \lambda_{ci} &= \frac{1}{2} \left(\alpha_i^2 + \frac{1}{\alpha_i^2} \right) \\
 \lambda_{cki} &= \frac{1}{2} \left[\frac{(\alpha_k^2 + \beta_k^2)^2}{\alpha_k^2} + \frac{\alpha_k^2}{(\alpha_k^2 + \beta_i^2)^2} \right] \\
 \alpha_i^2 &= i^2 \frac{Rt}{2c} \left(\frac{\pi}{L} \right)^2 \\
 \alpha_k^2 &= k^2 \frac{Rt}{2c} \left(\frac{\pi}{L} \right)^2 \\
 \beta_i^2 &= l^2 \frac{Rt}{2c} \left(\frac{1}{R} \right)^2 \\
 \beta_k^2 &= k^2 \frac{Rt}{2c} \left(\frac{1}{R} \right)^2 \\
 \delta_{ij} &= \text{Kronec ker delta}, j = 2k \\
 c &= \sqrt{3(1 - \mu)^2} \tag{3.10}
 \end{aligned}$$

3.3 Test of Simulated Cylindrical Shells

For calculation of buckling load, 50 cylindrical shells (GB1-GB50) were simulated using MathCAD code as listed in Table A.1 to Table A.50 in APPENDIX A.

The initial axisymmetric imperfections are represented by eq. (3.3) and Fourier coefficients were calculated. Table B.1 in APPENDIX B shows first eleven Fourier coefficients for GB Shells. Then sample mean was calculated using eq. (3.4) and are listed in Table B.1 in APPENDIX B. The elements of variance-covariance matrix were calculated using eq. (3.5) and are shown in Table C.1 in APPENDIX C. For 25 GB Shells variance-covariance matrix comes out to be matrix of 25X25. As can be seen from the matrix the maximum peaks are at the diagonal elements and as one moves away from the

diagonal elements the peaks vanishes, therefore the simulated shells do not follow classical axisymmetric buckling mode.

The auto-covariance function which gives the measure of linear association between two variables was calculated by eq. (3.6) using MathCAD code. Fig. 3.1 shows the auto-covariance function for GB Shells. The plot is non-uniform and thus concludes that the initial imperfections of GB shells make up non-homogenous random fields.

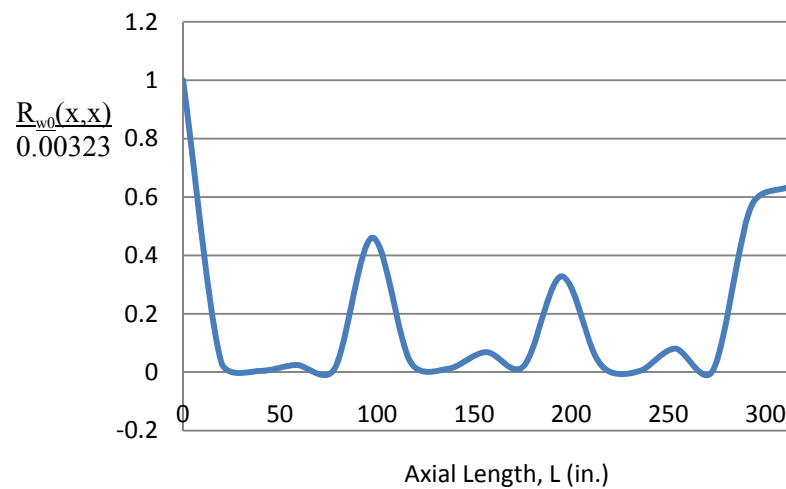


FIGURE 3.1: Auto-covariance Function for GB Shells

3.4 Calculation of Predicted Minimum Buckling Loads

Buckling loads for 50 GB Shells were calculated using eq. (3.9) by MathCAD code. A column plot showing number of buckled shells for specific values of non-dimensional buckling load (λ) are shown in Fig. 3.2. This plot will be used for calculating the reliability function from which experimental value of non-dimensional buckling load can be calculated.

Fig. 3.3 shows the reliability function for 50 GB Shells. The value of non-dimensional buckling load (λ) can be calculated at any desired reliability from this curve.

If the desired reliability is 0.95, then the non-dimensional buckling load (λ) comes to be 0.880. Depending on the sample size, there is difference in obtained value and theoretical value. From Table 1 of Massey [33] it can be concluded that for 50 sample sizes and 0.05 level of significance, absolute difference between calculated and theoretical value is 0.19. So, the value of non-dimensional buckling load (λ) comes to be (0.880-0.19) that is 0.690.

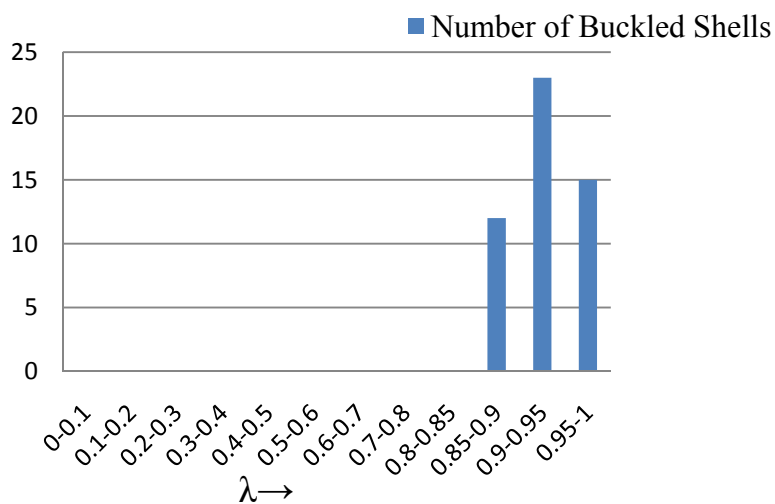


FIGURE 3.2: Non-dimensional Buckling Loads for 50 GB Shells (Axisymmetric Fourier Analysis)

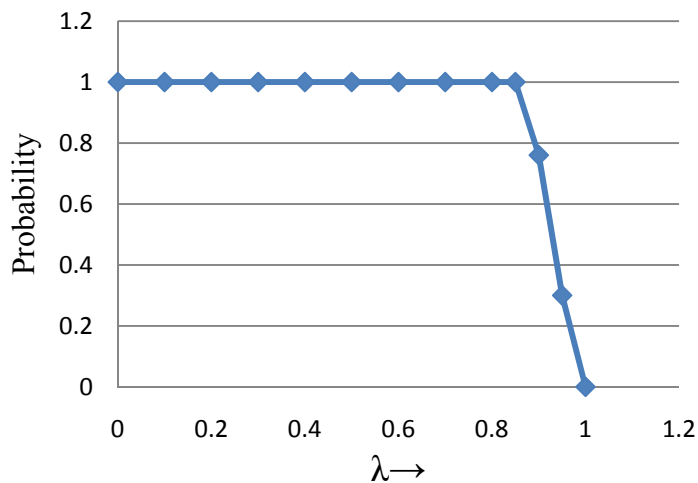


FIGURE 3.3: Calculated Reliability Function V/S Non-dimensional Buckling Load (Axisymmetric Fourier Analysis)

3.5 Predicted Buckling Loads by Koiter's Theory

Buckling loads can also be calculated for FGD vessel by Koiter method as illustrated in Koiter [12]. Koiter derived a second order quadratic equation for determining λ considering nonlinear equations of shallow shell theory, which may be linearized for the investigation of neutral equilibrium in the symmetric configuration. Koiter considered only those buckling modes which are periodic in the axial direction as well as in the circumferential direction.

$$2(1 - \lambda)^2 - 3c\xi\lambda = 0 \quad (3.11)$$

Buckling loads for 50 GB Shells were calculated by finding the eigenvalues of the eq. (3.11) and values are shown in Table D.1 in APPENDIX D and summarized in Fig. 3.4 shown below. Furthermore, the reliability function of 50 GB Shells is shown in Fig. 3.5.

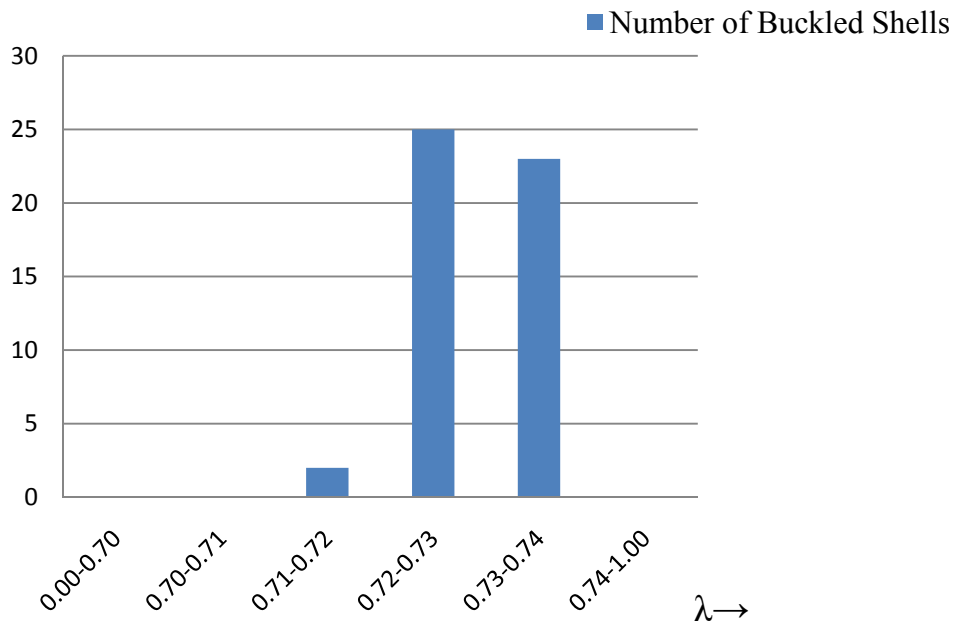


FIGURE 3.4: Non-dimensional Buckling Loads for 50 GB Shells (Koiter Axisymmetric Theory)

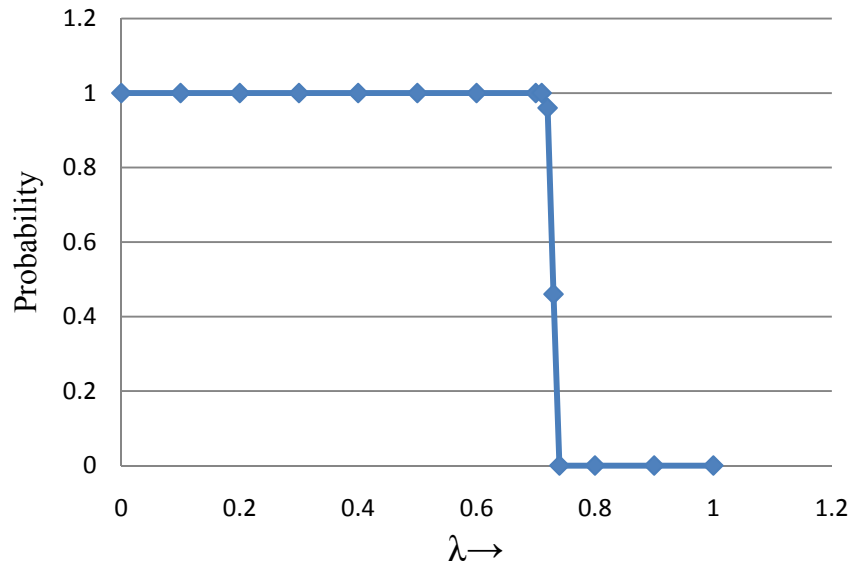


FIGURE 3.5: Calculated Reliability Function V/S Non-dimensional Buckling Load (Koiter Axisymmetric Theory)

3.6 Summary

Analysis of GB shells subjected to axial compressive end load considering shell wall thickness variations to be axisymmetric was carried out in this Chapter. Thickness variations were represented by coefficients of cosine Fourier series. Fourier coefficients associated with the imperfections were determined and variance-covariance matrix and auto-covariance function were determined to check the similarities between the simulated GB Shells. Reliability function curves are drawn by non-linear transfer function and Koiter's special theory techniques. Results obtained will be compared to ASME Boiler and Pressure Vessel Section VIII Division 2 Rules in Chapter VI. The load carrying capacity of the shell is reduced by 12% by Fourier series technique due to the presence of variations in shell wall thickness. Axial load reduces by 29% according to Koiter's special theory. Analysis is further extended in next Chapter to asymmetric form, which considers shell wall thickness variations in both axial and circumferential direction.

CHAPTER 4: ASYMMETRIC ANALYSIS OF AXIAL END LOAD ON CYLINDRICAL SHELL

4.1 Introduction

Reduction of buckling load for axial end load cylindrical shell having axisymmetric imperfections was studied in last Chapter. It was observed that load carrying capacity of GB shells reduced by 12% due to axisymmetric variations in shell wall thickness of simulated GB shells. In order to get clearer picture of effect of variations in shell wall thickness on load carrying capacity of GB shells detailed analysis considering variations to be asymmetric needs to be carried out. In this Chapter, non-dimensional buckling load is calculated for GB shells simulated by Monte Carlo technique considering imperfections to be asymmetric. Shell wall thickness is considered to vary in simulated GB shells in axial direction as well as in circumferential direction. Double Fourier series is used to represent this asymmetric imperfection. Multi-mode analysis is used for calculation of non-dimensional buckling loads. Results obtained will then be compared to non-dimensional buckling load values obtained by Koiter's special theory. Reliability function curves are drawn so that buckling load values can be calculated at any desired level of confidence.

4.2 Theory

The reliability approach for analysis of thin cylindrical shells, containing small asymmetric thickness variations while subjected to an axial end load, employs the

simulation of number of shells using Monte Carlo technique, calculation of buckling loads using Multimode analysis, and calculation of non-dimensional buckling load (λ) based on reliability function. Similar to the method described by Elishakoff et al. [31], any initial imperfection can be represented by series of cosines and sines. The initial imperfection function $W_n(\xi, \theta)$ can be represented as shown in eq. (3.1) and again shown below as eq. (4.1) as given by Elishakoff and Arbocz [20] and Arbocz and Williams [19]:

$$W_n(\xi, \theta) = \sum_{i=0}^{N_1} a_i \cos(i\pi\xi) + \sum_{k=1}^{N_2} \sum_{l=1}^{N_3} \left[\begin{array}{l} b_{kl} \sin(k\pi\xi) \cos(l\theta) \\ + c_{kl} \sin(k\pi\xi) \sin(l\theta) \end{array} \right] \quad (4.1)$$

The first summation term in eq. (4.1) denotes the axisymmetric part of imperfection and second double summation term denotes the non-symmetric or asymmetric part. Equation (4.1) can also be written in a more simplified way as shown in eq. (4.2):

$$W_0(\xi, \theta) = \sum_{i=1}^{N_1} A_i \cos(i\pi\xi) + \sum_{r=1}^N \left[\begin{array}{l} C_r \sin(k_r\pi\xi) \cos(l_r\theta) \\ + D_r \sin(k_r\pi\xi) \sin(l_r\theta) \end{array} \right] \quad (4.2)$$

The index, r is selected so that eq. (4.1) can be represented by eq. (4.2) and also $N = N_2 \times N_3$. The means of the Fourier coefficients of N simulated shells is determined by eq. (4.3):

$$\begin{aligned} K_{A_i A_j}^{(e)} &= \frac{1}{N-1} \sum_{m=1}^N (A_i^{(m)} - A_i^{(e)}) (A_j^{(m)} - A_j^{(e)}) \\ K_{C_r C_s}^{(e)} &= \frac{1}{N-1} \sum_{m=1}^N (C_r^{(m)} - C_r^{(e)}) (C_s^{(m)} - C_s^{(e)}) \end{aligned} \quad (4.3)$$

where,

$$\begin{aligned} A_i^{(e)} &= \frac{1}{N} \sum_{m=1}^N a_i^{(m)} \\ C_r^{(e)} &= \frac{1}{N} \sum_{m=1}^N c_r^{(m)} \end{aligned} \quad (4.4)$$

The elements of variance-covariance matrix are calculated by eq. (4.5):

$$\begin{aligned} \sigma_A^2(\xi) &= \sum_{i=0}^{N_1} \sum_{j=0}^{N_1} K_{A_i A_j} \delta_{ij} \cos(\pi i \xi) \cos(\pi j \xi) \\ \sigma_C^2(\xi, \theta) &= \sum_{r=1}^N \sum_{s=1}^N \begin{bmatrix} K_{C_r C_s} \sin(k_r \pi \xi) \sin(k_s \pi \xi) \\ \cos(l_r \theta) \cos(l_s \theta) \end{bmatrix} \\ \sigma_D^2(\xi, \theta) &= \sum_{r=1}^N \sum_{s=1}^N \begin{bmatrix} K_{D_r D_s} \sin(k_r \pi \xi) \sin(k_s \pi \xi) \\ \cos(l_r \theta) \cos(l_s \theta) \end{bmatrix} \end{aligned} \quad (4.5)$$

The simulation process should be checked by the auto-covariance function of the simulated N shells. The auto-covariance function $C_{w0}(\xi_1, \theta_1, \xi_2, \theta_2)$ is then calculated by eq. (4.6) and has to be compared to the auto-covariance function of the initial sample. The auto-covariance function gives a measure of linear association between two variables of the same process.

Once the auto-covariance function of the simulated shells agrees with the actual shell and variance-covariance matrix has been investigated, the next step is to calculate buckling load for each simulated shell using multi-mode analysis [17].

$$\begin{aligned}
C_{w_0}(\xi_1, \theta_1; \xi_2, \theta_2) &= \sum_{i=0}^{N_1} \sum_{j=0}^{N_1} K_{A_i A_j} \cos(i\pi\xi_1) \cos(j\pi\xi_2) \\
&+ \sum_{i=0}^{N_1} \sum_{s=1}^N K_{A_i C_s} \cos(i\pi\xi_1) \sin(k_s \pi\xi_2) \cos(l_s \theta_2) \\
&+ \sum_{i=0}^{N_1} \sum_{s=0}^N K_{A_i D_s} \cos(i\pi\xi_1) \sin(k_s \pi\xi_2) \sin(l_s \theta_2) \\
&+ \sum_{r=1}^N \sum_{j=0}^{N_1} K_{C_r A_j} \sin(k_r \pi\xi_1) \cos(j\pi\xi_2) \cos(l_r \theta_1) \\
&+ \sum_{r=1}^N \sum_{j=0}^{N_1} K_{D_r A_j} \sin(k_r \pi\xi_1) \cos(j\pi\xi_2) \sin(l_r \theta_1) \\
&+ \sum_{r=1}^N \sum_{s=1}^N K_{C_r C_s} \sin(k_r \pi\xi_1) \cos(l_s \theta_2) \sin(k_s \pi\xi_2) \cos(l_r \theta_1) \\
&+ \sum_{r=1}^N \sum_{s=1}^N K_{C_r D_s} \sin(k_r \pi\xi_1) \cos(l_r \theta_1) \sin(k_s \pi\xi_2) \sin(l_s \theta_2) \\
&+ \sum_{r=1}^N \sum_{s=1}^N K_{D_r C_s} \sin(k_r \pi\xi_1) \sin(l_r \theta_1) \sin(k_s \pi\xi_2) \cos(l_s \theta_2) \\
&+ \sum_{r=1}^N \sum_{s=1}^N K_{D_r D_s} \sin(k_r \pi\xi_1) \sin(l_r \theta_1) \sin(k_s \pi\xi_2) \sin(l_s \theta_2)
\end{aligned} \tag{4.6}$$

The auto-covariance function $C_{w_0}(\xi_1, \theta_1, \xi_2, \theta_2)$ can be written in simplified form as:

$$\begin{aligned}
C_{w_0}(\xi_1, \theta_1, \xi_2, \theta_2) &= \sum_{i=0}^{N_1} \sum_{j=0}^{N_1} K_{A_i A_j} \cos(i\pi\xi_1) \cos(j\pi\xi_2) \\
&+ \sum_{r=1}^N \sum_{s=1}^N K_{C_r C_s} \sin(k_r \pi\xi_1) \sin(k_s \pi\xi_2) \cos(l_r (\theta_2 - \theta_1))
\end{aligned} \tag{4.7}$$

The critical buckling loads for 50 simulated GB shells can be represented in a reliability v/s non-dimensional buckling load plot and critical non-dimensional buckling load at desired reliability can be calculated.

4.3 Simulated Cylindrical Shells

4.3.1 GB shells

Initial imperfections in 50 GB shells are in the form of wall thickness variations that vary in both axial and circumferential direction. Fifty cylindrical shells (GB1-GB50) as simulated using MathCAD code in Chapter II are considered to have asymmetric imperfections and are used to predict the non-dimensional buckling load. These shells are similar to FGD vessel and were simulated as per manufacturing tolerances laid out in ASME Boiler and Pressure Vessel Code Section VIII Division 2 Rules. Table A.1 to Table A.50 in APPENDIX A gives generated shell wall thickness values for GB shells. Each GB shell have 144 shell wall thickness values, consisting of 12 readings axially and 12 circumferentially at each elevation.

4.3.2 Koiter circle

Koiter circle gives the relation between the wave numbers k and l . For, an axially loaded cylinder, Koiter circle depends on length, radius and thickness of shell. The circumferential wave number, l must be an integer, while axial wave number, k can take any value. According to the classical theory all the combination of wave numbers on the Koiter circle are possible. The minimum critical load occurs for modes that satisfy the condition shown in eq. (4.8) [34]. This equation also governs the Koiter circle as shown in Fig. 4.1.

$$A^2 + B^2 = A \left[12 \frac{(1 - \mu^2)}{(Rt)^2} \right]^{\frac{1}{4}} \quad (4.8)$$

where,

$$A = \frac{k\pi}{L}, B = \frac{l}{R} \quad (4.9)$$

From the Koiter circle it is clear that k , number of half waves in axial direction can take values from 1 to 27 and l , number of full waves in circumferential direction can take values from 1 to 16.

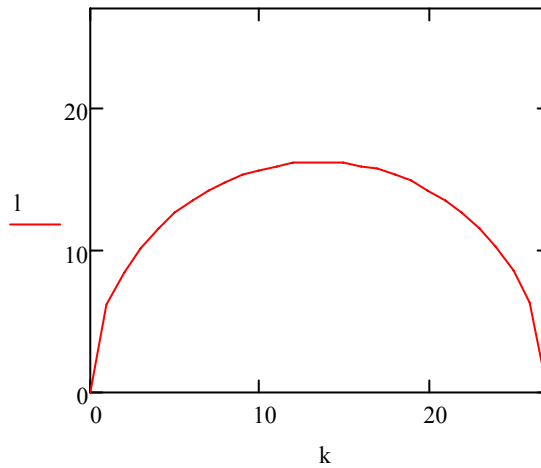


FIGURE 4.1: Koiter Circle for FGD Vessel ($L/R=2.6$, $R/t=320$)

4.3.3 Fourier coefficients

The initial asymmetric imperfections are represented by eq. (4.10) and Fourier coefficients were calculated. Table E.1 and Table E.2 in APPENDIX E shows the Fourier coefficient's for GB1 Shells.

$$W_n(\xi, \theta) = \sum_{k=1}^{27} \sum_{l=0}^{16} \sin(k\pi\xi) [C_{kl} \cos(l\theta) + D_{kl} \sin(l\theta)] \quad (4.10)$$

Fig. 4.2 and Fig. 4.3 shows the variation of the half wave sine Fourier series as a function of circumferential wave number, l and axial half wave number, k , respectively.

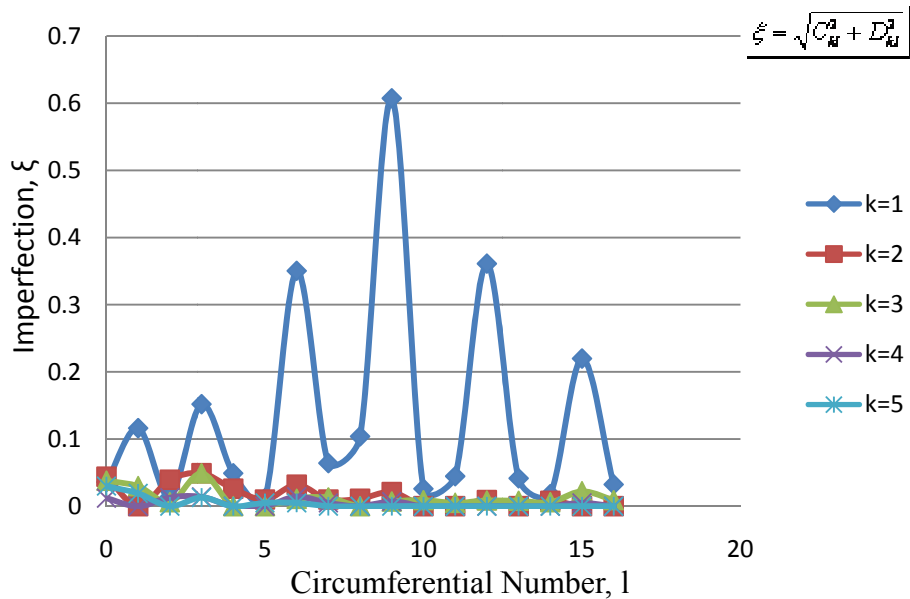


FIGURE 4.2: Circumferential Variation of the Half-wave Sine Fourier Representation

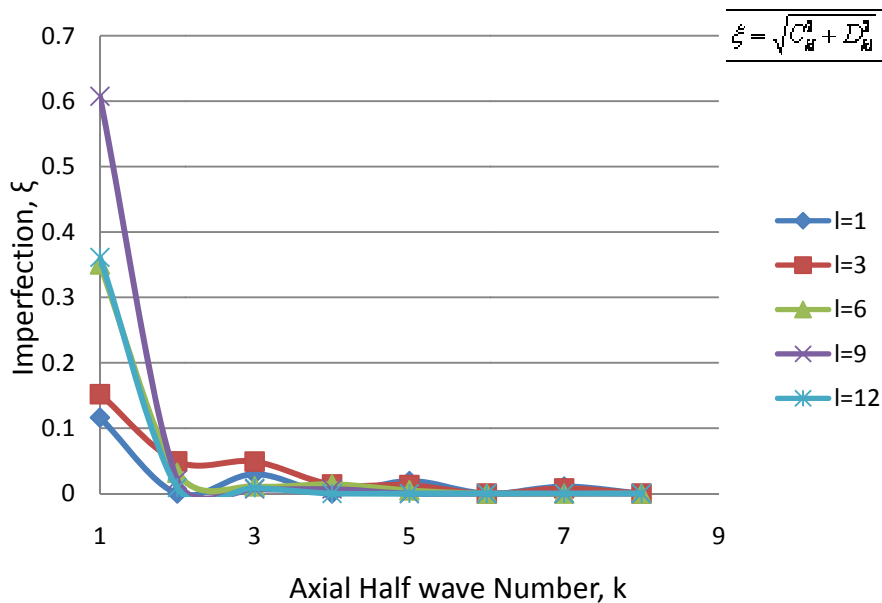


FIGURE 4.3: Axial Variation of the Half-wave Sine Fourier Representation

4.4 Calculation of Predicted Minimum Buckling Loads

Buckling loads for 50 GB Shells was calculated using Multi-mode method [17] using MathCAD code.

4.4.1 Buckling load maps

The buckling loads were calculated for a perfect cylindrical shell using classical simply supported boundary conditions. These maps are then used to determine the dominant mode shape. Table F.1 in APPENDIX F shows the classical buckling load map for GB1 shell.

4.4.2 Coupling of modes

From literature, it has been shown that coupling between one axisymmetric mode with wave number $(i,0)$ and two asymmetric modes with wave numbers (k,l) and (m,n) will occur, if the relation $i=|k\pm l|$ and $l=n$ are satisfied. For the degenerate case of one axisymmetric $(i,0)$ and one asymmetric (k,l) the coupling conditions reduce to the single relation $i=2k$. Further it has been found that coupling between three asymmetric modes with wave numbers (k,l) , (m,n) and (p,q) will occur if the relations $k+m+p=\text{odd integer}$ and $q=|l\pm n|$ are satisfied. If these coupling conditions are satisfied, then the resulting buckling load of the shell is generally lower than the buckling load each mode is considered separately.

For analysis of cylindrical shells subjected to axial loading multi-mode analysis considering 8-mode is used. The selected 8-modes are shown as tree in Fig. G.1 in APPENDIX G. Donnell's non-linear eq. (1.3) is then used to calculate buckling load for each GB Shell.

4.4.3 Calculation of buckling load

A column plot showing number of buckled shells for specific values of non-dimensional buckling load (λ) are shown in Fig. 4.4. This plot will be used for calculating

the reliability function from which experimental value of non-dimensional buckling load can be calculated.

Fig. 4.5 shows the reliability function for 50 GB Shells. The value of non-dimensional buckling load (λ) can be calculated at any desired reliability from this curve. If the desired reliability is 0.95, then the non-dimensional buckling load (λ) comes to be 0.61.

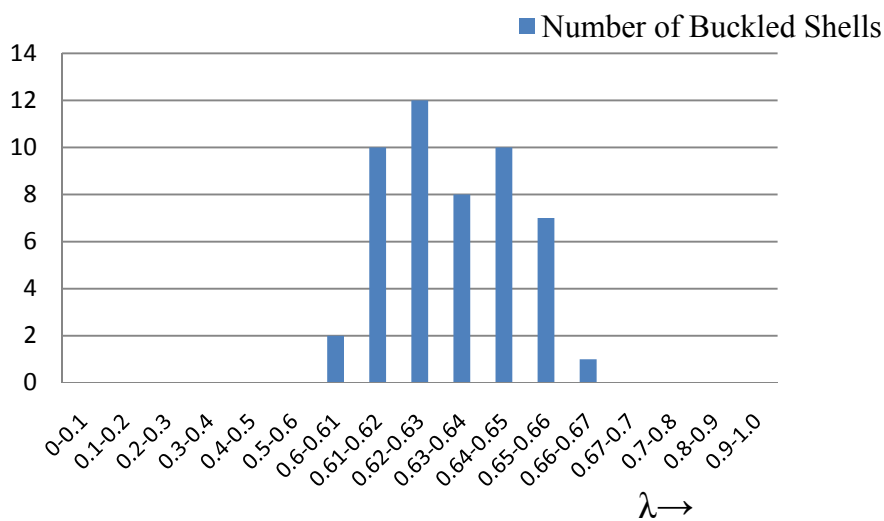


FIGURE 4.4: Non-dimensional Buckling Loads for 50 GB Shells (Multimode)

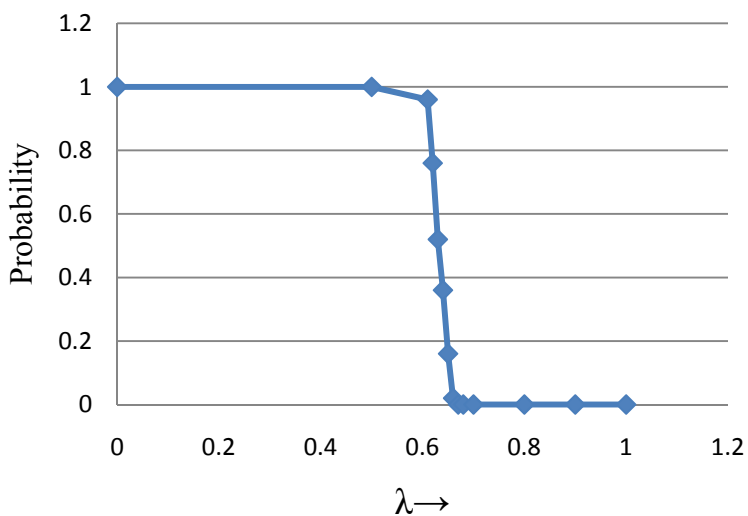


FIGURE 4.5: Calculated Reliability Function V/S Non-dimensional Buckling Load (Multimode)

4.5 Predicted Buckling Loads by Koiter's Theory

Buckling loads can also be calculated for GB shells by Koiter method as illustrated in Ref. [12]. Koiter assumed that if for an isotropic shell the initial imperfections are represented by the 3 modes as shown in eq. (4.11)

$$W = t\xi(\cos i_{cl}x + \sqrt{2} \frac{i_{cl}}{k_1} \sin k_1x \cos ly - \sqrt{2} \frac{i_{cl}}{k_2} \sin k_2x \cos ly) \quad (4.11)$$

where,

$$i_{cl} = \left(\frac{L}{\pi} \right) \sqrt{\frac{2c}{Rt}} \quad (4.12)$$

and k_1 and k_2 are the two roots of the quadratic equation

$$k^2 \frac{Rt}{2c} \left(\frac{\pi}{L} \right)^2 + l^2 \frac{Rt}{2c} \left(\frac{1}{R} \right)^2 + k \sqrt{\frac{Rt}{2c}} \left(\frac{\pi}{L} \right) = 0 \quad (4.13)$$

Koiter derived a second order quadratic equation for determining λ considering nonlinear equations of shallow shell theory, which may be linearized for the investigation of neutral equilibrium in the symmetric configuration. Koiter considered only those buckling modes which are periodic in the axial direction as well as in the circumferential direction.

$$(\lambda - 1)^2 + 6c\xi\lambda = 0 \quad (4.14)$$

Buckling loads for 50 GB Shells were calculated by finding the eigenvalues of the eq. (4.14) and values are shown in Table H.1 in APPENDIX H and summarized in Fig. 4.6 shown below. Furthermore, the reliability function of 50 GB Shells is shown in Fig. 4.7.

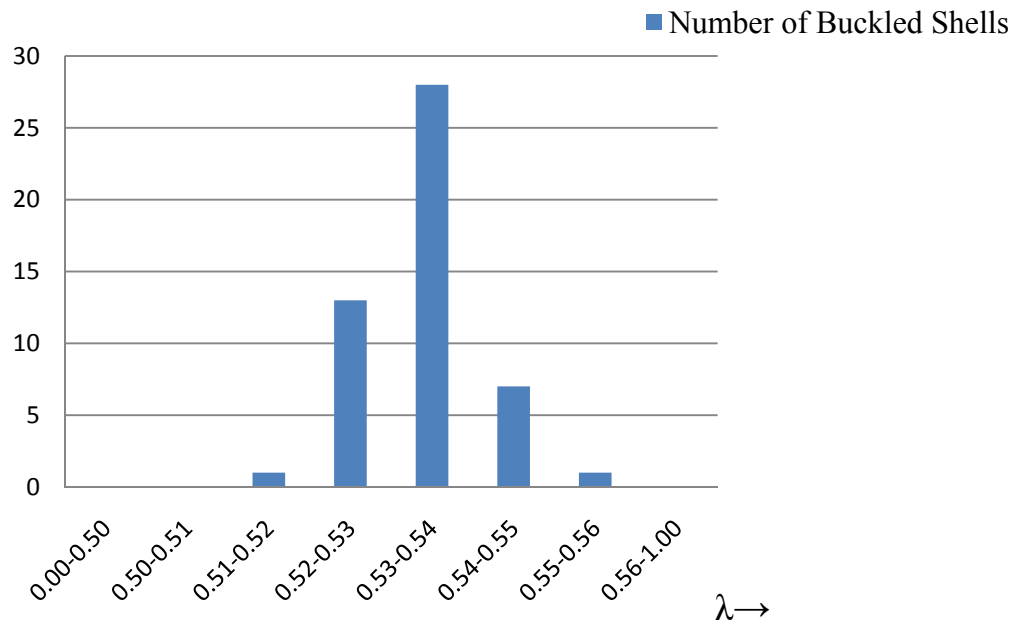


FIGURE 4.6: Non-dimensional Buckling Loads for 50 GB Shells (Koiter Asymmetric Theory)

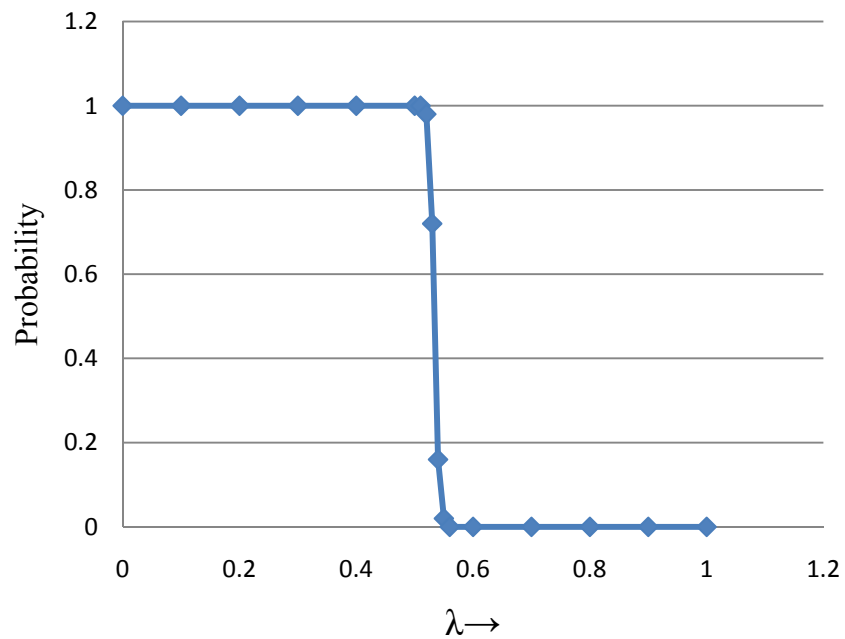


FIGURE 4.7: Calculated Reliability Function V/S Non-dimensional Buckling Load (Koiter Asymmetric Theory)

4.6 Summary

Simulated GB shells were analyzed considering shell wall thickness variations to be asymmetric. Double Fourier sine series was used to represent thickness variations. Sine series is used in comparison to cosine series as with sine series less number of Fourier coefficients are required to represent the thickness variations. Buckling load map was formed by calculating the buckling load for all combinations of k and l values. Lowest possible failure mode was determined and 8-mode failure was considered by considering the interaction of different modes. Buckling load was calculated by considering failure of shells in this 8-mode fashion. By asymmetric analysis, the load carrying capacity of the shell is reduced by 39% by Fourier series technique due to the presence of variations in wall thickness. Koiter's special theory gives the axial load reduction value of 49%.

After analysis of shells under axial compression, Chapter V considers the shell under vacuum or external pressure. The analysis of shells in vacuum is more important from Mechanical point of view as these shells are often used as pressure vessels.

CHAPTER 5: ANALYSIS OF EXTERNAL PRESSURE ON CYLINDRICAL SHELL

5.1 Introduction

Effects of imperfections in shell wall of cylindrical shells were studied in previous chapters of this dissertation. Cylindrical shells geometrically similar to FGD vessel were simulated and analysis under axial end load was carried out. This dissertation would be incomplete without the analysis of cylindrical shell under vacuum or external pressure which is important from mechanical point of view. In this Chapter, non-dimensional buckling load is calculated for GB shells simulated by Monte Carlo technique when shells are subjected to external pressure only. Imperfections in this Chapter are treated to be asymmetric i.e. varying in both axial and circumferential direction. Double Fourier series is used to represent this asymmetric imperfection. Fourier coefficients as calculated in the last chapter are used for analysis of shells under external pressure. Multi-mode analysis is again used for calculation of non-dimensional buckling loads. Donnell's linearized buckling equation for thin cylindrical shell which does not include the effect of pre-buckling and post-buckling is used to predict the non-dimensional buckling load when shells are subjected to external pressure or vacuum only. Reliability function curves are drawn so that buckling load values can be calculated at any desired level of confidence.

5.2 Simulated Shells

5.2.1 GB shells

For calculation of non-dimensional buckling load in case of shells subjected to external pressure or vacuum, 50 cylindrical shells (GB1-GB50) simulated by MathCAD code in Chapter II are used. Initial imperfections in simulated GB shells are shell wall thickness variations. As asymmetric analysis is to be carried out on GB shells variation of thickness values in both axial and circumferential direction are taken into consideration. Table A.1 to Table A.50 in APPENDIX A gives generated shell wall thickness values for GB shells.

5.2.2 Fourier coefficients

The initial asymmetric imperfections are represented by double Fourier sine series. For calculation of non-dimensional buckling load, the first step is calculation of Fourier coefficients. Fourier coefficients C_{kl} and D_{kl} as represented in eq. (5.1) were determined in chapter IV and these coefficients for GB1 shell are listed in Table E.1 and Table E.2 in APPENDIX E. The relation of non-dimensional numbers ξ and θ with axial and circumferential coordinates are given in eq. (5.2)

$$W_n(\xi, \theta) = \sum_k \sum_l \sin(k\pi\xi) [C_{kl} \cos(l\theta) + D_{kl} \sin(l\theta)] \quad (5.1)$$

where,

$$\begin{aligned} \xi &= \frac{x}{L}, 0 \leq x \leq L \\ \theta &= \frac{y}{R}, 0 \leq \theta \leq 2\pi \end{aligned} \quad (5.2)$$

5.3 Calculation of Predicted Minimum Buckling Loads

Buckling loads for 50 GB Shells was calculated using Multi-mode method [17] using MathCAD code.

5.3.1 Buckling load maps

Buckling load maps consists of buckling loads for different modes i.e. different combinations of wave numbers in axial and circumferential direction. The buckling loads were calculated for a perfect cylindrical shell subjected to external pressure and using classical simply supported boundary conditions as given by Donnell and shown in eq.

(5.3):

$$D\nabla^4(\nabla^4 w) - \nabla^4(N_{yy}w_{,yy} + N_{xx}w_{,xx}) + \frac{Et}{R^2}w_{,xxxx} = 0 \quad (5.3)$$

where, D is bending stiffness given by eq. (5.4) and $\nabla^4 w$ is given by eq. (5.5)

$$D = \frac{Et^3}{12(1 - \mu^2)} \quad (5.4)$$

$$\nabla^4(w) = w_{,xxxx} + \frac{2}{R^2}w_{,xxyy} + \frac{1}{R^4}w_{,yyyy} \quad (5.5)$$

The imperfections are assumed to follow the double Fourier sine series as shown in eq. (5.6). These maps are then used to determine the dominant mode shape. Table I.1 in APPENDIX I shows the classical buckling load map for GB1 shell when shells are subjected to external pressure.

$$w = C_{kl} \sin\left(\frac{k\pi x}{L}\right) \cos\left(\frac{ly}{R}\right) + D_{kl} \sin\left(\frac{k\pi x}{L}\right) \sin\left(\frac{ly}{R}\right) \quad (5.6)$$

5.3.2 Coupling of modes

Modes are coupled in similar way as done in the case of cylindrical shells under axial load in Chapter IV. Coupling between one axisymmetric mode with wave number $(i,0)$ and two asymmetric modes with wave numbers (k,l) and (m,n) will occur, if the relation $i=|k\pm l|$ and $l=n$ are satisfied. For the case of one axisymmetric $(i,0)$ and one asymmetric (k,l) the coupling conditions reduce to the single relation $i=2k$. The coupling between three asymmetric modes with wave numbers (k,l) , (m,n) and (p,q) will occur if the relations $k+m+p=\text{odd integer}$ and $q=|l\pm n|$ are satisfied. If these coupling conditions are satisfied, then the resulting buckling load of the shell is generally lower than the buckling load each mode is considered separately. The use of above conditions gave a 8-mode failure mode that is used for calculating the non-dimensional buckling load.

5.3.3 Calculation of Buckling Load

Donnell's linearized equation is again used for calculating the buckling load of GB shells subjected to external pressure. Initial imperfection, w is assumed to follow 8-mode fashion. A 8-mode deformation mode as shown in Fig. J.1 in APPENDIX J is considered for calculating the non-dimensional buckling loads when shells are subjected to external pressure.

A column plot showing number of buckled shells for specific values of non-dimensional buckling load (λ) are shown in Fig. 5.1. This plot will be used for calculating the reliability function from which experimental value of non-dimensional buckling load can be calculated.

Fig. 5.2 shows the reliability function for 50 GB Shells. The value of non-dimensional buckling load (λ) can be calculated at any desired reliability from this curve.

If the desired reliability is 0.95, then the non-dimensional buckling load (λ) comes to be 0.89.

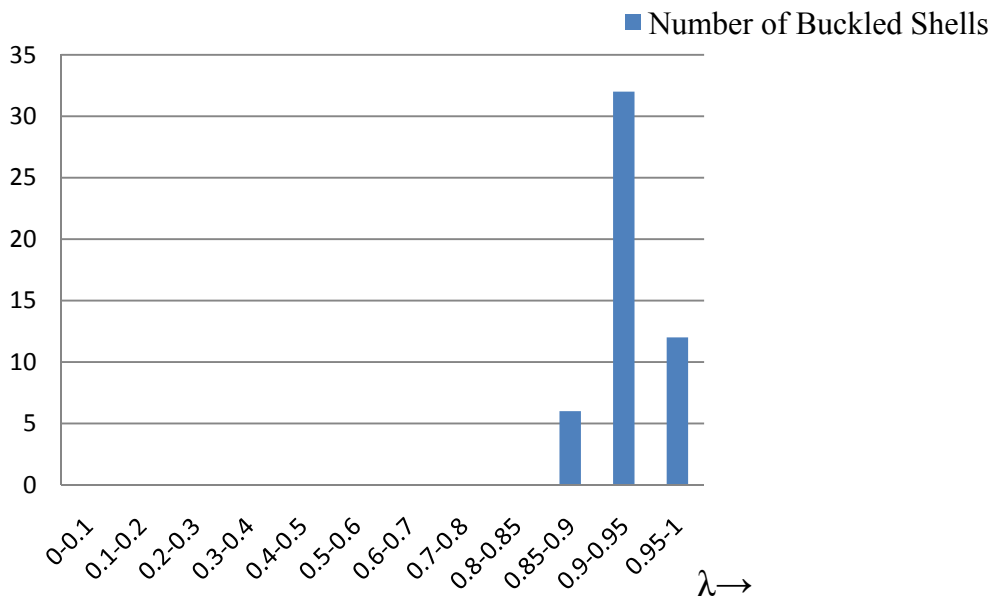


FIGURE 5.1: Non-dimensional Buckling Loads for 50 GB Shells (Shells Subjected to External Pressure)

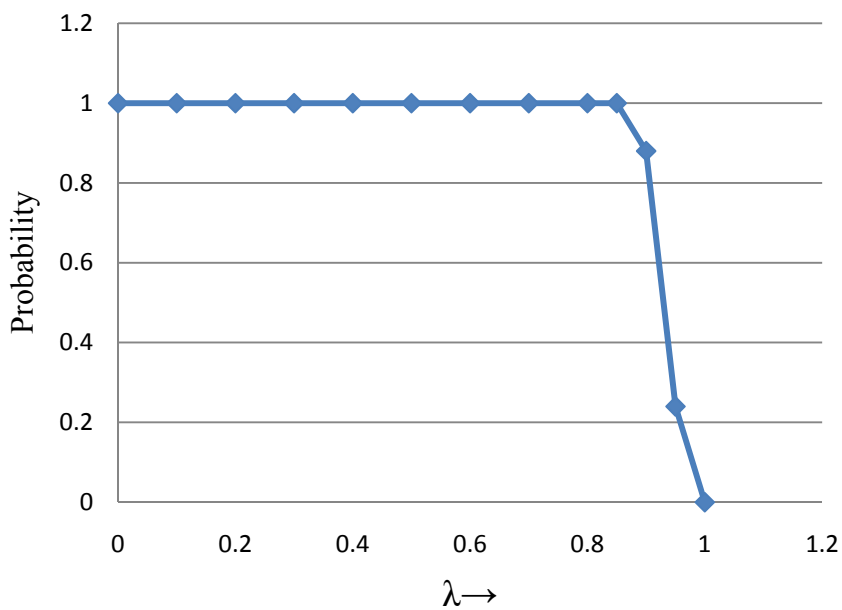


FIGURE 5.2: Calculated Reliability Function V/S Non-dimensional Buckling Load (Shells Subjected to External Pressure)

5.4 Summary

Analysis of the GB shells subjected to external pressure or vacuum considering shell wall thickness variations to be asymmetric was carried out in this Chapter. Double Fourier sine series was used to represent thickness variations. Buckling load map was formed by calculating the buckling load for all combinations of wave numbers in axial and circumferential directions. Lowest possible failure mode was determined and 8-mode failure was considered by considering the interaction of different modes. Buckling load was calculated by considering failure of shells in 8-mode fashion. The load carrying capacity of the shells subjected to external pressure is reduced by 11% by Fourier series technique due to the presence of variations in shell wall thickness.

Chapter VI covers the comparison of results from Fourier series method, Koiter's special theory and ASME Boiler and Pressure Vessel Code Section VIII Division 2 Rules when shells are subjected to axial end load and external pressure.

CHAPTER 6: RESULTS AND COMPARISON WITH ASME B&PV CODE

6.1 Introduction

Fifty simulated shells similar to FGD vessel, generated by using random numbers, were analyzed by Fourier series technique, Koiter's special theory and ASME B&PV Code Section VIII Division 2 Rules. Non-dimensional buckling loads were calculated for generated shells when subjected to axial loading and external pressure. This chapter enlists the results when shells were analyzed under different loading conditions and by different techniques. It was found that ASME B&PV Code provides adequate factor of safety when shells with imperfections are subjected to axial compressive load and external pressure. This Chapter also provides discussions of results obtained when imperfections were considered to be axisymmetric and asymmetric. Comparisons are also made between three different techniques employed in this dissertation i.e. Monte Carlo method, Koiter's special theory and ASME B&PV Code. Discussions related to behavior of shells under axial compressive load and external pressure is also carried out.

6.2 Results

As per ASME B&PV Code Section VIII Division 2 Rules [28], capacity reduction factors (β) that accounts for shape imperfections must be applied to the allowable stresses. Eq. (6.1) is used to calculate the capacity reduction factor for unstiffened cylinders subjected to axial compression loading.

$$\beta = 0.207 \text{ for } \frac{D_0}{t} \geq 1247$$

$$\beta = \frac{338}{389 + \frac{D_0}{t}} \text{ for } \frac{D_0}{t} < 1247 \quad (6.1)$$

The ratio D_0/t for FGD Stack comes out to be 642. Thus, using eq. (6.1) the value of β comes out to be 0.328.

The classical buckling load for FGD vessel under axial compressive load by eq. (1.4) comes out to be 56.75ksi. This load carrying capacity will be reduced due to presence of imperfections. The results obtained from the evaluation of non-dimensional buckling load by Koiter Formulae, Monte Carlo techniques and ASME B&PV Code leads to Table 6.1. These results show that the effect of shell wall thickness variation on buckling load deserves special attention. Thus, in the absence of initial geometric imperfection, this particular kind of thickness variation may constitute the most important factor in the buckling load reduction.

TABLE 6.1: Buckling Loads for FGD Vessel Subjected to Axial Compressive Load

Buckling Loads derived for different techniques	
ASME B&PV Code	0.328
Asymmetric (Monte Carlo)	0.610
Asymmetric (Koiter)	0.510
Axisymmetric (Koiter)	0.710
Axisymmetric (Monte Carlo)	0.880

For simulated shells, non-dimensional buckling load (λ) comes out to be 0.880 by Monte Carlo technique considering axisymmetric analysis. It means that due to presence of shell wall thickness variation as a result of non-repeatability in manufacturing process

even within tolerance limits, the load carrying capacity of shell under axial compressive loading decreases by 12%. If more detailed analysis is carried out considering imperfections to be Asymmetric the non-dimensional buckling load decreases to 0.61, reducing the load carrying capacity of FGD vessel by 39%.

According to ASME B&PV Code Section VIII Division 2 Rules, Capacity Reduction Factor (β) that accounts for shape imperfections for pressure vessels subjected to external pressure is given by eq. (6.2) as shown below:-

$$\beta = 0.8 \quad (6.2)$$

The results obtained from the evaluation of non-dimensional buckling load when FGD vessel is subjected to axial compression by Monte Carlo techniques and ASME B&PV Code leads to Table 6.2. For simulated shells under external pressure, non-dimensional buckling load comes out to be 0.89 by Monte Carlo technique considering Asymmetric Analysis making 11% decrease. The load carrying capacity of shell under external pressure decreases by 20% according to ASME Boiler and Pressure Vessel Code Section VIII Division 2 Rules.

TABLE 6.2: Buckling Loads for FGD Vessel Subjected to External Pressure

Buckling Loads derived for different techniques	
ASME B&PV Code	0.80
Asymmetric (Monte Carlo)	0.89

6.3 Comparison of Results With B&PV Code Section VIII Division 2 Rules

Simulated shells under axial compressive load and external pressure were analyzed by Koiter's special theory, Monte Carlo technique and ASME Boiler and Pressure Vessel Code. Comparison can be drawn between axisymmetric and asymmetric analysis. Also

comparison between Koiter's special theory, Monte Carlo technique and ASME B&PV Code are made in subsections below.

6.3.1 Comparison between axisymmetric and asymmetric analysis

The variations in simulated shells were first considered to be axisymmetric (i.e. shell wall thickness does not vary in circumferential direction) and then shell wall thickness variations were considered to be asymmetric (i.e. varying in both axial and circumferential direction). Fig. 6.1 shows the reliability curves for axisymmetric and asymmetric analysis by Monte Carlo technique. There is a difference of around 28% in the reduction of buckling loads when variations are treated as axisymmetric and when treated as asymmetric by analyzing by Monte Carlo technique.

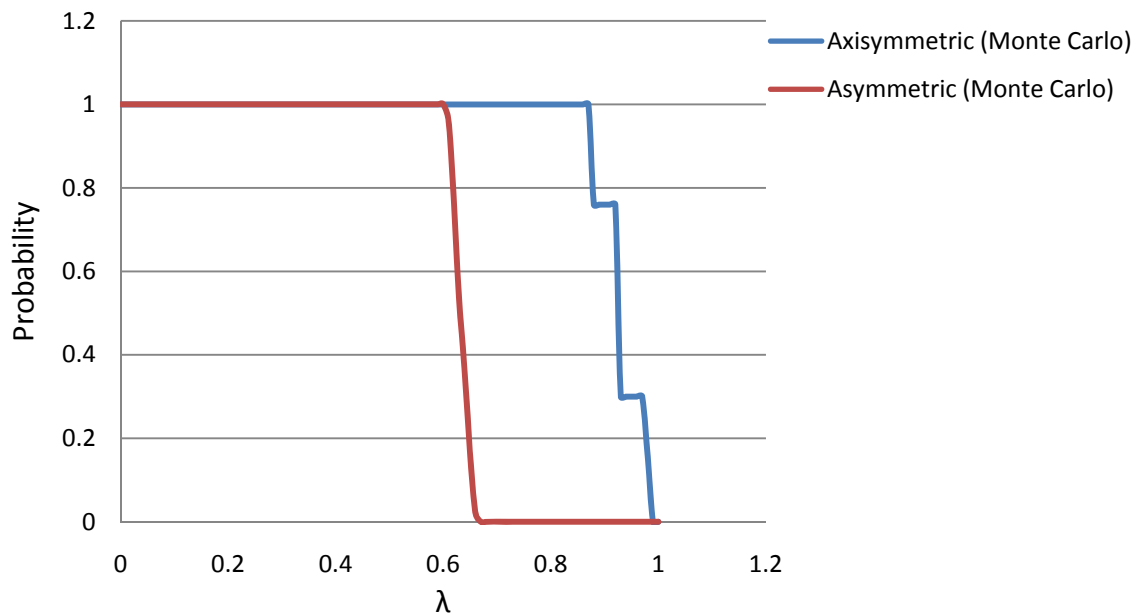


FIGURE 6.1: Reliability Curves for Shells Subjected to Axial Compressive Load by Monte Carlo Technique

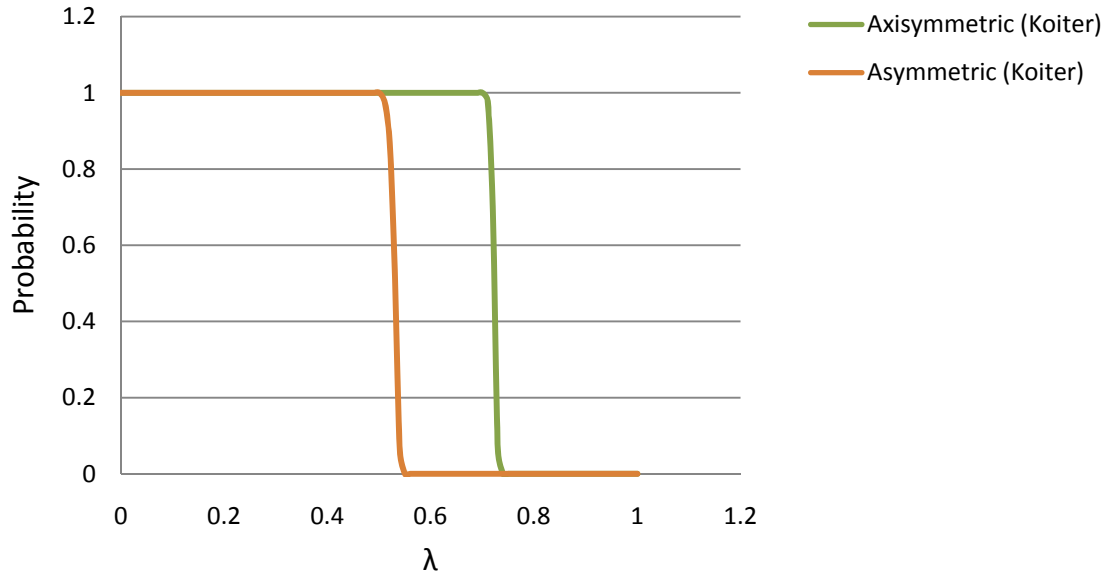


FIGURE 6.2: Reliability Curves for Shells Subjected to Axial Compressive Load by Koiter's Special Theory

Reliability curves for simulated shells subjected to axial compressive load analyzed by Koiter's special theory are shown in Fig. 6.2. At 95% reliability level the non-dimensional values for Axisymmetric and Asymmetric analysis by Koiter's special theory comes out to be 0.71 and 0.51 respectively. Thus critical buckling loads have to be reduced by 29% and 49% respectively for two cases. There is a difference of around 20% in the reduction of buckling loads when variations are treated as axisymmetric and when treated as asymmetric by analyzing by Monte Carlo technique.

The reason for more conservative results in case of asymmetric is due to the fact that more perturbations were considered in asymmetric analysis. Shell wall thickness variations were considered to vary in circumferential direction only in case of axisymmetric analysis while in case of asymmetric analysis variations in both axial and circumferential direction have been considered for analysis.

6.3.2 Comparison between Monte Carlo technique, Koiter's special theory and ASME B&PV Code

Comparison between three methods i.e. Monte Carlo technique, Koiter's special theory and ASME Boiler and Pressure Vessel Code, when shells are subjected to axial compressive load and variations in shell wall thickness were considered to be asymmetric are shown in Fig. 6.3. At 95% reliability level, non-dimensional buckling values comes out to be 0.328 according to ASME B&PV Code, 0.61 by Monte Carlo technique and 0.51 by Koiter's special theory. Critical buckling loads have to be reduced by 67.2% when ASME B&PV Code is used, while in case of Monte Carlo technique critical load has to be reduced by 39%. Critical buckling load reduces by 49% in case of Koiter's special theory. The reason behind lower critical buckling loads in case of Koiter's special theory is that theory is based on an eigen-value solution and higher order terms were neglected.

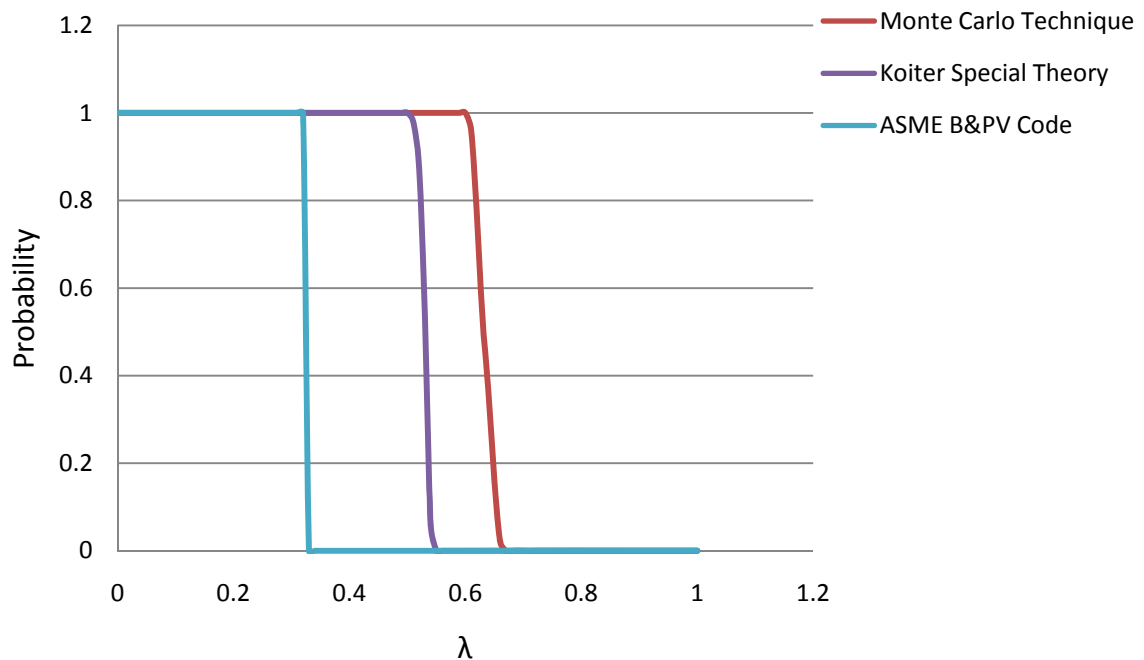


FIGURE 6.3: Reliability Curves for Shells Subjected to Axial Compressive Load

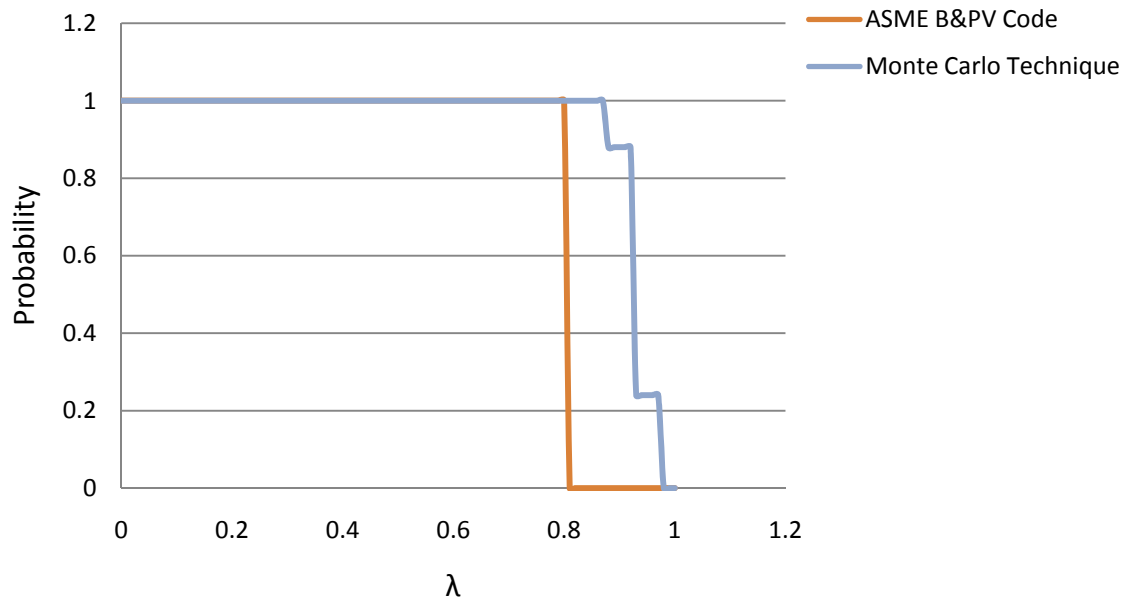


FIGURE 6.4: Reliability Curves for Shells Under External Pressure

Reliability curves for simulated GB shells subjected to external pressure are shown in Fig. 6.4. At 95% reliability level the non-dimensional values according to ASME B&PV Code and Monte Carlo technique comes out to be 0.89 and 0.8 respectively. There is a difference of around 9% in the reduction of buckling loads when simulated shells were analyzed by ASME B&PV Code and Monte Carlo technique.

The reason for more conservative results in case of ASME B&PV Code is due to the fact that ASME B&PV Code being a deterministic approach does not include the perturbations as considered in Monte Carlo technique which is a probabilistic approach.

CHAPTER 7: CONCLUSIONS

7.1 Recommendations

The results show that effect of shell wall thickness variation on buckling load deserves special attention. Thus, in the absence of initial geometric imperfection, thickness variation may constitute the most important factor in the buckling load reduction. The load carrying capacity will be reduced due to presence of imperfections when thin walled shells are subjected to axial compressive load or external pressure. In last chapter, results show that load carrying capacity of shells is reduced by 39% when shells are subjected to axial compressive end load using Monte Carlo method. Also by Monte Carlo method load carrying capacity reduces by 11% when shells are subjected to external pressure. The reduction values provided by ASME Boiler and Pressure Vessel Code Section VIII Division 2 Rules comes out to be 67.2% and 20% in case of shells subjected to axial end load and external loading respectively.

The reliability function of shells subjected to axial compressive end load obtained from Koiter's special theory, Monte Carlo techniques and ASME Boiler and Pressure Vessel Code leads to Fig. 7.1. Axisymmetric analysis of simulated shells shows the effect of shell wall thickness variations on the non-dimensional buckling load. More detailed analysis i.e. asymmetric analysis was carried out to include all perturbations when shells are subjected to axial compressive end load. ASME Boiler and Pressure Vessel Code give a more conservative non-dimensional buckling value.

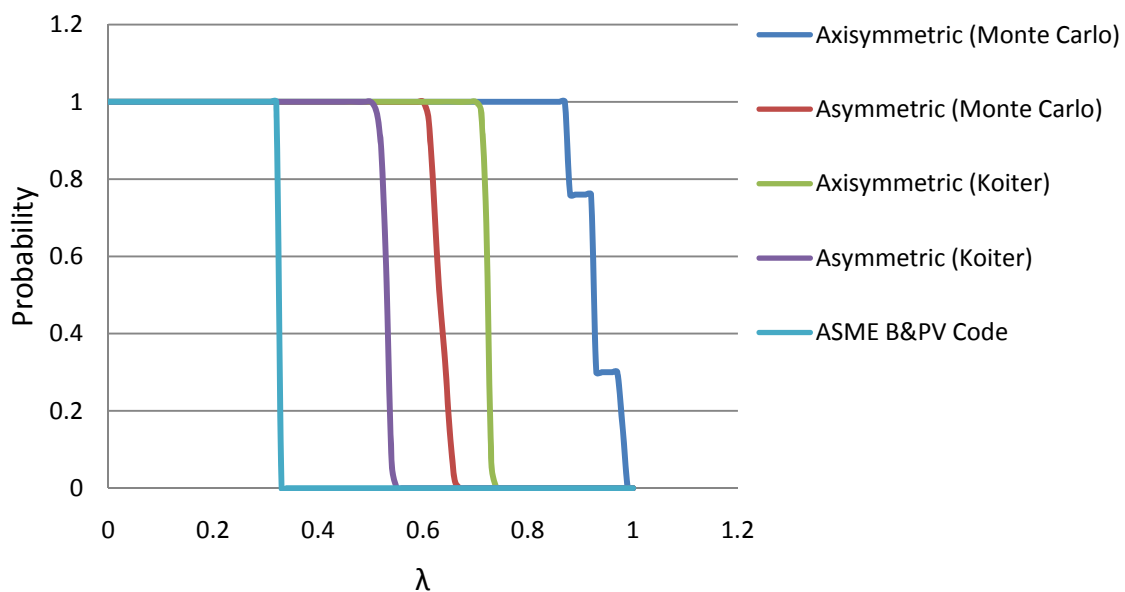


FIGURE 7.1: Reliability Curves of Simulated Shells Subjected to Axial Compressive Load by Different Methods

Fig. 7.2 shows the reliability function of shells subjected to external pressure obtained from Monte Carlo techniques and ASME Boiler and Pressure Vessel Code. ASME Boiler and Pressure Vessel Code again give a more conservative non-dimensional buckling value as compared to Monte Carlo method.

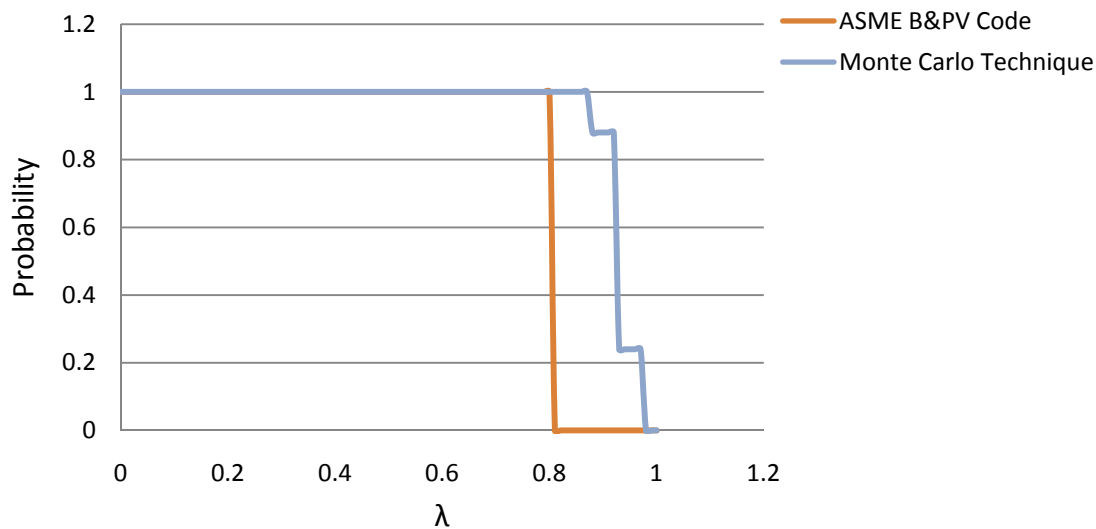


FIGURE 7.2: Reliability Curves of FGD Vessel Subjected to External Pressure by Different Methods

Two approaches were used for determining the buckling load of cylindrical shell, deterministic approach and stochastic approach. While the deterministic approach carries out analysis on the basis of some physical laws, stochastic (or probabilistic) approach takes into account several unknown factors that can affect the buckling loads. Deterministic approach does not include perturbations in the shell wall thicknesses. The use of stochastic or reliability approach is recommended in comparison to deterministic approach for calculating buckling load values for cylindrical shells in both axial compression end loading and under external pressure.

It can be concluded that imperfections in shell wall thickness have been addressed in ASME Boiler and Pressure Vessel Code by capacity reduction factor. The results obtained by Monte Carlo method agree well with those published by Elishakoff et al. [31] for the prediction of buckling loads for shells subjected to axial compressive loading. Based on the research carried out in this dissertation, further research on variation of material property in shell wall and effect of wrinkles or out of roundness of shells should be carried out. A reduction in amount of conversation provided by ASME Boiler and Pressure Vessel Code in form of capacity reduction factor is recommended.

7.2 Future Work

A lot of research has been going on the buckling of cylinders for last 100 years or so. Even then it is still challenging to work on this topic especially when cylinders have initial imperfections like thickness variations, wrinkles or are pre-buckled. The work carried out in this dissertation can be extended for calculating buckling loads for cylinders which are under other kind of loading conditions like lateral loading. Analysis can be extended to cylinder under axial load and external pressure. The results obtained

in this study can also be verified by finite element techniques. The analysis can be made by using FE codes like ABAQUS or ANSYS.

REFERENCES

1. Bazant, Z. P. and Cedolin, L., "Stability of Structures: Elastic, Inelastic, Fracture and Damage Theories", Oxford Univ. Press, New York 1991, 2nd ed. Dover, N.Y. 2002.
2. Koiter, W. T., "On the stability of elastic equilibrium", Ph.D. Thesis, Delft University, 1945.
3. Wang, C. M., Wang C. Y., Reddy, J. N., "Exact Solutions for Buckling of Structural Members", CRC Press, 2004.
4. Euler, L., "Methodus inveniendi lineas curvas maximi minimive proprietate gaudentes, (Appendix, De curvis elasticis)", Lausanne and Geneva, 1774.
5. Bryan, G. H., "On the Stability of Elastic Systems", Proc. Cambridge Phil. Soc., Vol. VI, 1888.
6. Southwell, R. V., "On the General Theory of Elastic Stability", Phil. Trans. Roy. Soc. London, Ser. A, Vol. 213, 1913.
7. Trefftz, E., "Derivation of Stability Criteria of Elastic Equilibrium from the Elastic Theory of Finite Deformations", Proc. Third Intern. Congr. Appl. Mech., Vol. III, Stockholm, 1930.
8. Kappus, R., "Theory of Elasticity of Finite Displacements", Z. Angew. Math. Mech., Vol. 19, 1939.
9. Biot, M., "Theory of Elasticity of the Second Order, with Practical Applications", Z. Angew. Math. Mech., Vol. 20, 1940.
10. Teng, J. G. and Rotter, J. M. (Eds), "Buckling of Thin Metal Shells", Spon Press, UK, 2004, pp. 41-87.
11. Donnell, L. H. and Wan, C. C., "Effect of Imperfections on Buckling of Thin Cylinders and Columns under Axial Compression", Journal of Applied Mechanics, March, 1950, pp. 73-83.
12. Koiter, W. T., "The Effect of Axisymmetric Imperfections on the Buckling of Cylindrical Shells under Axial Compression", , " Proceedings of Royal Netherlands Academy of Sciences, Amsterdam, Series 13, Vol. 66, 265-79, 1963, pp. 265-279.
13. Tennyson, R. C., Muggeridge, D. B., and Caswell, R. D., "Buckling of Circular Cylindrical Shells Having Axisymmetric Imperfection Distributions", AIAA Journal, Vol. 9, No. 5, May, 1971, pp. 924-930.

14. Roorda, J. and Hansen, J. S., "Random Buckling Behavior in Axially Loaded Cylindrical Shells with Axisymmetric Imperfections", *Journal of Spacecraft*, Vol. 9, No. 2, 1972, pp. 88-91.
15. Elishakoff, I. and Arbocz, J., "Reliability of Axially Compressed Cylindrical Shells with Random Axisymmetric Imperfections", *International Journal of Solids and Structures*, Vol. 18, No. 7, 1982, pp. 563-585.
16. Imbert, J. F., "The Effect of Imperfections on the Buckling of Cylindrical Shells", *Aeronautical Engineering Thesis*, California Institute of Technology, Pasadena, California, June, 1971.
17. Arbocz, J. and Babcock, C. D., "Prediction of Buckling Loads based on Experimentally Measured Initial Imperfections", In *Buckling of structures*, Budiansky B., ed., IUTAM Symposium, Cambridge, Mass., 1974, Springer Verlag, Berlin 1976, pp. 291-311.
18. Hansen, J., "Influence of General Imperfections in Axially Loaded Cylindrical Shells", *International Journal of Solids and Structures*, Vol. 11, 1975, pp. 1223-1233.
19. Arbocz, J. and Williams, J. G., "Imperfection Surveys on a 10-ft-Diameter Shell Structure", *AIAA Journal*, Vol. 15, No. 7, July, 1977, pp. 949-956.
20. Elishakoff, I. and Arbocz, J., "Reliability of Axially Compressed Cylindrical Shells with General Nonsymmetric Imperfections", *Journal of Applied Mechanics*, Vol. 52, March, 1985, pp. 122-128.
21. Fung, Y. C., and Sechler, E. E., "Instability of Thin Elastic Shells", *First Symposium on Naval Structural Mechanics* (edited by J. Norman Goodier and N. J. Hoff), Pergamon Press, New York, 115-68, 1960.
22. Amazigo, J. C., and Budiansky, B., "Asymptotic Formulas for the Buckling Stresses of Axially Compressed Cylinders with Localized or Random Axisymmetric Imperfections," *Journal of Applied Mechanics*, 39, 1972, pp. 179-184.
23. Roark, R. J., and Young, W. C., *Formulas for Stress and Strain*, McGraw-Hill, 5th ed., 1975.
24. Metropolis, N. and Ulam, S., "The Monte Carlo Method", *Journal of the American Statistical Association*, Vol. 44, No. 247, September, 1949, pp. 335-341.
25. Marsulex, 2003, "2003 Annual Meeting: 2002 Operating Review," www.marsulex.com, Toronto, Ontario.

26. API, 1998, Welded Steel Tanks for Oil Storage, API Standard 650, Tenth Edition, November 1998, American Petroleum Institute, Washington, DC.
27. Williams, D. K., 2004, "Buckling Considerations and the Use of Code Case 2286-1 for Analyzing a Flue Gas Desulphurization Vessel," Design & Analysis of Pressure Vessels, Heat Exchangers & Piping Components, ASME PVP Vol. 477, New York.
28. ASME, 2007, ASME Boiler & Pressure Vessel Code, Section VIII, Division 1 and 2, American Society of Mechanical Engineers, New York.
29. ASME, 2000, ASME STS-1-2000, Steel Stacks, American Society of Mechanical Engineers, New York.
30. Williams, D. K., Williams, J. R., and Hari, Y., "Buckling of Imperfect Axisymmetric Homogeneous Shells of Variable Thickness: Perturbation Solution", International Conference & Exhibition on Pressure Vessels and Piping "OPE 2006 – CHENNAI" February, 7-9, 2006, Chennai, India.
31. Elishakoff, I., Li, Y., and Starnes, J. H., Jr., 2001, Non-Classical Problems in the Theory of Elastic Stability, Cambridge University Press, Cambridge, UK.
32. Elishakoff, I., "Buckling of a Stochastically Imperfect Finite Column on a Nonlinear Elastic Foundation – A Reliability Study," Journal of Applied Mechanics, Vol. 46, 411-6, June, 1979.
33. Massey, F. J., Jr., "The Kolmogorov-Smirnov test for goodness of fit," Journal of American Statistical Assessment, Vol. 46, 68-78, 1951.
34. Godoy, L. A., "Theory of Elastic Stability – Analysis and Sensitivity", Taylor and Francis, Philadelphia, 1999.

APPENDIX A: SIMULATED GB SHELLS

TABLE A.1: Shell Wall Thickness (in.) of GB1 Shell

$\theta \backslash L(\text{in.})$	13	39	65	91	117	143	169	195	221	247	273	299
0	0.371	0.359	0.359	0.367	0.358	0.347	0.367	0.347	0.350	0.365	0.367	0.365
30	0.368	0.367	0.366	0.353	0.374	0.354	0.361	0.347	0.361	0.354	0.370	0.359
60	0.375	0.358	0.349	0.365	0.367	0.353	0.358	0.373	0.352	0.353	0.371	0.359
90	0.363	0.367	0.348	0.366	0.350	0.348	0.366	0.372	0.363	0.347	0.353	0.360
120	0.352	0.363	0.365	0.348	0.370	0.370	0.358	0.351	0.362	0.370	0.348	0.365
150	0.370	0.367	0.357	0.370	0.360	0.363	0.362	0.357	0.359	0.349	0.368	0.363
180	0.356	0.362	0.374	0.360	0.345	0.352	0.363	0.363	0.367	0.346	0.363	0.344
210	0.365	0.349	0.349	0.357	0.362	0.344	0.360	0.358	0.363	0.364	0.346	0.347
240	0.344	0.357	0.369	0.373	0.360	0.369	0.366	0.363	0.369	0.361	0.364	0.371
270	0.353	0.360	0.350	0.361	0.370	0.351	0.350	0.370	0.362	0.357	0.347	0.367
300	0.362	0.367	0.369	0.359	0.364	0.361	0.350	0.363	0.372	0.358	0.351	0.356
330	0.370	0.349	0.349	0.370	0.370	0.348	0.358	0.362	0.367	0.349	0.373	0.361

TABLE A.2: Shell Wall Thickness (in.) of GB2 Shell

$\theta \backslash L(\text{in.})$	13	39	65	91	117	143	169	195	221	247	273	299
0	0.374	0.349	0.354	0.372	0.362	0.360	0.351	0.349	0.369	0.362	0.350	0.366
30	0.349	0.355	0.369	0.349	0.365	0.348	0.372	0.371	0.346	0.363	0.365	0.366
60	0.348	0.355	0.353	0.373	0.358	0.367	0.372	0.350	0.362	0.346	0.355	0.364
90	0.374	0.369	0.372	0.345	0.344	0.345	0.346	0.364	0.350	0.352	0.347	0.347
120	0.345	0.360	0.367	0.354	0.363	0.364	0.349	0.372	0.354	0.372	0.350	0.346
150	0.346	0.369	0.355	0.356	0.362	0.347	0.368	0.373	0.363	0.367	0.364	0.358
180	0.348	0.348	0.351	0.373	0.351	0.373	0.351	0.349	0.358	0.356	0.365	0.367
210	0.371	0.356	0.351	0.361	0.344	0.353	0.344	0.362	0.356	0.372	0.346	0.365
240	0.366	0.348	0.361	0.365	0.347	0.374	0.348	0.373	0.362	0.356	0.345	0.356
270	0.344	0.346	0.346	0.352	0.371	0.353	0.354	0.362	0.373	0.355	0.354	0.346
300	0.366	0.362	0.360	0.360	0.369	0.355	0.345	0.352	0.356	0.367	0.348	0.349
330	0.351	0.361	0.347	0.356	0.365	0.351	0.350	0.355	0.350	0.367	0.346	0.354

TABLE A.3: Shell Wall Thickness (in.) of GB3 Shell

$\theta \backslash L(\text{in.})$	13	39	65	91	117	143	169	195	221	247	273	299
0	0.351	0.345	0.368	0.368	0.356	0.361	0.358	0.357	0.366	0.364	0.363	0.364
30	0.359	0.371	0.371	0.366	0.351	0.346	0.355	0.352	0.368	0.362	0.349	0.367
60	0.358	0.356	0.366	0.347	0.351	0.352	0.357	0.364	0.363	0.360	0.354	0.374
90	0.363	0.363	0.372	0.371	0.374	0.371	0.344	0.345	0.365	0.358	0.364	0.355
120	0.356	0.371	0.361	0.354	0.345	0.347	0.368	0.348	0.362	0.373	0.357	0.372
150	0.37	0.362	0.368	0.359	0.349	0.366	0.347	0.361	0.361	0.352	0.365	0.358
180	0.363	0.369	0.350	0.350	0.344	0.371	0.365	0.358	0.352	0.367	0.359	0.371
210	0.346	0.362	0.369	0.375	0.364	0.353	0.349	0.353	0.359	0.363	0.369	0.345
240	0.371	0.362	0.370	0.364	0.357	0.364	0.346	0.355	0.365	0.364	0.344	0.373
270	0.353	0.365	0.363	0.349	0.347	0.370	0.345	0.363	0.363	0.361	0.356	0.349
300	0.345	0.344	0.363	0.353	0.366	0.371	0.364	0.375	0.369	0.358	0.370	0.348
330	0.356	0.355	0.352	0.370	0.364	0.372	0.372	0.349	0.375	0.375	0.372	0.348

TABLE A.4: Shell Wall Thickness (in.) of GB4 Shell

$\theta \backslash L(\text{in.})$	13	39	65	91	117	143	169	195	221	247	273	299
0	0.362	0.368	0.361	0.355	0.351	0.353	0.360	0.354	0.369	0.358	0.361	0.353
30	0.367	0.344	0.360	0.369	0.371	0.374	0.367	0.350	0.348	0.355	0.356	0.371
60	0.365	0.357	0.366	0.374	0.370	0.366	0.351	0.348	0.345	0.359	0.373	0.350
90	0.369	0.358	0.367	0.353	0.345	0.364	0.368	0.372	0.367	0.357	0.374	0.372
120	0.375	0.367	0.372	0.371	0.350	0.367	0.361	0.351	0.372	0.345	0.362	0.345
150	0.350	0.361	0.369	0.347	0.358	0.348	0.370	0.361	0.368	0.363	0.357	0.346
180	0.356	0.373	0.356	0.348	0.372	0.356	0.361	0.357	0.364	0.357	0.359	0.352
210	0.362	0.371	0.346	0.354	0.361	0.372	0.371	0.371	0.365	0.356	0.371	0.348
240	0.374	0.359	0.344	0.369	0.360	0.345	0.351	0.352	0.360	0.344	0.368	0.359
270	0.356	0.367	0.367	0.369	0.375	0.358	0.356	0.365	0.352	0.371	0.362	0.346
300	0.348	0.352	0.349	0.372	0.371	0.351	0.345	0.374	0.364	0.366	0.353	0.354
330	0.345	0.369	0.365	0.352	0.349	0.349	0.356	0.368	0.352	0.363	0.371	0.360

TABLE A.5: Shell Wall Thickness (in.) of GB5 Shell

$\theta \backslash L(\text{in.})$	13	39	65	91	117	143	169	195	221	247	273	299
0	0.357	0.358	0.367	0.372	0.374	0.355	0.374	0.364	0.357	0.347	0.347	0.373
30	0.363	0.348	0.346	0.371	0.360	0.359	0.363	0.358	0.352	0.366	0.345	0.344
60	0.359	0.351	0.355	0.356	0.372	0.370	0.355	0.354	0.356	0.365	0.352	0.346
90	0.373	0.369	0.349	0.365	0.354	0.361	0.371	0.353	0.350	0.344	0.351	0.357
120	0.370	0.364	0.348	0.353	0.362	0.362	0.351	0.371	0.363	0.363	0.371	0.363
150	0.369	0.368	0.350	0.374	0.355	0.364	0.346	0.371	0.355	0.353	0.345	0.357
180	0.371	0.370	0.352	0.362	0.353	0.368	0.349	0.369	0.374	0.367	0.346	0.363
210	0.373	0.359	0.355	0.348	0.373	0.349	0.351	0.364	0.372	0.372	0.347	0.344
240	0.373	0.346	0.365	0.363	0.369	0.368	0.368	0.362	0.374	0.363	0.374	0.356
270	0.348	0.355	0.373	0.355	0.365	0.358	0.347	0.350	0.350	0.368	0.371	0.354
300	0.359	0.357	0.347	0.359	0.368	0.360	0.348	0.351	0.355	0.361	0.356	0.370
330	0.345	0.353	0.361	0.373	0.366	0.346	0.361	0.351	0.353	0.356	0.364	0.350

TABLE A.6: Shell Wall Thickness (in.) of GB6 Shell

$\theta \backslash L(\text{in.})$	13	39	65	91	117	143	169	195	221	247	273	299
0	0.359	0.363	0.370	0.349	0.371	0.365	0.370	0.361	0.349	0.375	0.364	0.352
30	0.357	0.353	0.357	0.346	0.366	0.370	0.347	0.355	0.374	0.348	0.360	0.366
60	0.357	0.358	0.367	0.374	0.373	0.352	0.372	0.372	0.350	0.366	0.353	0.348
90	0.362	0.351	0.347	0.358	0.347	0.371	0.372	0.355	0.345	0.353	0.369	0.371
120	0.354	0.360	0.370	0.350	0.346	0.374	0.374	0.351	0.345	0.360	0.371	0.351
150	0.373	0.344	0.355	0.359	0.356	0.351	0.354	0.346	0.347	0.360	0.358	0.354
180	0.357	0.368	0.347	0.352	0.360	0.350	0.372	0.352	0.362	0.370	0.358	0.363
210	0.368	0.374	0.350	0.353	0.348	0.350	0.357	0.348	0.351	0.347	0.356	0.374
240	0.349	0.372	0.372	0.369	0.346	0.374	0.352	0.363	0.353	0.373	0.361	0.356
270	0.347	0.351	0.354	0.364	0.372	0.367	0.360	0.350	0.357	0.359	0.370	0.351
300	0.359	0.359	0.355	0.344	0.367	0.365	0.369	0.368	0.352	0.372	0.344	0.362
330	0.354	0.357	0.352	0.353	0.347	0.373	0.359	0.364	0.360	0.355	0.345	0.345

TABLE A.7: Shell Wall Thickness (in.) of GB7 Shell

$\theta \backslash L(\text{in.})$	13	39	65	91	117	143	169	195	221	247	273	299
0	0.372	0.349	0.367	0.354	0.359	0.365	0.358	0.366	0.351	0.374	0.346	0.354
30	0.351	0.347	0.351	0.349	0.365	0.372	0.346	0.371	0.364	0.366	0.371	0.350
60	0.374	0.365	0.368	0.353	0.355	0.362	0.367	0.356	0.371	0.347	0.372	0.373
90	0.356	0.359	0.361	0.351	0.368	0.347	0.364	0.359	0.357	0.358	0.349	0.352
120	0.354	0.364	0.348	0.363	0.344	0.367	0.351	0.368	0.374	0.346	0.362	0.371
150	0.363	0.364	0.357	0.362	0.367	0.359	0.375	0.354	0.355	0.348	0.349	0.350
180	0.353	0.370	0.349	0.366	0.369	0.369	0.372	0.355	0.363	0.367	0.370	0.367
210	0.372	0.371	0.351	0.366	0.366	0.355	0.372	0.347	0.372	0.344	0.371	0.356
240	0.354	0.374	0.351	0.366	0.361	0.375	0.363	0.375	0.351	0.374	0.374	0.364
270	0.358	0.366	0.366	0.348	0.347	0.373	0.367	0.356	0.360	0.367	0.366	0.367
300	0.357	0.356	0.364	0.356	0.347	0.364	0.367	0.357	0.362	0.365	0.369	0.356
330	0.348	0.370	0.354	0.371	0.349	0.349	0.357	0.352	0.360	0.365	0.374	0.374

TABLE A.8: Shell Wall Thickness (in.) of GB8 Shell

$\theta \backslash L(\text{in.})$	13	39	65	91	117	143	169	195	221	247	273	299
0	0.354	0.356	0.367	0.372	0.373	0.347	0.363	0.348	0.346	0.353	0.362	0.363
30	0.363	0.374	0.367	0.363	0.353	0.351	0.373	0.367	0.356	0.351	0.368	0.356
60	0.359	0.358	0.355	0.369	0.360	0.350	0.366	0.351	0.367	0.353	0.371	0.372
90	0.352	0.360	0.369	0.369	0.372	0.372	0.346	0.348	0.362	0.371	0.374	0.369
120	0.346	0.369	0.357	0.347	0.345	0.346	0.344	0.358	0.361	0.370	0.357	0.373
150	0.358	0.367	0.347	0.374	0.353	0.366	0.375	0.363	0.350	0.362	0.355	0.350
180	0.364	0.346	0.363	0.359	0.352	0.361	0.353	0.363	0.350	0.358	0.354	0.360
210	0.352	0.375	0.354	0.362	0.355	0.347	0.348	0.353	0.354	0.369	0.368	0.370
240	0.363	0.364	0.359	0.371	0.369	0.368	0.350	0.371	0.370	0.374	0.346	0.365
270	0.347	0.372	0.361	0.375	0.354	0.354	0.356	0.349	0.371	0.347	0.356	0.356
300	0.359	0.372	0.366	0.356	0.374	0.348	0.365	0.374	0.358	0.362	0.358	0.374
330	0.366	0.359	0.356	0.356	0.373	0.354	0.366	0.362	0.345	0.362	0.362	0.352

TABLE A.9: Shell Wall Thickness (in.) of GB9 Shell

$\theta \backslash L(\text{in.})$	13	39	65	91	117	143	169	195	221	247	273	299
0	0.365	0.344	0.363	0.370	0.363	0.349	0.358	0.350	0.363	0.364	0.370	0.345
30	0.373	0.369	0.371	0.359	0.346	0.346	0.371	0.350	0.374	0.347	0.364	0.367
60	0.352	0.348	0.351	0.373	0.366	0.360	0.361	0.368	0.374	0.363	0.374	0.354
90	0.350	0.356	0.351	0.347	0.353	0.344	0.352	0.374	0.346	0.345	0.346	0.372
120	0.349	0.346	0.364	0.357	0.354	0.361	0.364	0.364	0.357	0.374	0.350	0.352
150	0.366	0.345	0.368	0.375	0.360	0.370	0.374	0.357	0.356	0.346	0.370	0.346
180	0.361	0.355	0.360	0.345	0.373	0.355	0.348	0.356	0.353	0.369	0.371	0.352
210	0.375	0.351	0.357	0.348	0.371	0.348	0.371	0.368	0.346	0.372	0.361	0.345
240	0.363	0.367	0.375	0.355	0.373	0.361	0.367	0.365	0.362	0.366	0.345	0.361
270	0.360	0.358	0.345	0.345	0.354	0.368	0.369	0.359	0.354	0.363	0.358	0.358
300	0.370	0.370	0.347	0.368	0.357	0.372	0.348	0.347	0.373	0.353	0.357	0.345
330	0.361	0.354	0.354	0.368	0.363	0.350	0.373	0.350	0.345	0.363	0.347	0.349

TABLE A.10: Shell Wall Thickness (in.) of GB10 Shell

$\theta \backslash L(\text{in.})$	13	39	65	91	117	143	169	195	221	247	273	299
0	0.355	0.349	0.356	0.360	0.356	0.358	0.362	0.368	0.350	0.345	0.372	0.371
30	0.349	0.354	0.350	0.362	0.350	0.351	0.362	0.352	0.368	0.357	0.358	0.360
60	0.359	0.345	0.346	0.372	0.345	0.368	0.371	0.352	0.367	0.352	0.367	0.357
90	0.356	0.353	0.354	0.351	0.368	0.357	0.357	0.367	0.356	0.362	0.356	0.346
120	0.366	0.345	0.346	0.372	0.355	0.350	0.371	0.345	0.360	0.373	0.349	0.346
150	0.356	0.370	0.359	0.363	0.362	0.358	0.348	0.374	0.353	0.356	0.348	0.350
180	0.375	0.363	0.368	0.364	0.369	0.345	0.355	0.344	0.371	0.364	0.357	0.351
210	0.355	0.365	0.364	0.369	0.352	0.349	0.372	0.365	0.369	0.368	0.368	0.370
240	0.351	0.359	0.357	0.362	0.354	0.375	0.358	0.357	0.357	0.354	0.359	0.361
270	0.372	0.365	0.371	0.365	0.358	0.370	0.344	0.347	0.362	0.348	0.348	0.369
300	0.357	0.367	0.354	0.348	0.359	0.361	0.361	0.355	0.374	0.355	0.350	0.346
330	0.353	0.361	0.346	0.345	0.360	0.365	0.369	0.369	0.360	0.355	0.374	0.349

TABLE A.11: Shell Wall Thickness (in.) of GB11 Shell

$\theta \backslash L(\text{in.})$	13	39	65	91	117	143	169	195	221	247	273	299
0	0.349	0.357	0.364	0.366	0.361	0.374	0.345	0.347	0.361	0.375	0.351	0.370
30	0.371	0.368	0.373	0.352	0.360	0.352	0.369	0.361	0.371	0.373	0.370	0.361
60	0.352	0.354	0.358	0.375	0.361	0.350	0.352	0.371	0.345	0.358	0.366	0.355
90	0.347	0.364	0.369	0.355	0.356	0.350	0.345	0.359	0.356	0.355	0.346	0.374
120	0.347	0.363	0.355	0.351	0.346	0.357	0.371	0.369	0.351	0.363	0.372	0.372
150	0.375	0.352	0.344	0.358	0.353	0.369	0.358	0.347	0.373	0.344	0.355	0.365
180	0.370	0.362	0.354	0.361	0.365	0.352	0.367	0.364	0.367	0.363	0.367	0.362
210	0.369	0.361	0.354	0.351	0.364	0.351	0.354	0.354	0.357	0.347	0.348	0.354
240	0.370	0.358	0.372	0.357	0.370	0.350	0.371	0.354	0.363	0.356	0.360	0.360
270	0.345	0.364	0.359	0.346	0.368	0.369	0.364	0.353	0.370	0.345	0.351	0.344
300	0.351	0.350	0.369	0.374	0.375	0.361	0.354	0.353	0.357	0.352	0.347	0.361
330	0.366	0.360	0.368	0.356	0.349	0.369	0.350	0.357	0.366	0.362	0.367	0.372

TABLE A.12: Shell Wall Thickness (in.) of GB12 Shell

$\theta \backslash L(\text{in.})$	13	39	65	91	117	143	169	195	221	247	273	299
0	0.352	0.365	0.353	0.361	0.366	0.348	0.349	0.369	0.369	0.355	0.366	0.346
30	0.356	0.349	0.375	0.364	0.360	0.354	0.355	0.355	0.374	0.345	0.350	0.354
60	0.361	0.350	0.371	0.351	0.352	0.369	0.348	0.364	0.370	0.350	0.354	0.348
90	0.372	0.375	0.359	0.374	0.356	0.363	0.363	0.353	0.374	0.355	0.356	0.358
120	0.352	0.349	0.364	0.359	0.369	0.347	0.349	0.361	0.355	0.352	0.358	0.370
150	0.371	0.373	0.364	0.369	0.348	0.369	0.360	0.354	0.344	0.345	0.353	0.351
180	0.372	0.371	0.371	0.371	0.353	0.366	0.345	0.356	0.363	0.353	0.361	0.358
210	0.371	0.352	0.371	0.348	0.356	0.355	0.350	0.349	0.374	0.367	0.361	0.365
240	0.351	0.365	0.373	0.347	0.366	0.364	0.375	0.349	0.372	0.369	0.362	0.363
270	0.358	0.375	0.345	0.374	0.375	0.359	0.345	0.345	0.345	0.358	0.355	0.352
300	0.345	0.363	0.371	0.367	0.368	0.354	0.368	0.352	0.345	0.357	0.356	0.371
330	0.366	0.366	0.367	0.348	0.351	0.369	0.346	0.345	0.344	0.350	0.351	0.350

TABLE A.13: Shell Wall Thickness (in.) of GB13 Shell

$\theta \backslash L(\text{in.})$	13	39	65	91	117	143	169	195	221	247	273	299
0	0.354	0.353	0.365	0.365	0.375	0.366	0.369	0.373	0.359	0.357	0.362	0.345
30	0.362	0.346	0.372	0.357	0.355	0.352	0.347	0.362	0.358	0.368	0.358	0.344
60	0.352	0.363	0.365	0.365	0.345	0.365	0.370	0.363	0.373	0.359	0.371	0.366
90	0.356	0.344	0.356	0.361	0.347	0.346	0.371	0.357	0.349	0.365	0.368	0.359
120	0.357	0.358	0.357	0.349	0.352	0.356	0.368	0.349	0.349	0.363	0.353	0.354
150	0.371	0.350	0.357	0.364	0.352	0.375	0.361	0.350	0.371	0.353	0.358	0.353
180	0.370	0.345	0.348	0.366	0.356	0.372	0.373	0.354	0.347	0.350	0.359	0.368
210	0.355	0.355	0.372	0.356	0.372	0.372	0.373	0.371	0.363	0.364	0.345	0.350
240	0.363	0.362	0.357	0.354	0.362	0.351	0.350	0.345	0.356	0.375	0.359	0.357
270	0.351	0.345	0.351	0.369	0.359	0.358	0.348	0.345	0.367	0.349	0.363	0.357
300	0.361	0.356	0.365	0.368	0.360	0.350	0.344	0.362	0.360	0.346	0.350	0.353
330	0.357	0.367	0.358	0.370	0.360	0.346	0.363	0.372	0.373	0.354	0.351	0.373

TABLE A.14: Shell Wall Thickness (in.) of GB14 Shell

$\theta \backslash L(\text{in.})$	13	39	65	91	117	143	169	195	221	247	273	299
0	0.352	0.375	0.362	0.346	0.370	0.375	0.348	0.374	0.360	0.371	0.362	0.366
30	0.348	0.367	0.371	0.374	0.371	0.362	0.357	0.372	0.353	0.370	0.352	0.357
60	0.352	0.360	0.350	0.350	0.363	0.364	0.365	0.363	0.348	0.348	0.363	0.373
90	0.355	0.361	0.364	0.371	0.345	0.349	0.366	0.354	0.352	0.363	0.371	0.352
120	0.352	0.365	0.361	0.349	0.363	0.373	0.346	0.345	0.350	0.368	0.351	0.350
150	0.362	0.347	0.345	0.361	0.357	0.362	0.358	0.358	0.360	0.348	0.372	0.370
180	0.352	0.363	0.366	0.375	0.358	0.352	0.374	0.353	0.368	0.367	0.345	0.358
210	0.348	0.361	0.349	0.348	0.370	0.351	0.374	0.349	0.364	0.373	0.368	0.356
240	0.361	0.375	0.366	0.347	0.360	0.352	0.353	0.359	0.362	0.365	0.359	0.375
270	0.351	0.367	0.358	0.365	0.350	0.372	0.361	0.361	0.350	0.361	0.372	0.345
300	0.359	0.367	0.356	0.353	0.370	0.355	0.350	0.358	0.356	0.357	0.362	0.374
330	0.347	0.359	0.359	0.349	0.374	0.345	0.350	0.357	0.350	0.350	0.370	0.352

TABLE A.15: Shell Wall Thickness (in.) of GB15 Shell

$\theta \backslash L(\text{in.})$	13	39	65	91	117	143	169	195	221	247	273	299
0	0.362	0.374	0.347	0.346	0.349	0.362	0.369	0.367	0.354	0.369	0.367	0.356
30	0.350	0.349	0.367	0.354	0.359	0.357	0.357	0.359	0.352	0.362	0.372	0.345
60	0.350	0.367	0.363	0.363	0.367	0.360	0.369	0.357	0.344	0.374	0.365	0.362
90	0.368	0.364	0.363	0.368	0.371	0.363	0.349	0.361	0.364	0.364	0.355	0.345
120	0.370	0.355	0.357	0.369	0.356	0.370	0.369	0.374	0.359	0.351	0.361	0.364
150	0.351	0.350	0.369	0.369	0.345	0.358	0.367	0.363	0.363	0.366	0.358	0.363
180	0.365	0.372	0.345	0.361	0.344	0.349	0.362	0.349	0.346	0.350	0.363	0.352
210	0.352	0.364	0.361	0.361	0.373	0.372	0.373	0.345	0.364	0.374	0.349	0.373
240	0.345	0.349	0.360	0.373	0.374	0.356	0.358	0.358	0.358	0.346	0.353	0.366
270	0.369	0.367	0.369	0.352	0.371	0.364	0.361	0.361	0.353	0.365	0.366	0.352
300	0.354	0.371	0.345	0.358	0.352	0.375	0.352	0.375	0.350	0.362	0.361	0.375
330	0.348	0.370	0.363	0.371	0.366	0.358	0.352	0.347	0.363	0.351	0.352	0.357

TABLE A.16: Shell Wall Thickness (in.) of GB16 Shell

$\theta \backslash L(\text{in.})$	13	39	65	91	117	143	169	195	221	247	273	299
0	0.346	0.369	0.369	0.360	0.351	0.359	0.370	0.361	0.363	0.367	0.362	0.369
30	0.367	0.371	0.345	0.349	0.355	0.360	0.369	0.353	0.363	0.346	0.355	0.374
60	0.366	0.345	0.346	0.365	0.374	0.375	0.354	0.368	0.350	0.363	0.347	0.353
90	0.366	0.357	0.367	0.352	0.358	0.353	0.356	0.372	0.370	0.354	0.350	0.354
120	0.366	0.359	0.365	0.368	0.362	0.359	0.349	0.347	0.358	0.372	0.371	0.356
150	0.365	0.372	0.367	0.354	0.352	0.349	0.365	0.359	0.358	0.367	0.359	0.373
180	0.360	0.351	0.361	0.350	0.357	0.368	0.348	0.365	0.354	0.370	0.363	0.373
210	0.373	0.366	0.350	0.374	0.349	0.366	0.363	0.361	0.349	0.349	0.365	0.364
240	0.358	0.366	0.374	0.365	0.369	0.369	0.353	0.353	0.354	0.366	0.373	0.356
270	0.349	0.353	0.374	0.345	0.368	0.351	0.348	0.363	0.361	0.352	0.350	0.372
300	0.362	0.368	0.360	0.354	0.350	0.348	0.349	0.351	0.353	0.362	0.374	0.356
330	0.346	0.374	0.367	0.344	0.346	0.349	0.358	0.365	0.350	0.373	0.370	0.370

TABLE A.17: Shell Wall Thickness (in.) of GB17 Shell

$\theta \backslash L(\text{in.})$	13	39	65	91	117	143	169	195	221	247	273	299
0	0.373	0.357	0.365	0.362	0.367	0.349	0.364	0.344	0.362	0.362	0.375	0.348
30	0.353	0.347	0.373	0.372	0.351	0.357	0.344	0.372	0.357	0.374	0.350	0.345
60	0.356	0.345	0.361	0.345	0.368	0.367	0.349	0.352	0.348	0.366	0.371	0.363
90	0.360	0.350	0.363	0.360	0.367	0.352	0.368	0.351	0.361	0.358	0.358	0.365
120	0.366	0.359	0.360	0.350	0.359	0.367	0.369	0.346	0.374	0.349	0.353	0.357
150	0.360	0.348	0.358	0.365	0.370	0.370	0.347	0.371	0.345	0.364	0.347	0.371
180	0.346	0.368	0.361	0.361	0.375	0.354	0.373	0.358	0.368	0.367	0.351	0.335
210	0.361	0.372	0.352	0.375	0.362	0.360	0.374	0.373	0.346	0.347	0.374	0.359
240	0.364	0.366	0.363	0.364	0.355	0.374	0.369	0.367	0.373	0.363	0.373	0.351
270	0.345	0.356	0.354	0.375	0.373	0.368	0.369	0.346	0.350	0.366	0.348	0.36
300	0.361	0.360	0.367	0.370	0.373	0.365	0.366	0.347	0.375	0.353	0.362	0.344
330	0.365	0.347	0.374	0.365	0.358	0.347	0.362	0.373	0.346	0.346	0.347	0.346

TABLE A.18: Shell Wall Thickness (in.) of GB18 Shell

$\theta \backslash L(\text{in.})$	13	39	65	91	117	143	169	195	221	247	273	299
0	0.370	0.350	0.346	0.373	0.370	0.358	0.347	0.352	0.368	0.363	0.353	0.372
30	0.347	0.369	0.351	0.358	0.361	0.350	0.345	0.360	0.353	0.362	0.366	0.364
60	0.362	0.353	0.374	0.349	0.363	0.351	0.352	0.355	0.350	0.366	0.369	0.346
90	0.360	0.360	0.346	0.373	0.372	0.365	0.368	0.362	0.365	0.373	0.353	0.373
120	0.348	0.347	0.358	0.363	0.373	0.371	0.365	0.370	0.351	0.365	0.352	0.352
150	0.370	0.359	0.352	0.347	0.349	0.355	0.361	0.351	0.375	0.359	0.346	0.345
180	0.362	0.362	0.351	0.350	0.372	0.371	0.348	0.345	0.364	0.374	0.363	0.350
210	0.363	0.361	0.349	0.353	0.357	0.355	0.347	0.364	0.354	0.363	0.372	0.362
240	0.368	0.363	0.357	0.360	0.351	0.370	0.357	0.374	0.357	0.349	0.349	0.371
270	0.369	0.363	0.371	0.371	0.374	0.348	0.371	0.369	0.345	0.345	0.375	0.350
300	0.360	0.372	0.356	0.371	0.368	0.360	0.363	0.356	0.359	0.360	0.347	0.365
330	0.368	0.366	0.360	0.349	0.358	0.359	0.363	0.373	0.362	0.358	0.366	0.370

TABLE A.19: Shell Wall Thickness (in.) of GB19 Shell

$\theta \backslash L(\text{in.})$	13	39	65	91	117	143	169	195	221	247	273	299
0	0.370	0.374	0.367	0.361	0.374	0.363	0.357	0.368	0.350	0.363	0.350	0.346
30	0.374	0.358	0.357	0.361	0.356	0.363	0.363	0.374	0.361	0.372	0.368	0.373
60	0.365	0.352	0.350	0.361	0.368	0.372	0.355	0.359	0.365	0.344	0.365	0.375
90	0.355	0.373	0.345	0.373	0.351	0.372	0.346	0.350	0.349	0.370	0.348	0.374
120	0.366	0.361	0.356	0.373	0.347	0.361	0.350	0.369	0.371	0.362	0.364	0.367
150	0.362	0.352	0.348	0.359	0.353	0.350	0.349	0.364	0.363	0.374	0.367	0.368
180	0.350	0.366	0.366	0.364	0.351	0.355	0.370	0.371	0.374	0.358	0.370	0.365
210	0.369	0.349	0.358	0.365	0.347	0.358	0.352	0.351	0.375	0.362	0.357	0.350
240	0.360	0.352	0.366	0.356	0.361	0.367	0.374	0.361	0.356	0.349	0.372	0.355
270	0.361	0.350	0.355	0.375	0.349	0.368	0.350	0.357	0.364	0.373	0.373	0.367
300	0.364	0.367	0.349	0.350	0.369	0.356	0.358	0.372	0.370	0.346	0.347	0.347
330	0.357	0.355	0.369	0.372	0.369	0.362	0.364	0.371	0.351	0.349	0.359	0.346

TABLE A.20: Shell Wall Thickness (in.) of GB20 Shell

$\theta \backslash L(\text{in.})$	13	39	65	91	117	143	169	195	221	247	273	299
0	0.354	0.371	0.372	0.371	0.347	0.354	0.352	0.357	0.351	0.364	0.370	0.344
30	0.359	0.354	0.364	0.358	0.361	0.347	0.346	0.371	0.348	0.362	0.345	0.363
60	0.373	0.354	0.372	0.361	0.359	0.347	0.351	0.344	0.367	0.373	0.349	0.366
90	0.367	0.352	0.362	0.350	0.349	0.359	0.358	0.358	0.352	0.355	0.359	0.373
120	0.361	0.358	0.366	0.360	0.360	0.371	0.349	0.369	0.374	0.358	0.368	0.349
150	0.351	0.357	0.364	0.354	0.373	0.360	0.368	0.371	0.369	0.358	0.350	0.347
180	0.372	0.346	0.344	0.353	0.345	0.364	0.375	0.355	0.365	0.375	0.371	0.372
210	0.374	0.354	0.369	0.349	0.350	0.348	0.370	0.356	0.357	0.346	0.365	0.368
240	0.371	0.372	0.351	0.367	0.369	0.356	0.365	0.357	0.367	0.368	0.370	0.348
270	0.345	0.347	0.346	0.357	0.358	0.368	0.356	0.348	0.349	0.370	0.365	0.363
300	0.345	0.368	0.362	0.360	0.347	0.374	0.369	0.352	0.348	0.359	0.347	0.372
330	0.370	0.368	0.355	0.360	0.358	0.370	0.372	0.374	0.361	0.354	0.358	0.366

TABLE A.21: Shell Wall Thickness (in.) of GB21 Shell

$\theta \backslash L(\text{in.})$	13	39	65	91	117	143	169	195	221	247	273	299
0	0.350	0.361	0.349	0.366	0.361	0.363	0.365	0.361	0.363	0.353	0.365	0.358
30	0.370	0.352	0.366	0.350	0.356	0.368	0.357	0.356	0.365	0.373	0.364	0.347
60	0.358	0.368	0.368	0.356	0.370	0.346	0.356	0.347	0.359	0.364	0.370	0.357
90	0.362	0.359	0.374	0.361	0.353	0.345	0.373	0.370	0.352	0.373	0.345	0.375
120	0.350	0.368	0.348	0.347	0.350	0.352	0.370	0.344	0.375	0.351	0.353	0.350
150	0.372	0.360	0.347	0.372	0.361	0.348	0.372	0.354	0.350	0.374	0.347	0.362
180	0.365	0.357	0.347	0.356	0.349	0.360	0.361	0.365	0.367	0.356	0.360	0.346
210	0.347	0.371	0.346	0.372	0.355	0.374	0.358	0.344	0.374	0.355	0.373	0.373
240	0.353	0.353	0.350	0.359	0.371	0.373	0.350	0.375	0.372	0.365	0.347	0.345
270	0.364	0.369	0.345	0.370	0.359	0.344	0.363	0.371	0.357	0.359	0.366	0.374
300	0.365	0.361	0.349	0.356	0.363	0.369	0.347	0.345	0.352	0.354	0.359	0.363
330	0.353	0.372	0.372	0.368	0.357	0.372	0.372	0.368	0.357	0.354	0.366	0.346

TABLE A.22: Shell Wall Thickness (in.) of GB22 Shell

$\theta \backslash L(\text{in.})$	13	39	65	91	117	143	169	195	221	247	273	299
0	0.366	0.374	0.358	0.353	0.344	0.373	0.348	0.369	0.363	0.358	0.367	0.363
30	0.369	0.367	0.345	0.355	0.374	0.354	0.355	0.355	0.359	0.372	0.361	0.359
60	0.355	0.367	0.354	0.351	0.372	0.374	0.358	0.372	0.372	0.354	0.350	0.349
90	0.372	0.364	0.363	0.372	0.357	0.357	0.363	0.345	0.363	0.346	0.364	0.363
120	0.359	0.374	0.371	0.370	0.360	0.363	0.369	0.346	0.367	0.352	0.354	0.372
150	0.358	0.369	0.357	0.375	0.346	0.360	0.365	0.347	0.344	0.351	0.371	0.361
180	0.356	0.359	0.367	0.349	0.359	0.365	0.352	0.347	0.371	0.352	0.363	0.354
210	0.354	0.368	0.352	0.352	0.360	0.362	0.369	0.348	0.352	0.369	0.365	0.357
240	0.362	0.357	0.349	0.374	0.348	0.373	0.360	0.345	0.363	0.371	0.350	0.354
270	0.357	0.363	0.372	0.360	0.359	0.370	0.367	0.348	0.372	0.370	0.348	0.360
300	0.357	0.362	0.351	0.353	0.349	0.356	0.365	0.363	0.346	0.346	0.362	0.363
330	0.355	0.367	0.352	0.362	0.374	0.361	0.348	0.373	0.366	0.363	0.361	0.357

TABLE A.23: Shell Wall Thickness (in.) of GB23 Shell

$\theta \backslash L(\text{in.})$	13	39	65	91	117	143	169	195	221	247	273	299
0	0.360	0.361	0.351	0.353	0.364	0.352	0.359	0.354	0.369	0.359	0.353	0.346
30	0.373	0.344	0.367	0.351	0.344	0.349	0.349	0.353	0.359	0.348	0.352	0.359
60	0.362	0.354	0.345	0.349	0.362	0.369	0.368	0.358	0.372	0.374	0.363	0.344
90	0.373	0.346	0.346	0.356	0.358	0.362	0.367	0.373	0.344	0.358	0.354	0.353
120	0.370	0.370	0.357	0.353	0.353	0.352	0.349	0.344	0.361	0.353	0.355	0.370
150	0.354	0.350	0.349	0.349	0.352	0.368	0.372	0.373	0.350	0.361	0.359	0.374
180	0.367	0.372	0.366	0.367	0.366	0.367	0.371	0.363	0.369	0.350	0.369	0.366
210	0.374	0.347	0.361	0.364	0.364	0.370	0.369	0.373	0.345	0.374	0.359	0.348
240	0.375	0.370	0.347	0.372	0.351	0.355	0.348	0.367	0.345	0.368	0.344	0.364
270	0.345	0.355	0.373	0.360	0.356	0.357	0.355	0.350	0.366	0.346	0.363	0.366
300	0.346	0.353	0.347	0.363	0.361	0.347	0.368	0.358	0.351	0.345	0.363	0.353
330	0.363	0.361	0.358	0.374	0.358	0.365	0.355	0.350	0.361	0.370	0.359	0.353

TABLE A.24: Shell Wall Thickness (in.) of GB24 Shell

$\theta \backslash L(\text{in.})$	13	39	65	91	117	143	169	195	221	247	273	299
0	0.366	0.347	0.353	0.368	0.375	0.368	0.346	0.364	0.350	0.349	0.347	0.368
30	0.356	0.370	0.362	0.368	0.371	0.354	0.371	0.355	0.351	0.370	0.375	0.358
60	0.345	0.361	0.352	0.349	0.367	0.361	0.365	0.366	0.354	0.359	0.356	0.370
90	0.375	0.347	0.345	0.354	0.359	0.365	0.369	0.358	0.351	0.373	0.350	0.368
120	0.374	0.364	0.370	0.356	0.367	0.371	0.352	0.352	0.346	0.360	0.353	0.370
150	0.365	0.351	0.363	0.362	0.358	0.365	0.345	0.350	0.353	0.373	0.365	0.357
180	0.358	0.351	0.365	0.347	0.358	0.349	0.375	0.352	0.348	0.364	0.366	0.350
210	0.359	0.348	0.351	0.365	0.374	0.365	0.358	0.367	0.350	0.360	0.347	0.347
240	0.350	0.357	0.356	0.356	0.353	0.360	0.371	0.365	0.369	0.350	0.372	0.346
270	0.370	0.363	0.349	0.357	0.368	0.358	0.362	0.371	0.365	0.350	0.363	0.364
300	0.354	0.374	0.373	0.366	0.357	0.351	0.362	0.368	0.358	0.359	0.365	0.370
330	0.374	0.365	0.365	0.350	0.356	0.356	0.359	0.359	0.349	0.371	0.345	0.355

TABLE A.25: Shell Wall Thickness (in.) of GB25 Shell

$\theta \backslash L(\text{in.})$	13	39	65	91	117	143	169	195	221	247	273	299
0	0.367	0.370	0.369	0.348	0.344	0.350	0.359	0.364	0.351	0.364	0.354	0.348
30	0.373	0.367	0.344	0.362	0.363	0.361	0.347	0.354	0.344	0.375	0.363	0.358
60	0.357	0.352	0.351	0.347	0.348	0.347	0.358	0.360	0.370	0.367	0.366	0.359
90	0.364	0.355	0.357	0.347	0.367	0.374	0.356	0.368	0.351	0.362	0.362	0.373
120	0.375	0.374	0.357	0.361	0.358	0.361	0.345	0.364	0.355	0.359	0.359	0.352
150	0.353	0.349	0.364	0.345	0.363	0.365	0.349	0.372	0.361	0.345	0.366	0.349
180	0.345	0.371	0.349	0.349	0.353	0.355	0.348	0.373	0.354	0.375	0.368	0.363
210	0.359	0.354	0.369	0.350	0.369	0.353	0.373	0.347	0.369	0.356	0.358	0.362
240	0.351	0.358	0.370	0.375	0.370	0.351	0.375	0.372	0.372	0.356	0.361	0.345
270	0.371	0.360	0.350	0.362	0.371	0.356	0.353	0.365	0.352	0.369	0.350	0.345
300	0.370	0.372	0.370	0.368	0.355	0.374	0.347	0.367	0.351	0.363	0.369	0.358
330	0.354	0.364	0.351	0.365	0.359	0.373	0.360	0.374	0.375	0.363	0.346	0.357

TABLE A.26: Shell Wall Thickness (in.) of GB26 Shell

$\theta \backslash L(\text{in.})$	13	39	65	91	117	143	169	195	221	247	273	299
0	0.344	0.344	0.371	0.359	0.359	0.367	0.358	0.347	0.367	0.347	0.350	0.365
30	0.350	0.360	0.368	0.367	0.366	0.353	0.374	0.354	0.361	0.347	0.361	0.354
60	0.362	0.363	0.375	0.358	0.349	0.365	0.367	0.353	0.358	0.373	0.352	0.353
90	0.355	0.349	0.363	0.367	0.348	0.366	0.350	0.348	0.366	0.372	0.363	0.347
120	0.370	0.358	0.352	0.363	0.365	0.348	0.370	0.370	0.358	0.351	0.362	0.370
150	0.349	0.346	0.370	0.367	0.357	0.370	0.360	0.363	0.362	0.357	0.359	0.349
180	0.366	0.368	0.356	0.362	0.374	0.360	0.345	0.352	0.363	0.363	0.367	0.346
210	0.353	0.360	0.365	0.349	0.349	0.357	0.362	0.344	0.360	0.358	0.363	0.364
240	0.347	0.371	0.344	0.357	0.369	0.373	0.360	0.369	0.366	0.363	0.369	0.361
270	0.349	0.374	0.353	0.360	0.350	0.361	0.370	0.351	0.350	0.370	0.362	0.357
300	0.375	0.361	0.362	0.367	0.369	0.359	0.364	0.361	0.350	0.363	0.372	0.358
330	0.348	0.358	0.370	0.349	0.349	0.370	0.370	0.348	0.358	0.362	0.367	0.349

TABLE A.27: Shell Wall Thickness (in.) of GB27 Shell

$\theta \backslash L(\text{in.})$	13	39	65	91	117	143	169	195	221	247	273	299
0	0.367	0.365	0.374	0.349	0.354	0.372	0.362	0.360	0.351	0.349	0.369	0.362
30	0.370	0.359	0.349	0.355	0.369	0.349	0.365	0.348	0.372	0.371	0.346	0.363
60	0.371	0.359	0.348	0.355	0.353	0.373	0.358	0.367	0.372	0.350	0.362	0.346
90	0.353	0.360	0.374	0.369	0.372	0.345	0.344	0.345	0.346	0.364	0.350	0.352
120	0.348	0.365	0.345	0.360	0.367	0.354	0.363	0.364	0.349	0.372	0.364	0.372
150	0.368	0.363	0.346	0.369	0.355	0.356	0.362	0.347	0.368	0.373	0.363	0.367
180	0.363	0.344	0.348	0.348	0.351	0.373	0.351	0.373	0.351	0.349	0.358	0.356
210	0.346	0.347	0.371	0.356	0.351	0.361	0.344	0.353	0.344	0.362	0.356	0.372
240	0.364	0.371	0.366	0.348	0.361	0.365	0.347	0.374	0.348	0.373	0.362	0.356
270	0.347	0.367	0.344	0.346	0.346	0.352	0.371	0.353	0.354	0.362	0.373	0.355
300	0.351	0.356	0.366	0.362	0.360	0.360	0.369	0.355	0.345	0.352	0.356	0.367
330	0.373	0.361	0.351	0.361	0.347	0.356	0.365	0.351	0.350	0.355	0.350	0.367

TABLE A.28: Shell Wall Thickness (in.) of GB28 Shell

$\theta \backslash L(\text{in.})$	13	39	65	91	117	143	169	195	221	247	273	299
0	0.350	0.366	0.351	0.345	0.368	0.368	0.356	0.361	0.358	0.357	0.366	0.364
30	0.365	0.366	0.359	0.371	0.371	0.366	0.351	0.346	0.355	0.352	0.368	0.362
60	0.355	0.364	0.358	0.356	0.366	0.347	0.351	0.352	0.357	0.364	0.363	0.360
90	0.347	0.347	0.363	0.363	0.372	0.371	0.374	0.371	0.344	0.345	0.365	0.358
120	0.350	0.346	0.356	0.371	0.361	0.354	0.345	0.347	0.368	0.348	0.362	0.373
150	0.364	0.358	0.370	0.362	0.368	0.359	0.349	0.366	0.347	0.361	0.361	0.352
180	0.365	0.367	0.363	0.369	0.350	0.350	0.344	0.371	0.365	0.358	0.352	0.367
210	0.346	0.365	0.346	0.362	0.369	0.375	0.364	0.353	0.349	0.353	0.359	0.363
240	0.345	0.356	0.371	0.362	0.370	0.364	0.357	0.364	0.346	0.355	0.365	0.364
270	0.354	0.346	0.353	0.365	0.363	0.349	0.347	0.370	0.345	0.363	0.363	0.361
300	0.348	0.349	0.345	0.344	0.363	0.353	0.366	0.371	0.364	0.375	0.369	0.358
330	0.346	0.354	0.356	0.355	0.352	0.370	0.364	0.372	0.372	0.349	0.375	0.375

TABLE A.29: Shell Wall Thickness (in.) of GB29 Shell

$\theta \backslash L(\text{in.})$	13	39	65	91	117	143	169	195	221	247	273	299
0	0.363	0.364	0.362	0.368	0.361	0.355	0.351	0.353	0.360	0.354	0.369	0.358
30	0.349	0.367	0.367	0.344	0.360	0.369	0.371	0.374	0.367	0.350	0.348	0.355
60	0.354	0.374	0.365	0.357	0.366	0.374	0.370	0.366	0.351	0.348	0.345	0.359
90	0.364	0.355	0.369	0.358	0.367	0.353	0.345	0.364	0.368	0.372	0.367	0.357
120	0.357	0.372	0.375	0.367	0.372	0.371	0.350	0.367	0.361	0.351	0.372	0.345
150	0.365	0.358	0.350	0.361	0.369	0.347	0.358	0.348	0.370	0.361	0.368	0.363
180	0.359	0.371	0.356	0.373	0.356	0.348	0.372	0.356	0.361	0.357	0.364	0.357
210	0.369	0.345	0.362	0.371	0.346	0.354	0.361	0.372	0.371	0.371	0.365	0.356
240	0.344	0.373	0.374	0.359	0.344	0.369	0.360	0.345	0.351	0.352	0.360	0.344
270	0.356	0.349	0.356	0.367	0.367	0.369	0.375	0.358	0.356	0.365	0.352	0.371
300	0.370	0.348	0.348	0.352	0.349	0.372	0.371	0.351	0.345	0.374	0.364	0.366
330	0.372	0.348	0.345	0.369	0.365	0.352	0.349	0.349	0.356	0.368	0.352	0.363

TABLE A.30: Shell Wall Thickness (in.) of GB30 Shell

$\theta \backslash L(\text{in.})$	13	39	65	91	117	143	169	195	221	247	273	299
0	0.364	0.352	0.372	0.349	0.351	0.353	0.359	0.365	0.358	0.366	0.351	0.374
30	0.360	0.366	0.351	0.347	0.368	0.351	0.365	0.372	0.346	0.371	0.364	0.366
60	0.353	0.348	0.374	0.365	0.361	0.363	0.355	0.362	0.367	0.356	0.371	0.347
90	0.369	0.371	0.356	0.359	0.348	0.351	0.368	0.347	0.364	0.359	0.357	0.358
120	0.371	0.351	0.354	0.364	0.357	0.363	0.344	0.367	0.351	0.368	0.374	0.346
150	0.358	0.354	0.363	0.370	0.349	0.362	0.367	0.359	0.375	0.354	0.355	0.348
180	0.358	0.363	0.353	0.371	0.351	0.366	0.369	0.369	0.372	0.355	0.363	0.367
210	0.356	0.374	0.372	0.374	0.351	0.366	0.366	0.355	0.372	0.347	0.372	0.344
240	0.361	0.356	0.354	0.366	0.366	0.366	0.361	0.375	0.363	0.375	0.351	0.374
270	0.370	0.351	0.358	0.356	0.364	0.348	0.347	0.373	0.367	0.356	0.360	0.367
300	0.344	0.362	0.357	0.370	0.354	0.356	0.347	0.364	0.367	0.357	0.362	0.365
330	0.345	0.345	0.348	0.367	0.349	0.371	0.349	0.349	0.357	0.352	0.360	0.365

TABLE A.31: Shell Wall Thickness (in.) of GB31 Shell

$\theta \backslash L(\text{in.})$	13	39	65	91	117	143	169	195	221	247	273	299
0	0.347	0.373	0.359	0.363	0.370	0.349	0.371	0.365	0.370	0.361	0.349	0.375
30	0.345	0.344	0.357	0.353	0.357	0.346	0.366	0.370	0.347	0.355	0.374	0.348
60	0.352	0.346	0.357	0.358	0.367	0.374	0.373	0.352	0.372	0.372	0.350	0.366
90	0.351	0.357	0.362	0.351	0.347	0.358	0.347	0.371	0.372	0.355	0.345	0.353
120	0.371	0.363	0.354	0.360	0.370	0.350	0.346	0.374	0.374	0.351	0.345	0.360
150	0.345	0.357	0.373	0.344	0.355	0.359	0.356	0.351	0.354	0.346	0.347	0.360
180	0.346	0.363	0.357	0.368	0.347	0.352	0.360	0.350	0.372	0.352	0.362	0.370
210	0.347	0.344	0.368	0.374	0.350	0.353	0.348	0.350	0.357	0.348	0.351	0.347
240	0.374	0.356	0.349	0.372	0.372	0.369	0.346	0.374	0.352	0.363	0.353	0.373
270	0.371	0.354	0.347	0.351	0.354	0.364	0.372	0.367	0.360	0.350	0.357	0.359
300	0.356	0.370	0.359	0.359	0.355	0.344	0.367	0.365	0.369	0.368	0.352	0.372
330	0.364	0.350	0.354	0.357	0.352	0.353	0.347	0.373	0.359	0.364	0.360	0.355

TABLE A.32: Shell Wall Thickness (in.) of GB32 Shell

$\theta \backslash L(\text{in.})$	13	39	65	91	117	143	169	195	221	247	273	299
0	0.346	0.354	0.354	0.356	0.367	0.372	0.373	0.347	0.363	0.348	0.346	0.353
30	0.371	0.350	0.363	0.374	0.367	0.363	0.353	0.351	0.373	0.367	0.356	0.351
60	0.372	0.373	0.359	0.358	0.355	0.369	0.360	0.350	0.366	0.351	0.367	0.353
90	0.349	0.352	0.352	0.360	0.369	0.369	0.372	0.372	0.346	0.348	0.362	0.371
120	0.362	0.371	0.346	0.369	0.357	0.347	0.345	0.346	0.344	0.358	0.361	0.370
150	0.349	0.350	0.358	0.367	0.347	0.374	0.353	0.366	0.375	0.363	0.350	0.362
180	0.370	0.367	0.364	0.346	0.363	0.359	0.352	0.361	0.353	0.363	0.350	0.358
210	0.371	0.356	0.352	0.375	0.354	0.362	0.355	0.347	0.348	0.353	0.354	0.369
240	0.374	0.364	0.363	0.364	0.359	0.371	0.369	0.368	0.350	0.371	0.370	0.374
270	0.366	0.367	0.347	0.372	0.361	0.375	0.354	0.354	0.356	0.349	0.371	0.347
300	0.369	0.356	0.359	0.372	0.366	0.356	0.374	0.348	0.365	0.374	0.358	0.362
330	0.374	0.374	0.366	0.359	0.356	0.356	0.373	0.354	0.366	0.362	0.345	0.362

TABLE A.33: Shell Wall Thickness (in.) of GB33 Shell

$\theta \backslash L(\text{in.})$	13	39	65	91	117	143	169	195	221	247	273	299
0	0.362	0.363	0.365	0.344	0.363	0.370	0.363	0.349	0.358	0.350	0.363	0.364
30	0.368	0.356	0.373	0.369	0.371	0.359	0.346	0.346	0.371	0.350	0.374	0.347
60	0.371	0.372	0.352	0.348	0.351	0.373	0.366	0.360	0.361	0.368	0.374	0.363
90	0.374	0.369	0.350	0.356	0.351	0.347	0.353	0.344	0.352	0.374	0.346	0.345
120	0.357	0.373	0.349	0.346	0.364	0.357	0.354	0.361	0.364	0.364	0.357	0.374
150	0.355	0.350	0.366	0.345	0.368	0.375	0.360	0.370	0.374	0.357	0.356	0.346
180	0.354	0.360	0.361	0.355	0.360	0.345	0.373	0.355	0.348	0.356	0.353	0.369
210	0.368	0.370	0.375	0.351	0.357	0.348	0.371	0.348	0.371	0.368	0.346	0.372
240	0.346	0.365	0.363	0.367	0.375	0.355	0.373	0.361	0.367	0.365	0.362	0.366
270	0.356	0.356	0.360	0.358	0.345	0.345	0.354	0.368	0.369	0.359	0.354	0.363
300	0.358	0.374	0.370	0.370	0.347	0.368	0.357	0.372	0.348	0.347	0.373	0.353
330	0.362	0.352	0.361	0.354	0.354	0.368	0.363	0.350	0.373	0.350	0.345	0.363

TABLE A.34: Shell Wall Thickness (in.) of GB34 Shell

$\theta \backslash L(\text{in.})$	13	39	65	91	117	143	169	195	221	247	273	299
0	0.370	0.345	0.355	0.349	0.356	0.360	0.356	0.358	0.362	0.368	0.350	0.345
30	0.364	0.367	0.349	0.354	0.350	0.362	0.350	0.351	0.365	0.352	0.368	0.357
60	0.374	0.354	0.359	0.345	0.346	0.372	0.345	0.368	0.371	0.352	0.367	0.352
90	0.346	0.372	0.356	0.353	0.354	0.351	0.368	0.357	0.357	0.367	0.356	0.362
120	0.350	0.352	0.366	0.345	0.346	0.372	0.355	0.350	0.371	0.345	0.360	0.373
150	0.370	0.346	0.356	0.370	0.359	0.363	0.362	0.358	0.348	0.374	0.353	0.356
180	0.371	0.352	0.375	0.363	0.368	0.364	0.369	0.345	0.355	0.344	0.371	0.364
210	0.361	0.345	0.355	0.365	0.364	0.369	0.352	0.349	0.372	0.365	0.369	0.368
240	0.345	0.361	0.351	0.359	0.357	0.362	0.354	0.375	0.358	0.357	0.357	0.354
270	0.358	0.358	0.372	0.365	0.371	0.365	0.358	0.370	0.344	0.347	0.362	0.348
300	0.357	0.345	0.357	0.367	0.354	0.348	0.359	0.361	0.361	0.355	0.374	0.355
330	0.347	0.349	0.353	0.361	0.346	0.345	0.360	0.365	0.369	0.369	0.360	0.355

TABLE A.35: Shell Wall Thickness (in.) of GB35 Shell

$\theta \backslash L(\text{in.})$	13	39	65	91	117	143	169	195	221	247	273	299
0	0.372	0.371	0.349	0.357	0.364	0.366	0.361	0.374	0.345	0.347	0.361	0.375
30	0.358	0.360	0.371	0.368	0.373	0.352	0.360	0.352	0.369	0.361	0.371	0.373
60	0.367	0.357	0.352	0.354	0.358	0.375	0.361	0.350	0.352	0.371	0.345	0.358
90	0.356	0.346	0.347	0.364	0.369	0.355	0.356	0.350	0.345	0.359	0.356	0.355
120	0.349	0.346	0.347	0.363	0.355	0.351	0.346	0.357	0.371	0.369	0.351	0.363
150	0.348	0.350	0.375	0.352	0.344	0.358	0.353	0.369	0.358	0.347	0.373	0.344
180	0.357	0.351	0.370	0.362	0.354	0.361	0.365	0.352	0.367	0.364	0.367	0.363
210	0.368	0.370	0.369	0.361	0.354	0.351	0.364	0.351	0.354	0.354	0.357	0.347
240	0.359	0.361	0.370	0.358	0.372	0.357	0.370	0.350	0.371	0.354	0.363	0.356
270	0.348	0.369	0.345	0.364	0.359	0.346	0.368	0.369	0.364	0.353	0.370	0.345
300	0.350	0.346	0.351	0.350	0.369	0.374	0.375	0.361	0.354	0.353	0.357	0.352
330	0.374	0.349	0.366	0.360	0.368	0.356	0.349	0.369	0.350	0.357	0.366	0.362

TABLE A.36: Shell Wall Thickness (in.) of GB36 Shell

$\theta \backslash L(\text{in.})$	13	39	65	91	117	143	169	195	221	247	273	299
0	0.351	0.370	0.352	0.365	0.353	0.361	0.366	0.348	0.349	0.369	0.369	0.355
30	0.370	0.361	0.356	0.349	0.375	0.364	0.360	0.354	0.355	0.355	0.374	0.345
60	0.366	0.355	0.361	0.350	0.371	0.351	0.352	0.369	0.348	0.364	0.370	0.350
90	0.346	0.374	0.372	0.375	0.359	0.374	0.356	0.363	0.363	0.353	0.374	0.355
120	0.372	0.372	0.352	0.349	0.364	0.359	0.369	0.347	0.349	0.361	0.355	0.352
150	0.355	0.365	0.371	0.373	0.364	0.369	0.348	0.369	0.360	0.354	0.344	0.345
180	0.367	0.362	0.372	0.371	0.371	0.371	0.353	0.366	0.345	0.356	0.363	0.353
210	0.348	0.354	0.371	0.352	0.371	0.348	0.356	0.355	0.350	0.349	0.374	0.367
240	0.360	0.360	0.351	0.365	0.373	0.347	0.366	0.364	0.375	0.349	0.372	0.369
270	0.351	0.344	0.358	0.375	0.345	0.374	0.375	0.359	0.345	0.345	0.345	0.358
300	0.347	0.361	0.345	0.363	0.371	0.367	0.368	0.354	0.368	0.352	0.345	0.357
330	0.367	0.372	0.366	0.366	0.367	0.348	0.351	0.369	0.346	0.345	0.344	0.350

TABLE A.37: Shell Wall Thickness (in.) of GB37 Shell

$\theta \backslash L(\text{in.})$	13	39	65	91	117	143	169	195	221	247	273	299
0	0.366	0.346	0.354	0.353	0.365	0.365	0.375	0.366	0.369	0.373	0.359	0.357
30	0.350	0.354	0.362	0.346	0.372	0.357	0.355	0.352	0.347	0.362	0.358	0.368
60	0.354	0.348	0.352	0.363	0.365	0.365	0.345	0.365	0.370	0.363	0.373	0.359
90	0.356	0.358	0.356	0.344	0.356	0.361	0.347	0.346	0.371	0.357	0.349	0.365
120	0.358	0.370	0.357	0.358	0.357	0.349	0.352	0.356	0.368	0.349	0.349	0.363
150	0.353	0.351	0.371	0.350	0.357	0.364	0.352	0.375	0.361	0.370	0.371	0.353
180	0.361	0.358	0.370	0.345	0.348	0.366	0.356	0.372	0.373	0.354	0.347	0.350
210	0.361	0.365	0.355	0.355	0.372	0.356	0.372	0.372	0.373	0.371	0.363	0.364
240	0.362	0.363	0.363	0.362	0.357	0.354	0.362	0.351	0.350	0.345	0.356	0.375
270	0.355	0.352	0.351	0.345	0.351	0.369	0.359	0.358	0.348	0.345	0.367	0.349
300	0.356	0.371	0.361	0.356	0.365	0.368	0.360	0.350	0.344	0.362	0.360	0.346
330	0.351	0.350	0.357	0.367	0.358	0.370	0.360	0.346	0.363	0.372	0.373	0.354

TABLE A.38: Shell Wall Thickness (in.) of GB38 Shell

$\theta \backslash L(\text{in.})$	13	39	65	91	117	143	169	195	221	247	273	299
0	0.362	0.345	0.352	0.375	0.362	0.346	0.370	0.375	0.348	0.374	0.360	0.371
30	0.358	0.344	0.348	0.367	0.371	0.374	0.371	0.362	0.357	0.372	0.353	0.370
60	0.371	0.366	0.352	0.360	0.350	0.350	0.363	0.364	0.365	0.363	0.348	0.348
90	0.368	0.359	0.355	0.361	0.364	0.371	0.345	0.349	0.366	0.354	0.352	0.363
120	0.353	0.354	0.352	0.365	0.361	0.349	0.363	0.373	0.346	0.345	0.350	0.368
150	0.358	0.353	0.362	0.347	0.345	0.361	0.357	0.362	0.358	0.358	0.360	0.348
180	0.359	0.368	0.352	0.363	0.366	0.375	0.358	0.352	0.374	0.353	0.368	0.367
210	0.345	0.350	0.348	0.361	0.349	0.348	0.370	0.351	0.374	0.349	0.364	0.373
240	0.359	0.357	0.361	0.375	0.366	0.347	0.360	0.352	0.353	0.359	0.362	0.365
270	0.363	0.357	0.351	0.367	0.358	0.365	0.350	0.372	0.361	0.361	0.350	0.361
300	0.350	0.353	0.359	0.367	0.356	0.353	0.370	0.355	0.350	0.358	0.356	0.357
330	0.351	0.373	0.347	0.359	0.359	0.349	0.374	0.345	0.350	0.357	0.350	0.350

TABLE A.39: Shell Wall Thickness (in.) of GB39 Shell

$\theta \backslash L(\text{in.})$	13	39	65	91	117	143	169	195	221	247	273	299
0	0.362	0.366	0.362	0.374	0.347	0.346	0.349	0.362	0.369	0.367	0.354	0.369
30	0.352	0.357	0.350	0.349	0.367	0.354	0.359	0.357	0.357	0.359	0.352	0.362
60	0.363	0.373	0.350	0.367	0.363	0.363	0.367	0.360	0.369	0.357	0.344	0.374
90	0.371	0.352	0.368	0.364	0.363	0.368	0.371	0.363	0.349	0.361	0.364	0.364
120	0.351	0.350	0.370	0.355	0.357	0.369	0.356	0.370	0.369	0.374	0.359	0.351
150	0.372	0.370	0.351	0.350	0.369	0.369	0.345	0.358	0.367	0.363	0.363	0.366
180	0.345	0.358	0.365	0.372	0.345	0.361	0.344	0.349	0.362	0.349	0.346	0.350
210	0.368	0.356	0.352	0.364	0.361	0.361	0.373	0.372	0.373	0.345	0.364	0.374
240	0.359	0.375	0.345	0.349	0.360	0.373	0.374	0.356	0.358	0.358	0.358	0.346
270	0.372	0.345	0.369	0.367	0.369	0.352	0.371	0.364	0.361	0.361	0.353	0.365
300	0.362	0.374	0.354	0.371	0.345	0.358	0.352	0.375	0.352	0.375	0.350	0.362
330	0.370	0.352	0.348	0.370	0.363	0.371	0.366	0.358	0.352	0.347	0.363	0.351

TABLE A.40: Shell Wall Thickness (in.) of GB40 Shell

$\theta \backslash L(\text{in.})$	13	39	65	91	117	143	169	195	221	247	273	299
0	0.367	0.356	0.346	0.369	0.369	0.360	0.351	0.359	0.370	0.361	0.363	0.367
30	0.372	0.345	0.367	0.371	0.345	0.349	0.355	0.360	0.369	0.353	0.363	0.346
60	0.365	0.362	0.366	0.345	0.346	0.365	0.374	0.375	0.354	0.368	0.350	0.363
90	0.355	0.345	0.366	0.357	0.367	0.352	0.358	0.353	0.356	0.372	0.370	0.354
120	0.361	0.364	0.366	0.359	0.365	0.368	0.362	0.359	0.349	0.347	0.358	0.372
150	0.358	0.363	0.365	0.372	0.367	0.354	0.352	0.349	0.365	0.359	0.358	0.367
180	0.363	0.352	0.360	0.351	0.361	0.350	0.357	0.368	0.348	0.365	0.354	0.370
210	0.349	0.373	0.373	0.366	0.350	0.374	0.349	0.366	0.363	0.361	0.349	0.349
240	0.353	0.366	0.358	0.366	0.374	0.365	0.369	0.369	0.353	0.353	0.354	0.366
270	0.366	0.352	0.349	0.353	0.374	0.345	0.368	0.351	0.348	0.363	0.361	0.352
300	0.361	0.375	0.362	0.368	0.360	0.354	0.350	0.348	0.349	0.351	0.353	0.362
330	0.352	0.357	0.346	0.374	0.367	0.344	0.346	0.349	0.358	0.365	0.350	0.373

TABLE A.41: Shell Wall Thickness (in.) of GB41 Shell

$\theta \backslash L(\text{in.})$	13	39	65	91	117	143	169	195	221	247	273	299
0	0.362	0.369	0.373	0.357	0.365	0.362	0.367	0.349	0.364	0.344	0.362	0.362
30	0.355	0.374	0.353	0.347	0.373	0.372	0.351	0.357	0.344	0.372	0.357	0.374
60	0.347	0.353	0.356	0.345	0.361	0.345	0.368	0.367	0.349	0.352	0.348	0.366
90	0.350	0.354	0.360	0.350	0.363	0.360	0.367	0.352	0.368	0.351	0.361	0.358
120	0.371	0.356	0.366	0.359	0.360	0.350	0.359	0.367	0.369	0.346	0.374	0.349
150	0.359	0.373	0.360	0.348	0.358	0.365	0.370	0.370	0.347	0.371	0.345	0.364
180	0.363	0.373	0.346	0.368	0.361	0.361	0.375	0.354	0.373	0.358	0.368	0.367
210	0.365	0.364	0.361	0.372	0.352	0.375	0.362	0.360	0.374	0.373	0.346	0.347
240	0.373	0.356	0.364	0.366	0.363	0.364	0.355	0.374	0.369	0.367	0.373	0.363
270	0.350	0.372	0.345	0.356	0.354	0.375	0.373	0.368	0.369	0.346	0.350	0.366
300	0.374	0.356	0.361	0.360	0.367	0.370	0.373	0.365	0.366	0.347	0.375	0.353
330	0.370	0.370	0.365	0.347	0.374	0.365	0.358	0.347	0.362	0.373	0.346	0.346

TABLE A.42: Shell Wall Thickness (in.) of GB42 Shell

$\theta \backslash L(\text{in.})$	13	39	65	91	117	143	169	195	221	247	273	299
0	0.375	0.348	0.370	0.350	0.346	0.373	0.370	0.358	0.347	0.352	0.368	0.363
30	0.350	0.345	0.347	0.369	0.351	0.358	0.361	0.350	0.345	0.360	0.353	0.362
60	0.371	0.363	0.362	0.353	0.374	0.349	0.363	0.351	0.352	0.355	0.350	0.366
90	0.358	0.365	0.360	0.360	0.346	0.373	0.372	0.365	0.368	0.362	0.365	0.373
120	0.353	0.357	0.348	0.347	0.358	0.363	0.373	0.371	0.365	0.370	0.351	0.365
150	0.347	0.371	0.370	0.359	0.352	0.347	0.349	0.355	0.361	0.351	0.375	0.359
180	0.351	0.346	0.362	0.362	0.351	0.350	0.372	0.371	0.348	0.345	0.364	0.374
210	0.374	0.359	0.363	0.361	0.349	0.353	0.357	0.355	0.347	0.364	0.354	0.363
240	0.373	0.351	0.368	0.363	0.357	0.360	0.351	0.370	0.357	0.374	0.357	0.349
270	0.348	0.360	0.369	0.363	0.371	0.371	0.374	0.348	0.371	0.369	0.345	0.345
300	0.362	0.344	0.360	0.372	0.356	0.371	0.368	0.360	0.363	0.356	0.359	0.360
330	0.347	0.346	0.368	0.366	0.360	0.349	0.358	0.359	0.363	0.373	0.362	0.358

TABLE A.43: Shell Wall Thickness (in.) of GB43 Shell

$\theta \backslash L(\text{in.})$	13	39	65	91	117	143	169	195	221	247	273	299
0	0.353	0.372	0.370	0.374	0.367	0.361	0.374	0.363	0.357	0.368	0.350	0.363
30	0.366	0.364	0.374	0.358	0.357	0.361	0.356	0.363	0.363	0.374	0.361	0.372
60	0.369	0.346	0.365	0.352	0.350	0.361	0.368	0.372	0.355	0.359	0.365	0.344
90	0.353	0.373	0.355	0.373	0.345	0.373	0.351	0.372	0.346	0.350	0.349	0.370
120	0.352	0.352	0.366	0.361	0.356	0.373	0.347	0.361	0.350	0.369	0.371	0.362
150	0.346	0.345	0.362	0.352	0.348	0.359	0.353	0.350	0.349	0.364	0.363	0.374
180	0.363	0.350	0.350	0.366	0.366	0.364	0.351	0.355	0.370	0.371	0.374	0.358
210	0.372	0.362	0.369	0.349	0.358	0.365	0.347	0.358	0.352	0.351	0.375	0.362
240	0.349	0.371	0.360	0.352	0.366	0.356	0.361	0.367	0.374	0.361	0.356	0.349
270	0.375	0.350	0.361	0.350	0.355	0.375	0.349	0.368	0.350	0.357	0.364	0.373
300	0.347	0.365	0.364	0.367	0.349	0.350	0.369	0.356	0.358	0.372	0.370	0.346
330	0.366	0.370	0.357	0.355	0.369	0.372	0.369	0.362	0.364	0.371	0.351	0.349

TABLE A.44: Shell Wall Thickness (in.) of GB44 Shell

$\theta \backslash L(\text{in.})$	13	39	65	91	117	143	169	195	221	247	273	299
0	0.350	0.346	0.354	0.371	0.372	0.371	0.347	0.354	0.352	0.357	0.351	0.364
30	0.368	0.373	0.359	0.354	0.364	0.358	0.361	0.347	0.346	0.371	0.348	0.362
60	0.365	0.375	0.373	0.354	0.372	0.361	0.359	0.347	0.351	0.344	0.367	0.373
90	0.348	0.374	0.367	0.352	0.362	0.350	0.349	0.359	0.358	0.358	0.352	0.355
120	0.364	0.367	0.361	0.358	0.366	0.360	0.360	0.371	0.349	0.369	0.374	0.358
150	0.367	0.368	0.351	0.357	0.364	0.354	0.373	0.360	0.368	0.371	0.369	0.358
180	0.370	0.365	0.372	0.346	0.344	0.353	0.345	0.364	0.375	0.355	0.365	0.375
210	0.357	0.350	0.374	0.354	0.369	0.349	0.350	0.348	0.370	0.356	0.357	0.346
240	0.372	0.355	0.371	0.372	0.351	0.367	0.369	0.356	0.365	0.357	0.367	0.368
270	0.373	0.367	0.345	0.347	0.346	0.357	0.358	0.368	0.356	0.348	0.349	0.367
300	0.347	0.347	0.345	0.368	0.362	0.360	0.347	0.374	0.369	0.352	0.348	0.359
330	0.359	0.346	0.370	0.368	0.355	0.360	0.358	0.370	0.372	0.374	0.361	0.354

TABLE A.45: Shell Wall Thickness (in.) of GB45 Shell

$\theta \backslash L(\text{in.})$	13	39	65	91	117	143	169	195	221	247	273	299
0	0.370	0.344	0.350	0.361	0.349	0.366	0.361	0.363	0.365	0.361	0.363	0.353
30	0.345	0.363	0.370	0.352	0.366	0.350	0.356	0.368	0.357	0.356	0.365	0.373
60	0.349	0.366	0.358	0.368	0.368	0.356	0.370	0.346	0.356	0.347	0.359	0.364
90	0.359	0.373	0.362	0.359	0.374	0.361	0.353	0.345	0.373	0.370	0.352	0.373
120	0.368	0.349	0.350	0.368	0.348	0.347	0.350	0.352	0.370	0.344	0.375	0.351
150	0.350	0.347	0.372	0.360	0.347	0.372	0.361	0.348	0.372	0.354	0.350	0.374
180	0.371	0.372	0.365	0.357	0.347	0.356	0.349	0.360	0.361	0.365	0.367	0.356
210	0.365	0.368	0.347	0.371	0.346	0.372	0.355	0.374	0.358	0.344	0.374	0.355
240	0.370	0.348	0.353	0.353	0.350	0.359	0.371	0.373	0.350	0.375	0.372	0.365
270	0.365	0.363	0.364	0.369	0.345	0.370	0.359	0.344	0.363	0.371	0.357	0.359
300	0.347	0.372	0.365	0.361	0.349	0.356	0.363	0.369	0.347	0.345	0.352	0.354
330	0.358	0.366	0.353	0.372	0.372	0.368	0.357	0.372	0.372	0.368	0.357	0.354

TABLE A.46: Shell Wall Thickness (in.) of GB46 Shell

$\theta \backslash L(\text{in.})$	13	39	65	91	117	143	169	195	221	247	273	299
0	0.365	0.358	0.366	0.374	0.358	0.353	0.344	0.373	0.348	0.369	0.363	0.358
30	0.364	0.347	0.369	0.367	0.345	0.355	0.374	0.354	0.355	0.355	0.359	0.372
60	0.370	0.357	0.355	0.367	0.354	0.351	0.372	0.374	0.358	0.372	0.372	0.354
90	0.345	0.375	0.372	0.364	0.363	0.372	0.357	0.357	0.363	0.345	0.363	0.346
120	0.353	0.350	0.359	0.374	0.371	0.370	0.360	0.363	0.369	0.346	0.367	0.352
150	0.347	0.362	0.358	0.369	0.357	0.375	0.346	0.360	0.365	0.347	0.344	0.351
180	0.360	0.346	0.356	0.359	0.367	0.349	0.359	0.365	0.352	0.347	0.371	0.352
210	0.373	0.373	0.354	0.368	0.352	0.352	0.360	0.362	0.369	0.348	0.352	0.369
240	0.347	0.345	0.362	0.357	0.349	0.374	0.348	0.373	0.360	0.345	0.363	0.371
270	0.366	0.374	0.357	0.363	0.372	0.360	0.359	0.370	0.367	0.348	0.372	0.370
300	0.359	0.363	0.357	0.362	0.351	0.353	0.349	0.356	0.365	0.363	0.346	0.346
330	0.366	0.346	0.355	0.367	0.352	0.362	0.374	0.361	0.348	0.373	0.366	0.363

TABLE A.47: Shell Wall Thickness (in.) of GB47 Shell

$\theta \backslash L(\text{in.})$	13	39	65	91	117	143	169	195	221	247	273	299
0	0.367	0.363	0.360	0.361	0.351	0.353	0.364	0.352	0.359	0.354	0.369	0.359
30	0.361	0.359	0.373	0.344	0.367	0.351	0.344	0.349	0.349	0.353	0.359	0.348
60	0.350	0.349	0.362	0.354	0.345	0.349	0.362	0.369	0.368	0.358	0.372	0.374
90	0.364	0.363	0.373	0.346	0.346	0.356	0.358	0.362	0.367	0.373	0.344	0.358
120	0.354	0.372	0.370	0.370	0.357	0.353	0.353	0.352	0.349	0.344	0.361	0.353
150	0.371	0.361	0.354	0.350	0.349	0.349	0.352	0.368	0.372	0.373	0.350	0.361
180	0.363	0.354	0.367	0.372	0.366	0.367	0.366	0.367	0.371	0.363	0.369	0.350
210	0.365	0.357	0.374	0.347	0.361	0.364	0.364	0.370	0.369	0.373	0.345	0.374
240	0.350	0.354	0.375	0.370	0.347	0.372	0.351	0.355	0.348	0.367	0.345	0.368
270	0.348	0.360	0.345	0.355	0.373	0.360	0.356	0.357	0.355	0.350	0.366	0.346
300	0.362	0.363	0.346	0.353	0.347	0.363	0.361	0.347	0.368	0.358	0.351	0.345
330	0.361	0.357	0.363	0.361	0.358	0.374	0.358	0.365	0.355	0.350	0.361	0.370

TABLE A.48: Shell Wall Thickness (in.) of GB48 Shell

$\theta \backslash L(\text{in.})$	13	39	65	91	117	143	169	195	221	247	273	299
0	0.353	0.346	0.366	0.347	0.353	0.368	0.375	0.368	0.346	0.364	0.350	0.349
30	0.352	0.359	0.356	0.370	0.362	0.368	0.371	0.354	0.371	0.355	0.351	0.370
60	0.363	0.344	0.345	0.361	0.352	0.349	0.367	0.361	0.365	0.366	0.354	0.359
90	0.354	0.353	0.375	0.347	0.345	0.354	0.359	0.365	0.369	0.358	0.351	0.373
120	0.355	0.370	0.374	0.364	0.370	0.356	0.367	0.371	0.352	0.352	0.346	0.360
150	0.359	0.374	0.365	0.351	0.363	0.362	0.358	0.365	0.345	0.350	0.353	0.373
180	0.369	0.366	0.358	0.351	0.365	0.347	0.358	0.349	0.375	0.352	0.348	0.364
210	0.359	0.348	0.359	0.348	0.351	0.365	0.374	0.365	0.358	0.367	0.350	0.360
240	0.344	0.364	0.350	0.357	0.356	0.356	0.353	0.360	0.371	0.365	0.369	0.350
270	0.363	0.366	0.370	0.363	0.349	0.357	0.368	0.358	0.362	0.371	0.365	0.350
300	0.363	0.353	0.354	0.374	0.373	0.366	0.357	0.351	0.362	0.368	0.358	0.359
330	0.359	0.353	0.374	0.365	0.365	0.350	0.356	0.356	0.359	0.359	0.349	0.371

TABLE A.49: Shell Wall Thickness (in.) of GB49 Shell

$\theta \backslash L(\text{in.})$	13	39	65	91	117	143	169	195	221	247	273	299
0	0.347	0.368	0.367	0.370	0.369	0.348	0.344	0.350	0.359	0.364	0.351	0.364
30	0.375	0.358	0.373	0.367	0.344	0.362	0.363	0.361	0.347	0.354	0.344	0.375
60	0.356	0.370	0.357	0.352	0.351	0.347	0.348	0.347	0.358	0.360	0.370	0.367
90	0.350	0.368	0.364	0.355	0.357	0.347	0.367	0.374	0.356	0.368	0.351	0.362
120	0.353	0.370	0.375	0.374	0.357	0.361	0.358	0.361	0.345	0.364	0.355	0.359
150	0.365	0.357	0.353	0.349	0.364	0.345	0.363	0.365	0.349	0.372	0.361	0.345
180	0.366	0.350	0.345	0.371	0.349	0.349	0.353	0.355	0.348	0.373	0.354	0.375
210	0.347	0.347	0.359	0.354	0.369	0.350	0.369	0.353	0.373	0.347	0.369	0.356
240	0.372	0.346	0.351	0.358	0.370	0.375	0.370	0.351	0.375	0.372	0.372	0.356
270	0.363	0.364	0.371	0.360	0.350	0.362	0.371	0.356	0.353	0.365	0.352	0.369
300	0.365	0.370	0.370	0.372	0.370	0.368	0.355	0.374	0.347	0.367	0.351	0.363
330	0.345	0.355	0.354	0.364	0.351	0.365	0.359	0.373	0.360	0.374	0.375	0.363

TABLE A.50: Shell Wall Thickness (in.) of GB50 Shell

$\theta \backslash L(\text{in.})$	13	39	65	91	117	143	169	195	221	247	273	299
0	0.354	0.348	0.360	0.356	0.358	0.353	0.345	0.364	0.371	0.366	0.365	0.358
30	0.363	0.358	0.346	0.371	0.345	0.372	0.372	0.350	0.347	0.367	0.366	0.349
60	0.366	0.359	0.360	0.352	0.348	0.368	0.355	0.350	0.349	0.364	0.347	0.358
90	0.362	0.373	0.360	0.361	0.352	0.353	0.362	0.373	0.351	0.351	0.348	0.359
120	0.359	0.352	0.359	0.372	0.374	0.360	0.358	0.370	0.365	0.357	0.373	0.350
150	0.366	0.349	0.363	0.369	0.368	0.344	0.358	0.371	0.347	0.370	0.370	0.348
180	0.368	0.363	0.345	0.349	0.364	0.368	0.364	0.363	0.367	0.355	0.370	0.360
210	0.358	0.362	0.368	0.350	0.372	0.346	0.364	0.373	0.364	0.363	0.345	0.360
240	0.361	0.345	0.362	0.364	0.363	0.364	0.371	0.364	0.350	0.368	0.367	0.374
270	0.350	0.345	0.369	0.374	0.352	0.373	0.361	0.352	0.374	0.369	0.360	0.350
300	0.369	0.358	0.346	0.349	0.369	0.371	0.371	0.356	0.354	0.360	0.346	0.357
330	0.346	0.357	0.369	0.348	0.364	0.372	0.362	0.366	0.366	0.371	0.362	0.349

APPENDIX B: FOURIER COEFFICIENTS FOR GB SHELLS

TABLE B.1: Fourier Coefficients (a_i) for GB Shells

a_i	GB1	GB2	GB3	GB4	GB5	GB6	GB7	GB8	GB9	GB10	GB11	GB12	GB13
0	0.36000	0.35756	0.36006	0.36006	0.35939	0.35876	0.36081	0.36022	0.35897	0.35863	0.35949	0.35898	0.35881
1	0.00085	0.00002	-0.00054	0.00111	0.00155	-0.00012	-0.00132	0.00010	0.00056	-0.00015	0.00005	0.00336	0.00001
2	0.00045	-0.00079	0.00111	-0.00006	-0.00098	-0.00097	0.00007	0.00157	-0.00121	-0.00099	0.00071	0.00112	-0.00147
3	0.00024	0.00042	-0.00019	0.00052	0.00013	-0.00026	0.00049	-0.00184	0.00105	0.00077	-0.00072	-0.00102	0.00001
4	-0.00033	-0.00150	-0.00225	-0.00081	-0.00017	0.00182	0.00124	-0.00120	-0.00016	-0.00027	-0.00007	-0.00138	-0.00071
5	-0.00026	0.00032	-0.00003	0.00051	0.00230	0.00073	0.00013	-0.00099	0.00124	0.00034	-0.00047	-0.00024	-0.00002
6	0.00207	0.00122	-0.00120	-0.00045	0.00196	-0.00253	-0.00133	0.00017	-0.00003	0.00037	0.00059	-0.00001	0.00036
7	0.00063	-0.00044	-0.00144	0.00091	0.00028	0.00030	-0.00020	0.00027	0.00198	0.00044	-0.00112	-0.00154	0.00132
8	-0.00073	0.00028	0.00150	-0.00149	-0.00010	0.00030	-0.00039	-0.00092	0.00023	0.00049	0.00043	0.00039	0.00143
9	-0.00030	-0.00047	0.00096	0.00059	-0.00055	-0.00055	-0.00005	-0.00171	-0.00013	-0.00011	0.00020	0.00110	0.00053
10	-0.00072	0.00101	-0.00035	-0.00092	0.00030	0.00058	-0.00138	-0.00035	0.00053	-0.00147	0.00012	-0.00056	-0.00016
a_i	GB14	GB15	GB16	GB17	GB18	GB19	GB20	GB21	GB22	GB23	GB24	GB25	Mean (A_i)
0	0.35943	0.36008	0.35993	0.35996	0.35993	0.36083	0.35976	0.35974	0.36004	0.35874	0.35974	0.35976	0.35959
1	-0.00096	0.00044	-0.00057	0.00173	0.00017	-0.00063	-0.00052	-0.00026	0.00113	0.00032	0.00048	0.00023	0.00028
2	0.00028	-0.00076	0.00264	-0.00264	0.00024	0.00016	0.00084	-0.00040	0.00046	-0.00018	-0.00035	0.00019	-0.00004
3	-0.00167	-0.00115	-0.00028	-0.00112	-0.00002	0.00061	0.00075	0.00093	-0.00010	0.00116	-0.00063	0.00209	0.00001
4	-0.00033	0.00020	0.00037	-0.00113	0.00044	-0.00008	0.00051	-0.00007	0.00068	0.00143	0.00163	-0.00048	-0.00010
5	0.00007	-0.00003	-0.00070	0.00105	0.00169	0.00040	-0.00012	0.00071	0.00082	0.00075	0.00096	0.00101	0.00041
6	-0.00173	-0.00132	-0.00088	-0.00031	0.00124	0.00153	-0.00061	-0.00028	-0.00119	0.00064	-0.00003	-0.00020	-0.00008
7	-0.00094	0.00032	-0.00060	0.00140	-0.00009	0.00058	0.00049	-0.00004	-0.00155	0.00118	0.00090	-0.00017	0.00011
8	-0.00200	-0.00058	-0.00039	0.00027	-0.00101	0.00014	0.00107	-0.00007	0.00024	0.00065	-0.00043	-0.00173	-0.00010
9	-0.00108	-0.00096	0.00009	0.00017	-0.00064	0.00084	0.00011	-0.00129	-0.00049	-0.00015	-0.00068	0.00038	-0.00017
10	0.00031	-0.00017	0.00092	0.00031	0.00052	-0.00086	0.00046	-0.00141	-0.00189	-0.00004	0.00167	0.00099	-0.00010

APPENDIX D: BUCKLING LOAD OF GB SHELLS
(KOITER AXISYMMETRIC METHOD)

TABLE D.1: Non-Dimensional Buckling Load of GB Shells
(Koiter Axisymmetric Method)

GB Shell	λ	GB Shell	λ
1	0.731	26	0.728
2	0.714	27	0.720
3	0.732	28	0.725
4	0.732	29	0.733
5	0.727	30	0.732
6	0.722	31	0.719
7	0.737	32	0.734
8	0.733	33	0.730
9	0.724	34	0.720
10	0.721	35	0.724
11	0.727	36	0.728
12	0.724	37	0.723
13	0.722	38	0.722
14	0.727	39	0.734
15	0.732	40	0.727
16	0.731	41	0.739
17	0.731	42	0.727
18	0.731	43	0.735
19	0.738	44	0.731
20	0.729	45	0.731
21	0.729	46	0.731
22	0.731	47	0.724
23	0.722	48	0.727
24	0.729	49	0.731
25	0.729	50	0.731

APPENDIX F: BUCKLING LOAD MAP FOR GB SHELLS (AXIAL LOADING)

TABLE F.1: Buckling Load Map for GB Shells (All values normalized by factor 21,320 lb/in.)

k\l	0	1	2	3	4	5	6	7	8	9	10	11	12	13	14	15	16
1	360.0	127.0	25.9	7.09	2.63	1.33	1.00	1.13	1.57	2.31	3.40	4.90	6.88	9.42	12.6	16.6	21.4
2	90.1	65.7	31.8	14.0	6.51	3.32	1.91	1.27	1.03	1.02	1.18	1.49	1.95	2.57	3.37	4.37	5.59
3	40.0	34.6	23.6	14.2	8.20	4.82	2.96	1.94	1.38	1.10	1.00	1.03	1.17	1.40	1.73	2.16	2.70
4	22.5	20.7	16.4	11.8	7.98	5.32	3.57	2.46	1.77	1.35	1.12	1.01	1.01	1.08	1.23	1.45	1.74
5	14.4	13.7	11.7	9.31	7.02	5.14	3.73	2.73	2.04	1.58	1.28	1.10	1.01	1.00	1.06	1.17	1.33
6	10.0	9.67	8.68	7.34	5.93	4.66	3.61	2.78	2.16	1.72	1.40	1.19	1.07	1.01	1.01	1.05	1.15
7	7.39	7.19	6.64	5.85	4.97	4.11	3.34	2.69	2.18	1.78	1.48	1.26	1.12	1.04	1.00	1.01	1.06
8	5.68	5.56	5.23	4.74	4.17	3.58	3.02	2.53	2.11	1.77	1.51	1.31	1.16	1.07	1.01	1.00	1.02
9	4.50	4.43	4.22	3.91	3.53	3.12	2.71	2.34	2.01	1.73	1.50	1.32	1.18	1.09	1.03	1.00	1.01
10	3.67	3.62	3.49	3.28	3.01	2.72	2.43	2.15	1.89	1.66	1.47	1.31	1.19	1.10	1.04	1.01	1.00

APPENDIX G: 8-MODE TREE FOR GB SHELLS (AXIAL LOADING)

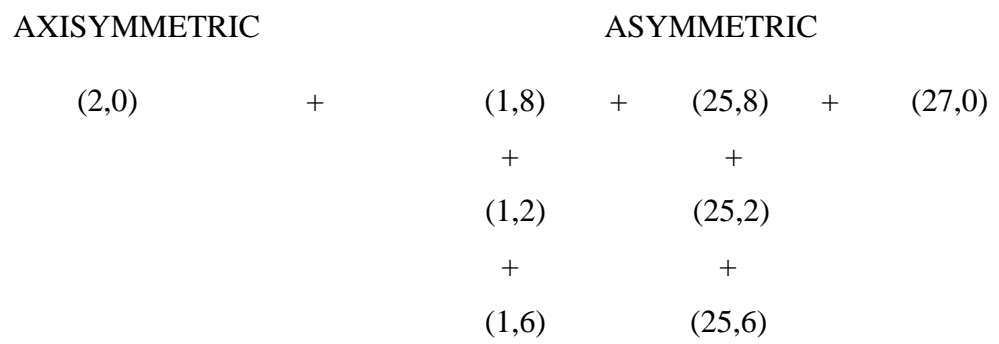


FIGURE G.1: 8-Mode Tree for GB Shells (Axial Loading)

APPENDIX H: BUCKLING LOAD OF GB SHELLS
(KOITER ASYMMETRIC METHOD)

TABLE H.1: Non-Dimensional Buckling Load of GB Shells
(Koiter Asymmetric Method)

GB Shell	λ	GB Shell	λ
1	0.539	26	0.534
2	0.514	27	0.523
3	0.539	28	0.53
4	0.539	29	0.541
5	0.532	30	0.539
6	0.526	31	0.522
7	0.548	32	0.542
8	0.541	33	0.537
9	0.528	34	0.523
10	0.524	35	0.528
11	0.533	36	0.534
12	0.528	37	0.527
13	0.526	38	0.526
14	0.533	39	0.543
15	0.539	40	0.532
16	0.538	41	0.55
17	0.538	42	0.533
18	0.538	43	0.544
19	0.548	44	0.538
20	0.536	45	0.539
21	0.536	46	0.538
22	0.539	47	0.528
23	0.525	48	0.533
24	0.536	49	0.539
25	0.536	50	0.538

APPENDIX I: BUCKLING LOAD MAP FOR GB SHELLS (EXTERNAL PRESSURE)

TABLE I.1: Buckling Load Map for GB Shells (All values normalized by factor 5.975 lb/in.²)

k/l	1	2	3	4	5	6	7	8	9	10	11	12	13	14	15	16
1	5530.0	282.0	34.3	7.2	2.3	1.2	1.0	1.1	1.2	1.5	1.8	2.1	2.4	2.8	3.2	3.6
2	11400.0	1380.0	271.0	70.8	23.1	9.2	4.5	2.8	2.2	2.1	2.2	2.4	2.7	3.0	3.4	3.8
3	13500.0	2310.0	615.0	201.0	75.5	32.2	15.5	8.5	5.3	3.9	3.3	3.2	3.3	3.5	3.8	4.1
4	14400.0	2860.0	910.0	347.0	148.0	69.0	35.0	19.3	11.6	7.8	5.8	4.9	4.5	4.4	4.5	4.7
5	14900.0	3190.0	1120.0	477.0	223.0	113.0	60.6	34.6	21.1	13.9	9.9	7.7	6.5	5.9	5.6	5.7
6	15100.0	3390.0	1280.0	580.0	292.0	157.0	88.9	52.9	33.2	22.0	15.4	11.6	9.3	8.0	7.3	7.2
7	15300.0	3530.0	1380.0	661.0	350.0	197.0	117.0	72.4	46.7	31.5	22.3	16.6	13.1	10.9	9.6	8.8
8	15500.0	3640.0	1470.0	725.0	398.0	234.0	144.0	91.9	61.0	41.9	30.0	22.4	17.5	14.4	12.4	11.1
9	15600.0	3720.0	1530.0	776.0	439.0	265.0	168.0	111.0	75.2	52.8	38.4	28.9	22.7	18.5	15.7	13.8
10	15800.0	3790.0	1580.0	819.0	474.0	293.0	190.0	128.0	89.2	63.9	47.1	35.9	28.3	23.0	19.4	17.0

APPENDIX J: 8-MODE TREE FOR GB SHELLS (EXTERNAL PRESSURE)

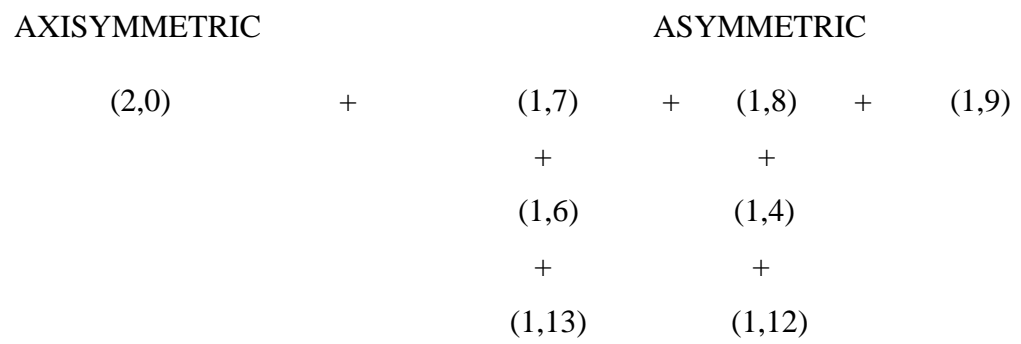


FIGURE J.1: 8-Mode Tree for GB Shells (External Pressure)